AD-A165 442 UNDERGROUND DYNAMIC AIRBLAST SIMULATOR INVESTIGATIONS 1/2
TUNNEL RESPONSE MEA..(U) MERRITT CASES INC REDLANDS CA
D N BURGESS ET AL. 31 OCT 84 84-015-T1 DNA-TR-84-404
UNCLASSIFIED DNA001-84-C-0085 F/G 19/4 NL

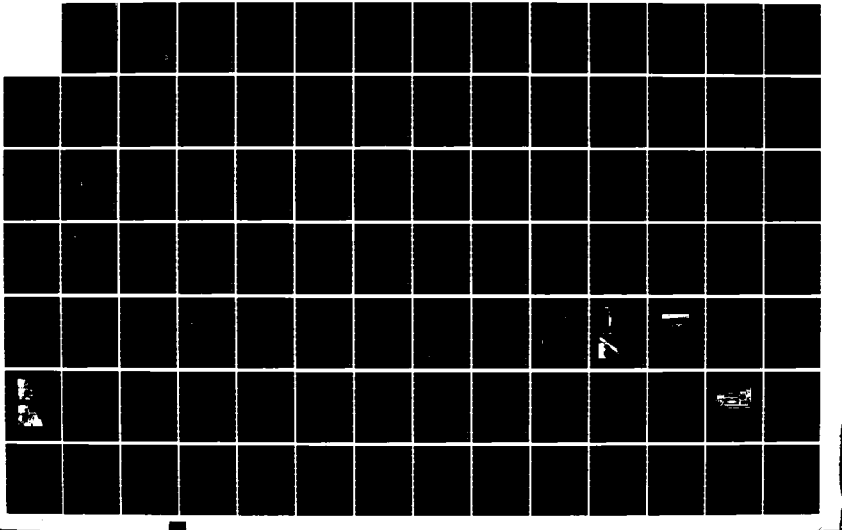

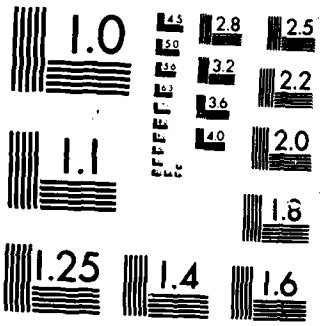

E301909

(12)

AD-A165 442

DNA-TR-84-404

UNDERGROUND DYNAMIC AIRBLAST SIMULATOR INVESTIGATIONS

Tunnel Response Measurements and Theoretical Analyses

D.N. Burgess
K.B. Morrill
G.L. Wintergerst
H.C. Davis
Merritt CASES, Inc.
P.O. Box 1206
Redlands, CA 92373-0401

31 October 1984

Technical Report

CONTRACT No. DNA 001-84-C-0085

Approved for public release;
distribution is unlimited.

THIS WORK WAS SPONSORED BY THE DEFENSE NUCLEAR AGENCY
UNDER RDT&E RMSS CODE B342084466 Y99QMXSH00004 H2590D.

Prepared for
Director
DEFENSE NUCLEAR AGENCY
Washington, DC 20305-1000

Destroy this report when it is no longer needed. Do not return to sender.

PLEASE NOTIFY THE DEFENSE NUCLEAR AGENCY, ATTN: STTI, WASHINGTON, DC 20305-1000, IF YOUR ADDRESS IS INCORRECT, IF YOU WISH IT DELETED FROM THE DISTRIBUTION LIST, OR IF THE ADDRESSEE IS NO LONGER EMPLOYED BY YOUR ORGANIZATION.

UNCLASSIFIED
SECURITY CLASSIFICATION OF THIS PAGE

AD-A165442

REPORT DOCUMENTATION PAGE

Form Approved
OMB No. 0704-0188
Exp. Date: Jun 30, 1986

1a. REPORT SECURITY CLASSIFICATION UNCLASSIFIED	1b. RESTRICTIVE MARKINGS
2a. SECURITY CLASSIFICATION AUTHORITY	3. DISTRIBUTION / AVAILABILITY OF REPORT Approved for public release; distribution is unlimited.
2b. DECLASSIFICATION / DOWNGRADING SCHEDULE N/A since UNCLASSIFIED	
4. PERFORMING ORGANIZATION REPORT NUMBER(S) 84-015-T1	5. MONITORING ORGANIZATION REPORT NUMBER(S) DNA-TR-84-404
6a. NAME OF PERFORMING ORGANIZATION Merritt CASES, Inc. 6b. OFFICE SYMBOL (If applicable)	7a. NAME OF MONITORING ORGANIZATION Director Defense Nuclear Agency
6c. ADDRESS (City, State, and ZIP Code) P.O. Box 1206 Redlands, CA 92373-0401	7b. ADDRESS (City, State, and ZIP Code) Washington, DC 20305-1000
8a. NAME OF FUNDING / SPONSORING ORGANIZATION 8b. OFFICE SYMBOL (If applicable)	9. PROCUREMENT INSTRUMENT IDENTIFICATION NUMBER DNA 001-84-C-0085
8c. ADDRESS (City, State, and ZIP Code)	10. SOURCE OF FUNDING NUMBERS

PROGRAM ELEMENT NO.	PROJECT NO	TASK NO	WORK UNIT ACCESSION NO.
62715H	Y99QMXS	H	DH008236

11. TITLE (Include Security Classification)
UNDERGROUND DYNAMIC AIRBLAST SIMULATOR INVESTIGATIONS, Tunnel Response Measurements and Theoretical Analyses

12. PERSONAL AUTHOR(S)
D.N. Burgess, K.B. Morrill, G.L. Wintergerst, and H.C Davis

13a. TYPE OF REPORT	13b. TIME COVERED	14. DATE OF REPORT (Year, Month, Day)	15. PAGE COUNT
Technical	FROM 831101 TO 840930	1984, October 31	168

16. SUPPLEMENTARY NOTATION
This work was sponsored by the Defense Nuclear Agency under RDT&E RMSS Code B342084466 Y99QMXSH00004 H2590D.

17 COSATI CODES			18. SUBJECT TERMS (Continue on reverse if necessary and identify by block number)	
FIELD	GROUP	SUB-GROUP		
14	2		Dynamic Airblast Simulation	DABS
			Tunnel Response Tests	Tunnel Behavior
8	7		Rock Deformation Measurements	Rock Strain

19. ABSTRACT (Continue on reverse if necessary and identify by block number)

This report describes preliminary design investigations for a reusable large scale underground dynamic airblast simulator. It also describes dynamic measurements of rock displacement and passive measurements of residual rock deformation which were made during two explosively loaded tunnel response tests at Little Skull Mountain, Nevada Test Site. Correlations between theoretical finite element analyses and active measurements are also described.

20. DISTRIBUTION / AVAILABILITY OF ABSTRACT	21. ABSTRACT SECURITY CLASSIFICATION	
☐ UNCLASSIFIED/UNLIMITED ☒ SAME AS RPT. ☐ DTIC USERS	UNCLASSIFIED	
22a. NAME OF RESPONSIBLE INDIVIDUAL Betty L. Fox	22b. TELEPHONE (Include Area Code) (202) 325-7042	22c. OFFICE SYMBOL DNA/STTI

DD FORM 1473, 84 MAR

83 APR edition may be used until exhausted
All other editions are obsolete.

SECURITY CLASSIFICATION OF THIS PAGE
UNCLASSIFIED

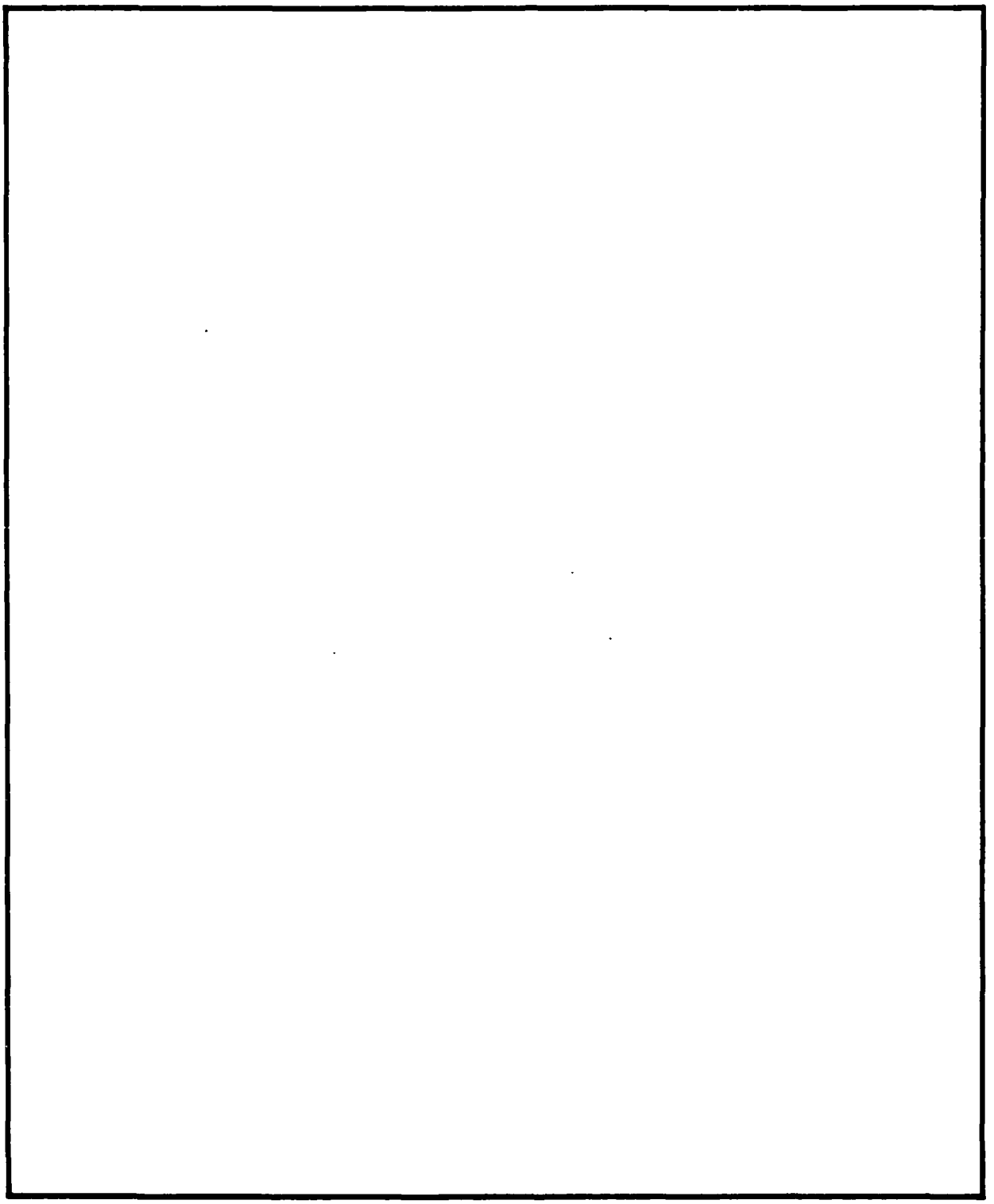

SUMMARY

One of the concepts for basing the new, small ICBM currently under development by the Air Force is the Hard Mobile Launcher (HML). As part of the concept development and selection process, it was judged necessary to simulate the effects of nuclear airblast on a large scale model of the HML. Because of the requirement to conduct several airblast simulation tests during the HML concept validation phase, it was decided to investigate the development of a reusable large scale dynamic airblast simulator. The simulator was envisioned to be similar to a very large shock tube driven by a high explosive detonation.

One of the reusable simulator concepts considered consists of a tunnel excavated into a mountain. Merritt CASES, Inc. (CASES) performed preliminary design analyses for a one-half scale underground simulator and participated in conducting and evaluating the results of two tunnel response tests. These tests, using an Iremite driver, were performed during June 1984 in an existing tunnel, 18 feet-seven inches (5.66 m) in diameter and 704 feet (214.6 m) long. This program was conducted at Little Skull Mountain, Area 25, Nevada Test Site. The overall objective of the program was to evaluate the behavior of a tunnel subjected to repeated high explosive detonations and to the resulting airblast waves propagating along the tunnel.

CASES performed a series of two dimensional finite element calculations to predict the behavior of a one-half scale underground simulator. The simulator was assumed to be located in ashfall tuff at Little Skull Mountain. The cross section was assumed to be 45 feet (13.7 m) wide and 30 feet (9.1 m) high (a 45 foot (13.7 m) semicircle over a 45 by 7.5 foot (13.7 by 2.3 m) rectangle). The driver section was assumed to be loaded with a triangular pressure pulse with a peak of 400 psi (2.76 MPa). We also performed response prediction calculations for the tunnel response

tests in the existing tunnel. The results of both series of calculations indicated that rock strains would be quite small and that tunnel behavior should be essentially elastic.

CASES developed and fielded 24 gages to measure dynamic relative rock displacements in the driver section, near the portal, and at one intermediate location. The primary objective of the active measurements was to obtain displacement-time histories which could be used to confirm or calibrate our finite element calculations of tunnel response for later use in designing a one-half scale underground simulator and in predicting its behavior.

The dynamic relative displacement gage consists of a borehole extensometer which employs a linear variable differential transformer as a transducer. The gages measured the displacement of the rock between the collars of the boreholes and points located either two or three tunnel radii from the collar. These gages performed very well during both tunnel response tests, providing detailed dynamic response data. Measured relative displacements were quite small, generally on the order of 0.07 inches (0.18 cm) or less. Following the first test, the finite element calculational model was calibrated against two of the gage records. The calibrated model was then used to calculate relative displacement-time histories at the other gage locations for Test 1 and at all gage locations for Test 2. The calculated and measured peak relative displacements were generally in good agreement. The calculations also provided reasonably good matches to the "structure" of the gage records beyond the peaks. We concluded that the objective of obtaining dynamic displacement data and calibrating the calculational model was satisfied.

Passive measurements of residual rock deformations were also made, using the H-Gage (similar in principal to a Whittemore gage) developed by CASES and used

previously on the HURON LANDING structures experiment. The primary objective of the passive measurements was to supplement active data with residual tangential and "diametral" rock strain measurements around the periphery of the tunnel in the event inelastic behavior occurred. The H-Gage accurately measures the distance between gage points (predrilled lag screws) installed prior to a test, in the rock around the tunnel perimeter at a nominal spacing of 20 inches (50.8 cm). Both tangential and diametral measurements were made before and after each test. Measured residual displacements were very small, many of them less than the estimated precision of the gage. However, the measurement technique is sufficiently accurate (better than 0.2 percent for tangential strain and 0.02 percent for diametral strain) to measure any strains which are large enough to cause significant damage to the tunnel.

The tunnel was able to withstand two high explosive detonations with negligible damage. The small measured displacements, when coupled with pretest predictions and observations of the tunnel following both tests, led us to conclude that tunnel response was essentially elastic. Consequently, there is a high degree of confidence that a one-half scale simulator could be constructed and repeatedly operated successfully at Little Skull Mountain or in a similar geology.

PREFACE

The work described in this report was performed under Contract DNA001-84-C-0085. The technical monitor during the period of performance was Lt. Col. Gary Ganong, FCDNA (since retired) and the work was funded by the Air Force's Ballistic Missile Office where the Project Officer was Lt. David Emary. The able assistance of both these individuals is greatly appreciated.

Successfully conducting a program of this type on such a compressed schedule would not have been possible without the willing support and advice provided by numerous individuals from DNA, AFWL, and NMERI. The authors particularly wish to thank Mr. Joe LaComb of DNA, Mr. Joe Renick of AFWL, and Dr. Leo Stockham of NMERI.

The authors also wish to thank Dr. Rey Shunk of Electromechanical Systems for his assistance and advice on gage design; Dr. Jon Collins of Acta for his advice on the statistical treatment of the passive measurement data; and Dr. Joel Sweet of our staff for performing the finite element calculations.

Conversion factors for U.S. customary to metric (SI) units of measurement.

To Convert From	To	Multiply By
angstrom	meters (m)	1.000 000 X E -10
atmosphere (normal)	kilo pascal (kPa)	1.013 25 X E +2
bar	kilo pascal (kPa)	1.000 000 X E +2
barn	meter^2 (m^2)	1.000 000 X E -28
British thermal unit (thermochemical)	joule (J)	1.054 350 X E +3
cal (thermochemical)/cm^2§	mega joule/m^2 (MJ/m^2)	4.184 000 X E -2
calorie (thermochemical)§	joule (J)	4.184 000
calorie (thermochemical)/g§	joule per kilogram (J/kg)*	4.184 000 X E +3
curie§	giga becquerel (GBq)†	3.700 000 X E +1
degree Celsius‡	degree kelvin (K)	$t_K = t°_C + 273.15$
degree (angle)	radian (rad)	1.745 329 X E -2
degree Fahrenheit	degree kelvin (K)	$t_K = (t°_F + 459.67)/1.8$
electron volt§	joule (J)	1.602 19 X E -19
erg§	joule (J)	1.000 000 X E -7
erg/second	watt (W)	1.000 000 X E -7
foot	meter (m)	3.048 000 X E -1
foot-pound-force	joule (J)	1.355 818
gallon (U.S. liquid)	meter^3 (m^3)	3.785 412 X E -3
inch	meter (m)	2.540 000 X E -2
jerk	joule (J)	1.000 000 X E +9
joule/kilogram (J/kg) (radiation dose absorbed)§	gray (Gy)*	1.000 000
kilotons§	terajoules	4.183
kip (1000 lbf)	newton (N)	4.448 222 X E +3
kip/inch^2 (ksi)	kilo pascal (kPa)	6.894 757 X E +3
ktap	newton-second/m^2 ($N-s/m^2$)	1.000 000 X E +2
micron	meter (m)	1.000 000 X E -6
mil	meter (m)	2.540 000 X E -5
mile (international)	meter (m)	1.609 344 X E +3
ounce	kilogram (kg)	2.834 952 X E -2
pound-force (lbf avoirdupois)	newton (N)	4.448 222
pound-force inch	newton-meter (N·m)	1.129 848 X E -1
pound-force/inch	newton/meter (N/m)	1.751 268 X E +2
pound-force/foot^2	kilo pascal (kPa)	4.788 026 X E -2
pound-force/inch^2 (psi)	kilo pascal (kPa)	6.894 757
pound-mass (lbm avoirdupois)	kilogram (kg)	4.535 924 X E -1
pound-mass-foot^2 (moment of inertia)	kilogram-meter^2 ($kg·m^2$)	4.214 011 X E -2
pound-mass/foot^3	kilogram-meter^3 (kg/m^3)	1.601 846 X E +1
rad (radiation dose absorbed)§	gray (Gy)*	1.000 000 X E -2
roentgen§	coulomb/kilogram (C/kg)	2.579 760 X E -4
shake	second (s)	1.000 000 X E -8
slug	kilogram (kg)	1.459 390 X E +1
torr (mm Hg, 0° C)	kilo pascal (kPa)	1.333 22 X E -1

*The gray (Gy) is the accepted SI unit equivalent to the energy imparted by ionizing radiation to a mass of energy corresponding to one joule/kilogram.
†The becquerel (Bq) is the SI unit of radioactivity; 1 Bq = 1 event/s.
‡Temperature may be reported in degree Celsius as well as degree kelvin.
§These units should not be converted in DNA technical reports; however, a parenthetical conversion is permitted at the author's discretion.

TABLE OF CONTENTS

TABLE OF CONTENTS (Concluded)

LIST OF ILLUSTRATIONS

LIST OF ILLUSTRATIONS (Continued)

LIST OF ILLUSTRATIONS (Continued)

LIST OF ILLUSTRATIONS (Continued)

LIST OF ILLUSTRATIONS (Concluded)

LIST OF TABLES

LIST OF TABLES (Concluded)

SECTION 1

INTRODUCTION

1.1 BACKGROUND

Following the release of the Scowcroft Commission report (Reference 1) in April 1983, the Air Force began the concept validation phase of a program to develop a new small ICBM with a single warhead. The development of alternative basing modes was included in the program and one of the basing mode concepts selected for development was the Hard Mobile Launcher (HML).

As part of the concept development and selection process, it was judged necessary to simulate the effects of nuclear airblast on a large scale model of the HML. One alternative for the simulation was to use an enlarged version of the Dynamic Airblast Simulator (DABS) previously developed and used by the Air Force. This simulation technique involves the use of a corrugated steel arch covered by a soil overburden. The simulator structure is destroyed during the test and, consequently, the technique has been termed the disposable DABS.

Since there was a requirement to conduct several airblast simulation tests during the HML concept validation phase, it was decided to investigate the development of a reusable large scale dynamic airblast simulator. The simulator was envisioned to be similar to a very large shock tube driven by a high explosive detonation.

This report describes a portion of our work in developing preliminary structural design concepts and conducting trade-offs among concepts on the basis of cost, schedule, and risk, for a reusable dynamic airblast simulator for use in testing HML concepts. The work not reported here will be discussed later in the

contract final report. Originally, preliminary designs were to be accomplished for a full scale simulator, followed by designs for three-quarter and one-half scale simulators. However, early in the program, we were directed to limit our investigations to one-half scale simulators.

As provided in Reference 2, the approximate simulator dimensions required to test a full scale model of the HML are 100 feet (30.48 m) wide, 50 feet (15.24 m) high (e.g., a semi-circle 100 feet (30.48 m) in diameter), and 3000 feet (914.4 m) long. Each of these dimensions is reduced by one-half for a one-half scale simulator. It was further stipulated that changes to the shape of the simulator cross section were permissible as long as the area was preserved. Reference 2 also provided for the simulator to be driven by detonating a mixture of methane and air with a maximum pressure in the driver section of 270 psi (1.86 MPa).

One of the reusable simulator concepts considered consists of a tunnel excavated into a mountain. Based on a preliminary comparison of full scale tunnel and above ground simulator concepts, we concluded that the tunnel concept appeared feasible, but that major uncertainties were associated with finding a site that would permit construction of a very large, stable opening.

Following the decision to concentrate our efforts on the one-half scale facility, we concluded that there was a high probability that such a facility could be successfully constructed in ashfall tuff at the Department of Energy's Nevada Test Site (NTS). This conclusion was based, in part, on the fact that a chamber of comparable cross section had been constructed as part of the Air Force's Deep Basing Egress Demonstration Program. This program was conducted at Little Skull Mountain, Area 25, NTS.

Several questions were raised regarding the behavior of a tunnel subjected to the effects of repeated high explosive detonations in the tunnel. There was also

speculation that major rehabilitation of the tunnel would be required following each detonation. Because of the short HML validation schedule (all testing to be completed prior to the end of fiscal year 1986), a requirement for major rehabilitation following each test would clearly make the tunnel simulator concept unacceptable. Therefore, it was decided, in March 1984, to conduct a series of tunnel response tests prior to making a decision to design and construct a one-half scale simulator. The tunnel response tests were to be completed prior to 1 July 1984.

The tunnel response test series, as originally planned, consisted of three tests. The first test was planned for a peak pressure level of approximately one-half that which would eventually be required in the HML simulator. The second test was planned for a peak pressure level approximately equal that required in the simulator. The third test was planned as a repeat of the second. Although three tests were planned, the tunnel response test program was terminated after the second test. Also, the actual test pressures (discussed later) were somewhat less than originally planned.

The two tunnel response tests were conducted in an existing tunnel with the portal located on the west face of Little Skull Mountain. The tunnel was constructed (as part of the Air Force's Egress Demonstration Program) in ashfall tuff by a tunnel boring machine. It was circular in cross section, 18 feet-seven inches (5.66 m) in diameter, and 704 feet (214.6 m) long. The depth of overburden above the tunnel varied from approximately 20 feet (6.1 m) at the portal to approximately 600 feet (182.9 m) at the face of the tunnel (Construction Station 7+04).

The cross section of the proposed one-half scale simulator was considered to be too large to be excavated economically by a tunnel boring machine and would likely

be mined with a flat invert ("horseshoe" shape). Therefore, it was decided to modify the existing circular tunnel by mining the bottom (below the springlines) with a roadheader to provide a tunnel with a "horseshoe" shape, in order to more nearly match the shape of the proposed one-half scale simulator.

Iremite was used as the explosive source for both of the tunnel response tests. In each case the length of the driver was 75 feet (22.9 m). In the first test, conducted on 1 June 1984, 30 strands of Iremite (1057 pounds (479.5 kg)) were used. The second test was conducted on 14 June 1984 and the driver section was loaded with 58 strands (2044 pounds (927.1 kg)) of Iremite. The details of the driver configurations are reported in Reference 3.

1.2 SCOPE AND OBJECTIVES

The responsibilities of Merritt CASES, Inc. (CASES) related to development of an underground reusable dynamic airblast simulator included:

a. Performing preliminary analyses of tunnel behavior.

b. Participating in planning for tunnel response tests.

c. Making active and passive rock deformation measurements.

d. Analyzing and evaluating the results of the tunnel response tests.

e. Predicting the behavior of a one-half scale underground simulator.[1]

Our work in these areas is described in this report, with primary emphasis on the tunnel response tests at Little Skull Mountain.

---

[1]This last area of responsibility was eliminated when it was decided, following the second tunnel response test, not to pursue the underground reusable simulator concept further during the HML Validation Phase.

The overall objective of the tunnel response test program was to evaluate the behavior of a tunnel subjected to repeated high explosive detonations and to the resulting airblast waves propagating along the tunnel. The specific objective of the rock deformation measurements made by CASES was to obtain data which could be used to confirm or calibrate our calculational techniques for subsequent use during the design of a one-half scale underground reusable dynamic airblast simulator.

The New Mexico Engineering Research Institute (NMERI) was responsible for designing, loading, and arming the explosive charges. They also made static pressure, stagnation pressure, and temperature measurements (Reference 3).

Design and construction of the required tunnel modifications, as well as general support to experimenters were provided by DNA Field Command, through various contractors. They also provided instrumentation cables, data recording, and overall management of the tunnel response tests.

1.3 REPORT ORGANIZATION

Preliminary design investigations for a one-half scale underground simulator and planning for a series of tunnel response tests are described in Section 2. Details of the design, fabrication, installation and recording of dynamic relative displacement gages are included in Section 3. In Section 4, the equipment and procedures used to make residual rock deformation measurements are described. Sections 5 and 6 present active and passive measurement data and some concluding remarks are provided in Section 7.

SECTION 2

PRELIMINARY DESIGN INVESTIGATIONS FOR UNDERGROUND REUSABLE DYNAMIC AIRBLAST SIMULATOR

2.1 PRELIMINARY ANALYSES OF ONE-HALF SCALE SIMULATOR

As stated in Section 1, siting an underground simulator in ashfall tuff at NTS appeared feasible, once the decision was made to limit simulation size to one-half scale. Consequently, we performed a series of preliminary two dimensional finite element calculations to predict the behavior of such a simulator. All finite element calculations described in this and subsequent sections were done using the SATURN code (Reference 4).

The preliminary analyses were done assuming the one-half scale simulator would be sited at Little Skull Mountain. The tuff material properties used in the calculations are shown in Table 2-1. These properties are based on data obtained during the Air Force's Deep Basing Egress Demonstration Program (Reference 5). Somewhat different properties were used for the static overburden portion of the analysis to more accurately reproduce the gravity stress field. This was accomplished by changing Poissons ratio and the shear modulus, while keeping the bulk modulus the same. Also shown in Table 2-1 is the Drucker-Prager yield condition used in these calculations. The tunnel was assumed to be 45 feet (13.7 m) wide and 30 feet (9.1 m) high (a 45 foot (13.7 m) semicircle over a 45 by 7.5 foot (13.7 by 2.3 m) rectangle). Static overpressure-time histories for use in the calculations were provided by the Air Force Weapons Laboratory. The assumed pressure loadings are shown in Figure 2-1. In each case, the pressure at each time step was assumed to be applied uniformly around the perimeter of the tunnel. In one case, representing the driver section, the depth of rock above the back of the

Table 2-1. Assumed Little Skull Mountain material properties used in finite element calculations.

DYNAMIC	STATIC
G = 100,000 psi	G = 50,000 psi
E = 240,000 psi	E = 133,333 psi
K = 133,333 psi	K = 133,333 psi
ν = 0.2	ν = 1/3
C = 200 psi	C = 200 psi
ϕ = 33°	ϕ = 33°

FAILURE MODEL

Drucker-Prager Yield Condition

$$\sqrt{J_2'} = \tau_o + \alpha \frac{\sigma_{KK}}{3}$$

α = 0.768; τ_o = 237 psi

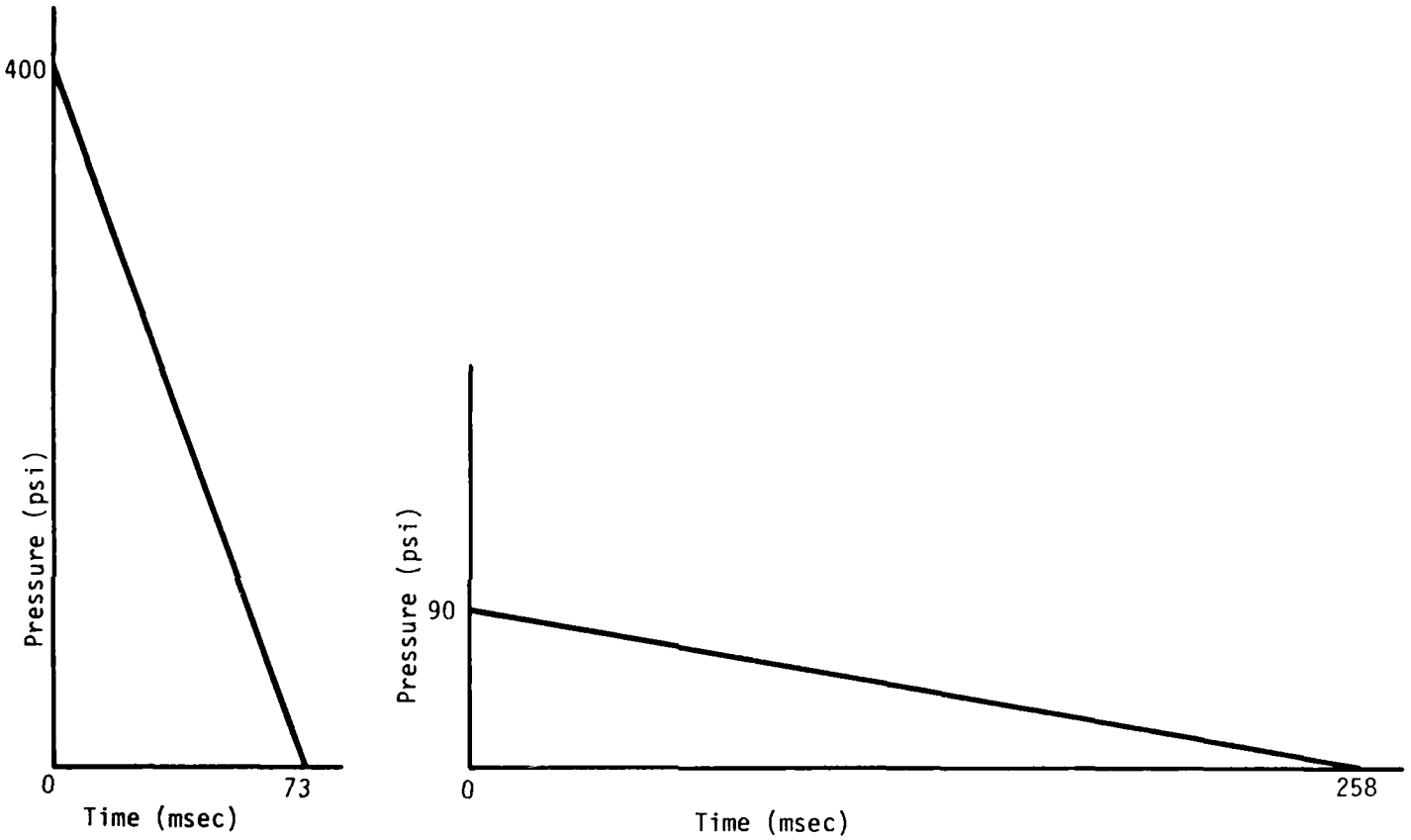

a. Driver section loading.

b. Runout section loading.

Figure 2-1. Assumed pressure loading for preliminary analyses of one-half scale underground simulator.

tunnel was assumed to be 570 feet (173.7 m). The finite element grid is shown in Figure 2-2. This section was loaded with the 400 psi (2.76 MPa) triangular pulse shown in Figure 2-1a. In the other case, representing the runout section near the portal, the depth of rock above the back of the tunnel was assumed to be 20 feet (6.1 m). The finite element grid is shown in Figure 2-3. This tunnel section was loaded with the 90 psi (0.62 MPa) triangular pulse shown in Figure 2-1b.

Two separate calculations were performed at each location. The first was a static calculation with overburden stresses determined by applying the appropriate gravity load to each element of the grid (equivalent to assuming lithostatic stress varies linearly with depth). For the second calculation, gravity loads were removed and the tunnel was loaded dynamically with the appropriate pressure-time pulse from Figure 2-1. Calculational output included stresses, strains, and displacements at selected elements around the tunnel. Element locations for which output was recorded are shown in Figure 2-4.

Selected results of the preliminary calculations are shown in Figure 2-5 through 2-8. In each case, compressive stresses are shown as positive. The dynamic tangential stress-time responses for the driver section (400 psi (2.76 MPa) peak pressure and 570 feet (173.7 m) of overburden) are shown in Figure 2-5. In this figure and those which follow, the responses for the crown, springline, and wall locations are shown in the "a" part of the figure. The response at the wall location is repeated and the responses of the floor and invert locations are shown in the "b" part of the figure. It should be noted that, except for the invert, tensile stresses occur in the absence of the lithostatic stresses.

In Figure 2-6 the superposition of the dynamic stresses from Figure 2-5 and the static tangential stresses is shown. The static overburden stresses are sufficient to prevent any tensile tangential stresses from occurring.

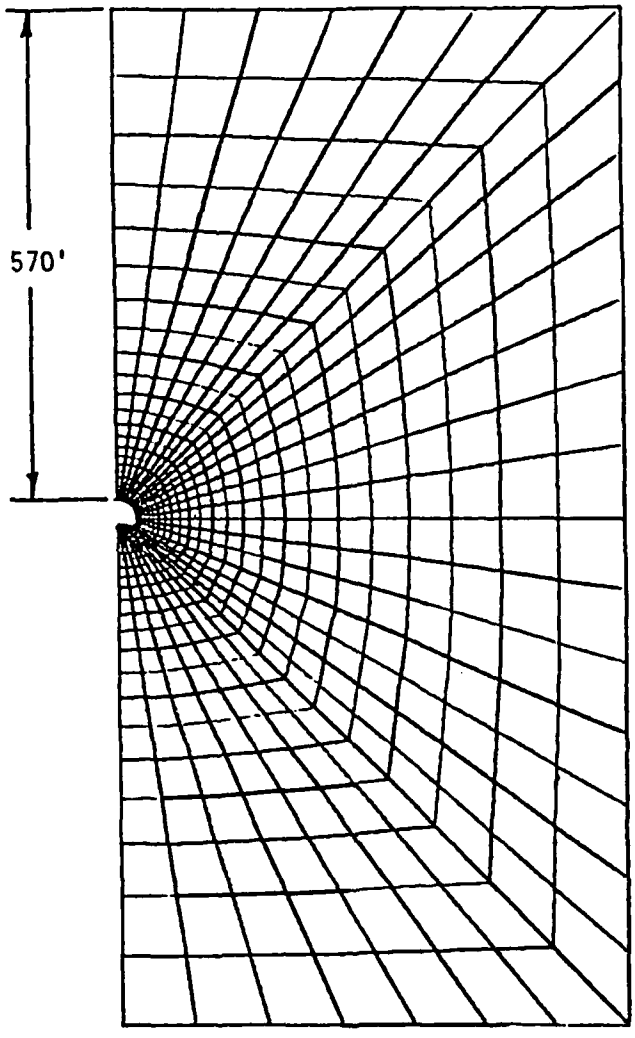

Figure 2-2. Finite element grid for tunnel with 570 feet of overburden, 400 psi peak pressure.

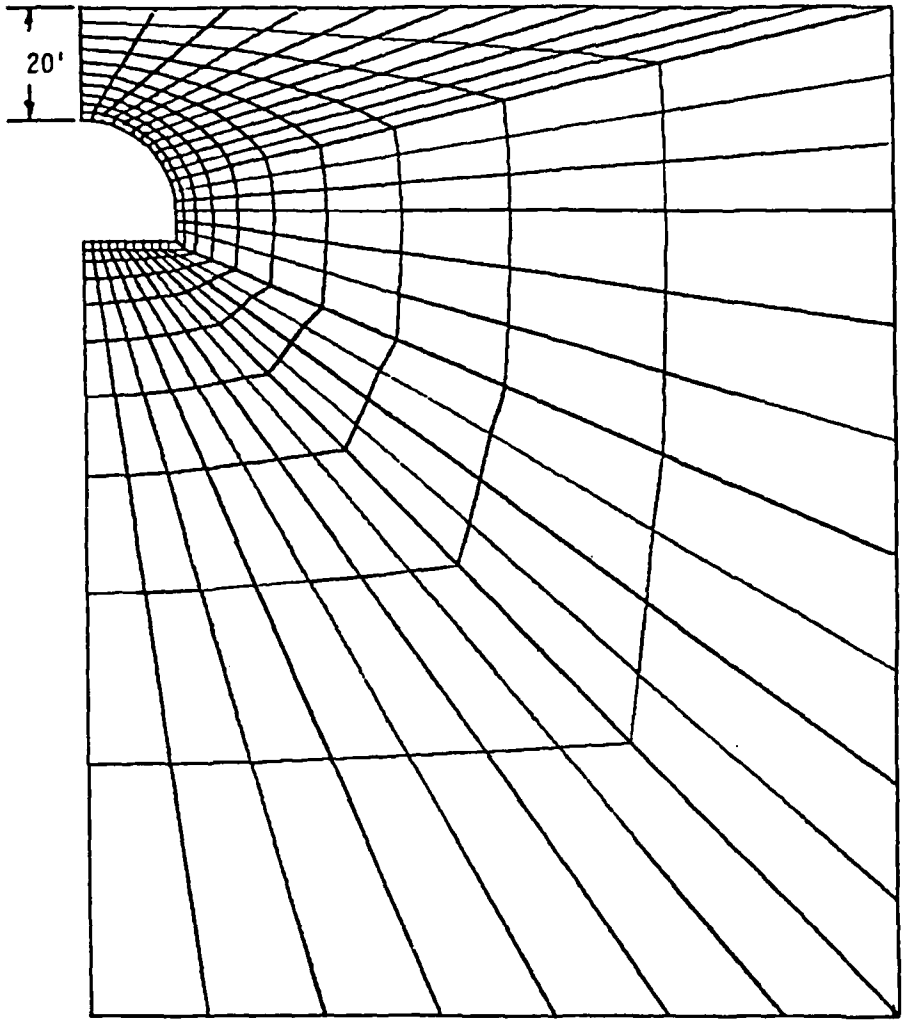

Figure 2-3. Finite element grid for tunnel with 20 feet of overburden, 90 psi peak pressure.

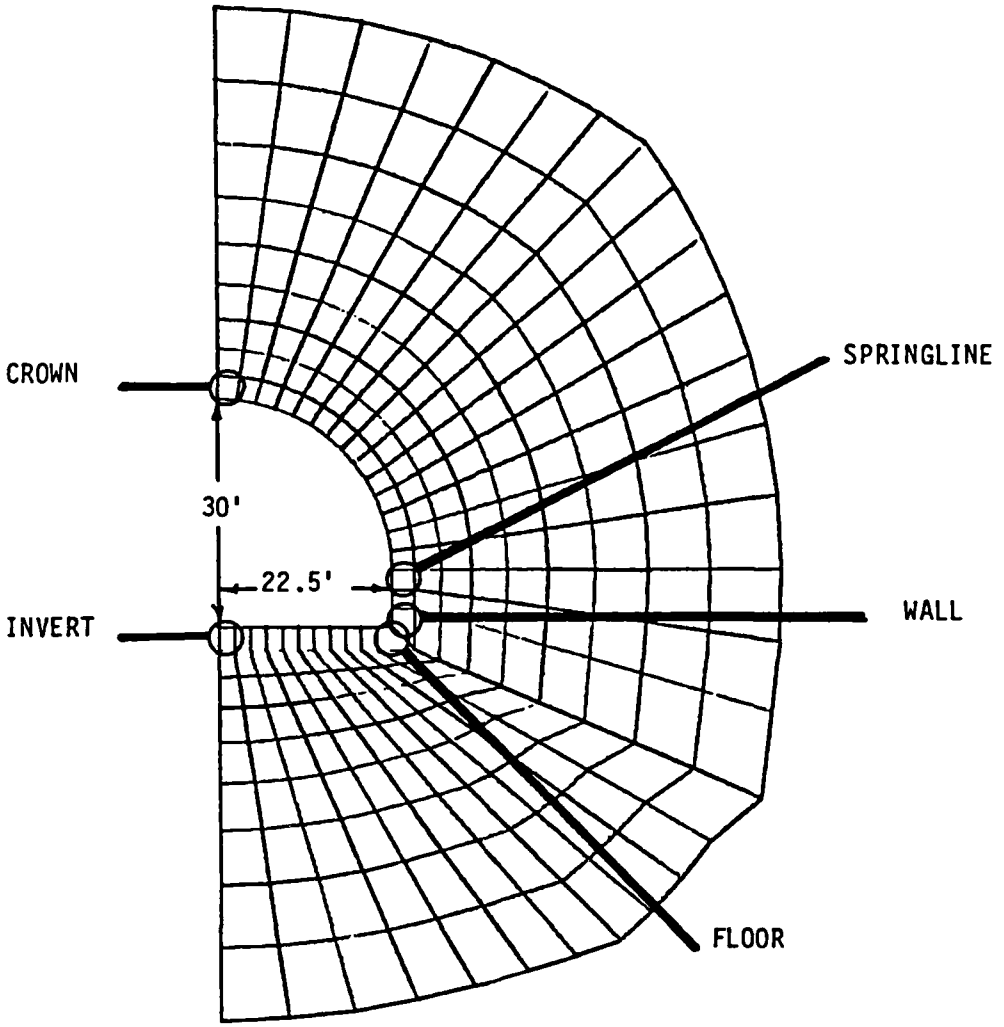

Figure 2-4. Detail of finite element grid near the tunnel with computer output locations identified.

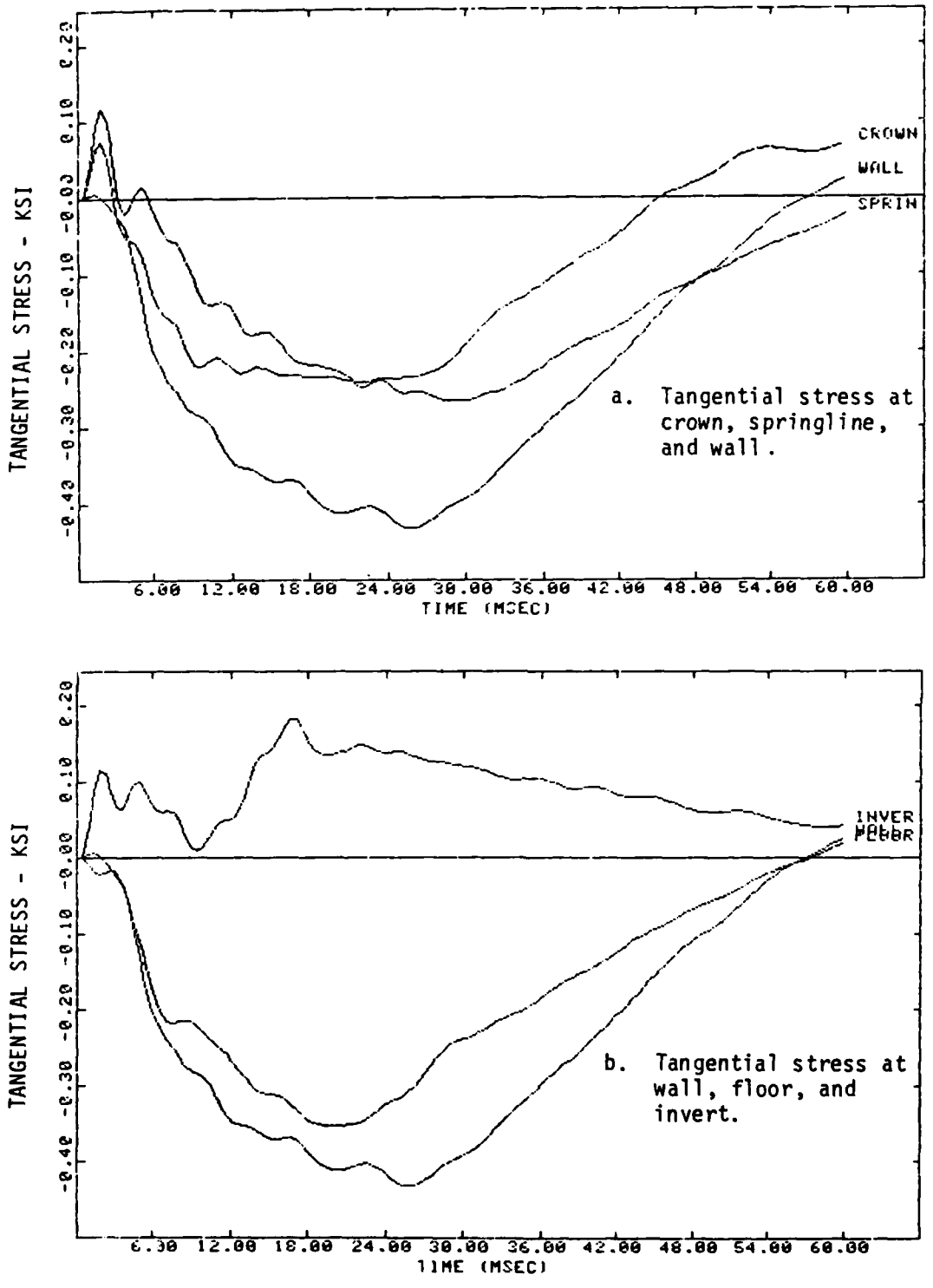

Figure 2-5. Dynamic tangential stress, 400 psi peak pressure, 570 feet of overburden.

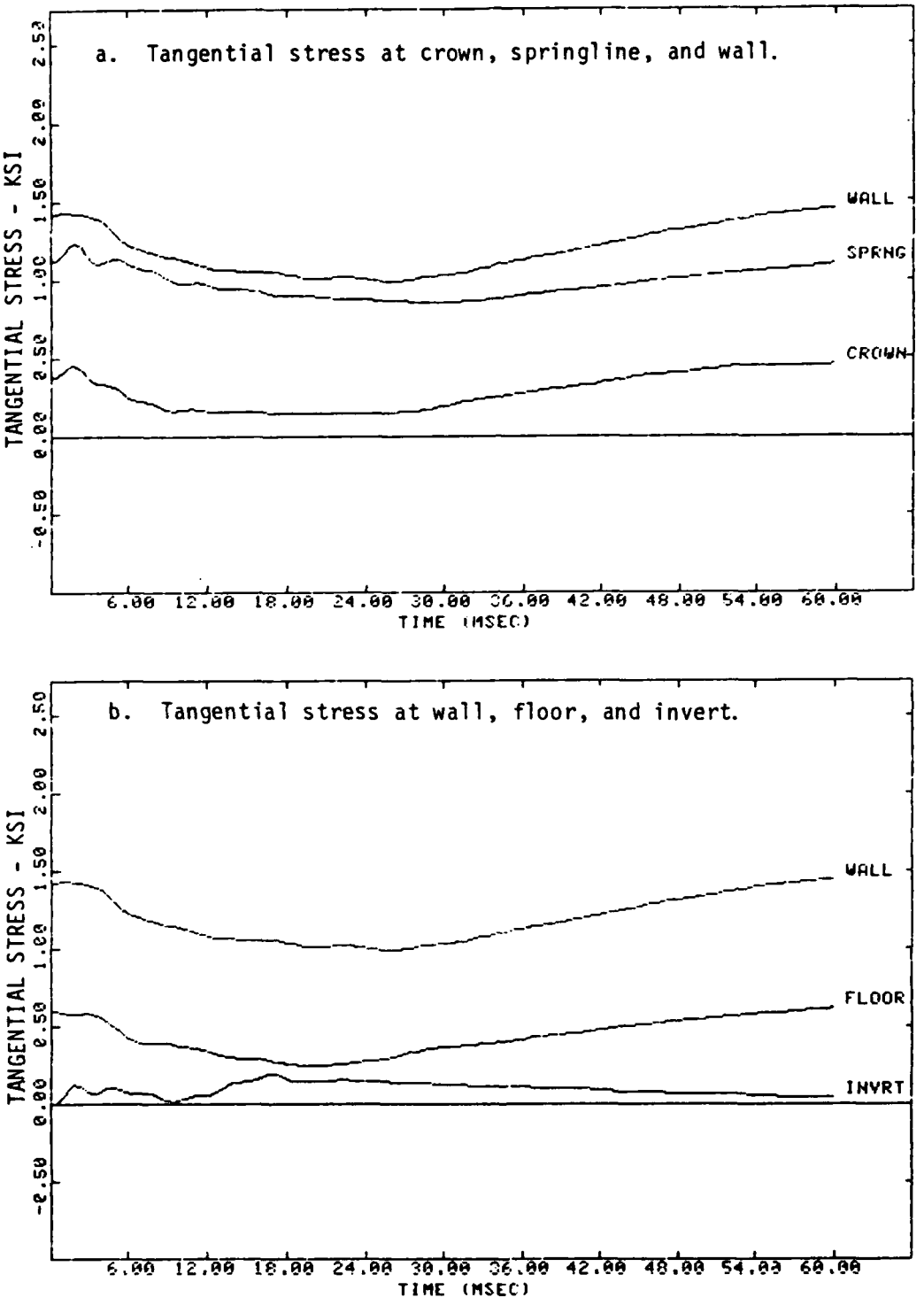

Figure 2-6. Superposition of static and dynamic tangential stress, 400 psi peak pressure, 570 feet of overburden.

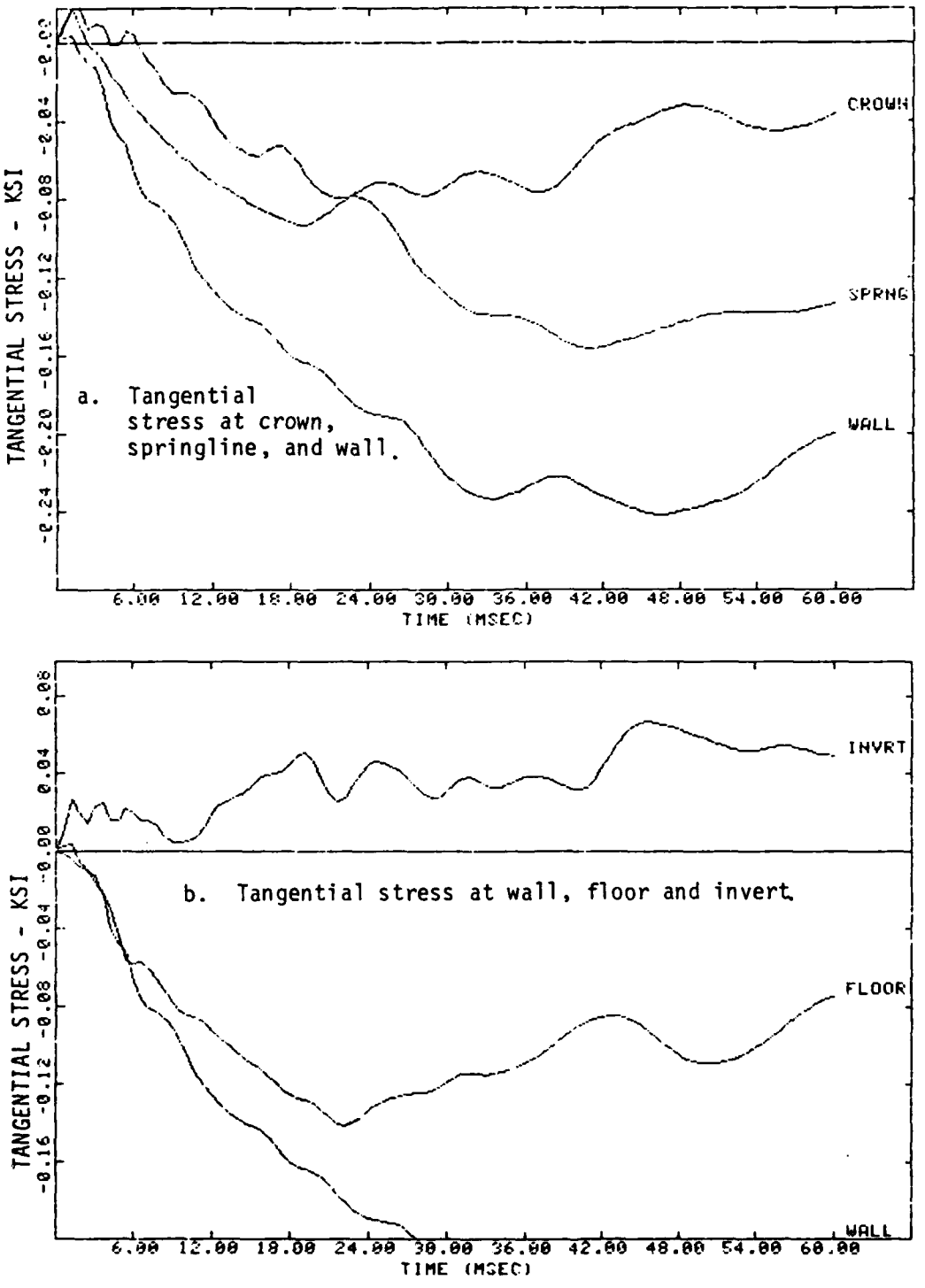

Figure 2-7. Dynamic tangential stress, 90 psi peak stress, 20 feet of overburden.

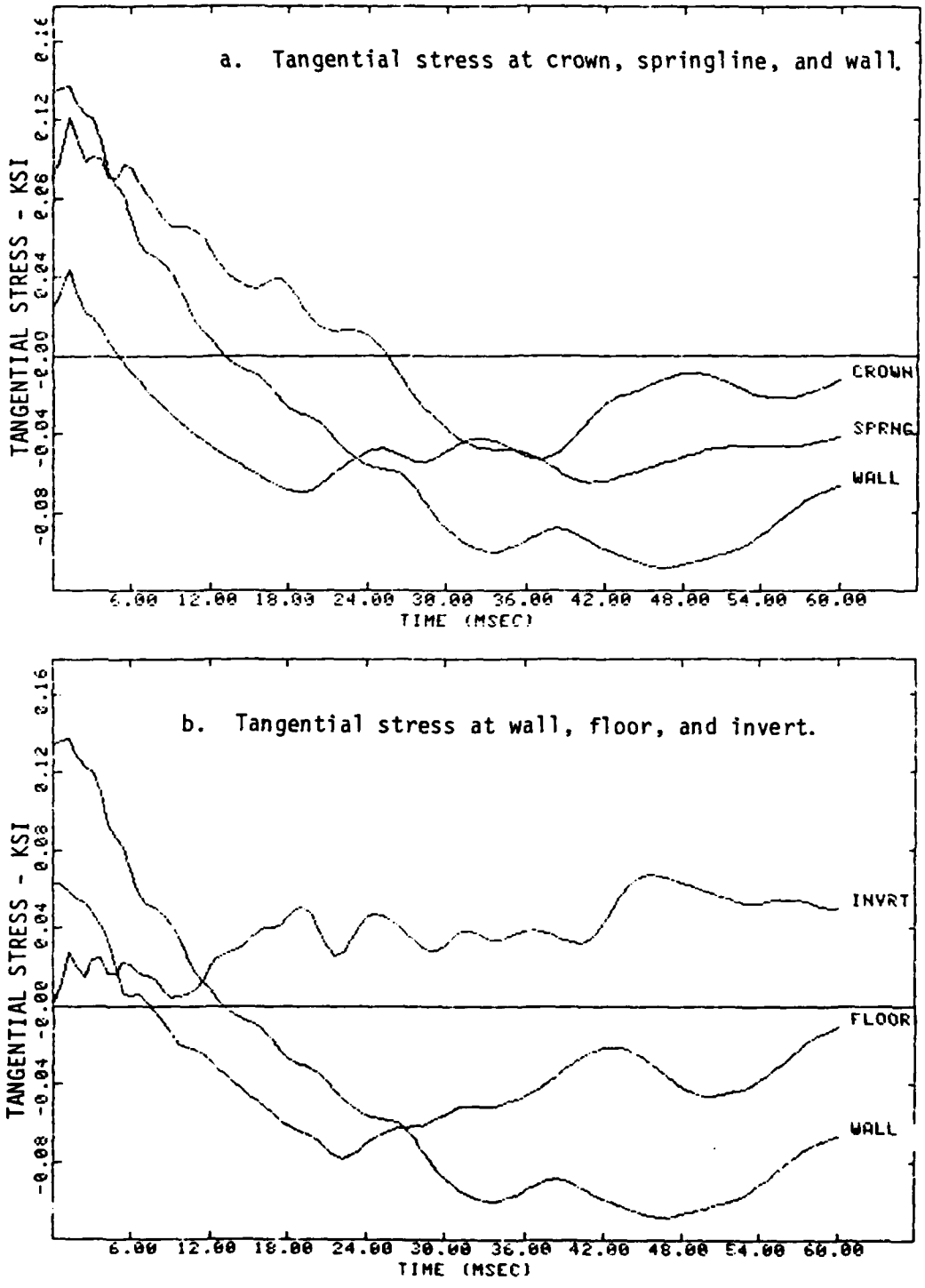

Figure 2-8. Superposition of static and dynamic tangential stress, 90 psi peak pressure, 20 feet of overburden.

The dynamic tangential stress-time responses for the runout section (90 psi (0.62 MPa) peak pressure and 20 feet (6.1 m) of overburden) are shown in Figure 2-7. Again, tensile stresses occur in the absence of the lithostatic stresses. However, in this case, when the dynamic and static stresses are combined by superposition (Figure 2-8), it is apparent that the static compressive stresses due to 20 feet (6.1 m) of overburden are not sufficient to prevent tensile stresses from occurring.

As noted above, the pressure loadings shown in Figure 2-1 were provided by the Air Force Weapons Laboratory. These pressure pulses had been developed earlier for use in preparing preliminary designs of an above ground reusable simulator. The 90 psi (0.62 MPa) peak pressure (based on preliminary calculations by S-Cubed) was intended to approximate the effects of non-uniform pressure distribution on the above ground simulator structure at the test section where the desired peak pressure should not exceed 60 psi (0.41 MPa). Consequently, 90 psi (0.62 MPa) is probably substantially higher than the actual loading which would occur near the portal of a tunnel simulator.

Following completion of the series of preliminary calculations described above, we again discussed pressure loadings with personnel of the Air Force Weapons Laboratory and it was agreed that a pressure pulse with 50 psi (0.34 MPa) peak and a duration of 100 milliseconds was a more realistic estimate of the loading which might be expected near the portal. This pulse was used in the next series of calculations described below. It was also agreed that the next series of calculations would model the existing tunnel (described in Section 1) at Little Skull Mountain, which had been selected for the tunnel response tests. A portion of the finite element mesh is shown in Figure 2-9.

In addition to refining the estimate of pressure loading near the portal, we concluded it was necessary to improve the accuracy of modeling the rock response.

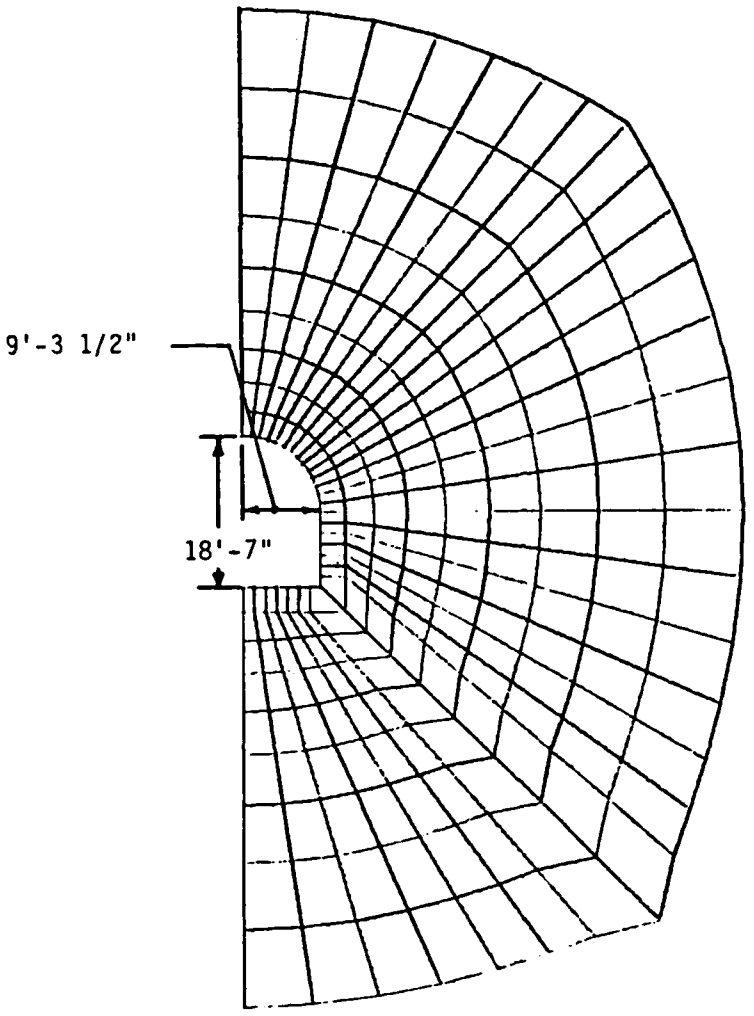

Figure 2-9. Partial finite element mesh for tunnel response test geometry.

The approach taken was to perform a static calculation to estimate the in situ (gravitational) stresses and then use this state of stress as the initial condition for the dynamic calculation.

The in situ stress determination was composed of two distinct calculational phases. Starting with the finite element mesh containing the tunnel opening, the gravitational stresses were determined as if the tunnel was not present. This was accomplished by applying forces, along the inner surface of the tunnel opening, whose magnitudes were chosen so as to prevent horizontal deformation, in addition to applying nodal forces which represent the gravity loading. The next step was to simulate the construction of the tunnel opening. This was done by reducing the inner surface forces incrementally until they reached zero. At this point, the state of stress in the finite element mesh was predicted for the continuum containing the tunnel opening.

The application of the internal dynamic pressure has the tendency to form tensile stresses tangent to the inner surface of the tunnel. These dynamic stress components were combined with the static in situ stress components to determine if tensile failure could occur. The tensile failure model utilized for this study is very similar to the model previously documented in Reference 6. For this model, tensile failure occurs according to the behavior of the principal stress components. The calculational procedure is as follows: (a) the dynamic state of stress is first assumed to be elastic and the stress tensor is determined, (b) the principal stresses are then determined from the X-Y components, (c) if any of these stresses exceed the tensile strength for an uncracked state or zero for a previously cracked state, an inelastic tensile strain component is introduced to make this principal stress zero, and (d) the resulting state of stress is then compared to the plasticity failure surface for further modification. Once an element has failed in

tension, further loading adds to the accumulated tensile (porosity) strain. Future loading can decrease this strain if the loading has a compressive tendency. Once this strain reduces to zero the element is considered "healed" with a zero tensile strength and compressive stresses can accumulate.

To determine the effect of tensile cracking on tunnel response, we performed a series of calculations using the approach described above. The finite element grid shown in Figure 2-9 and the revised loading pulse (50 psi (0.34 MPa) peak pressure and 100 milliseconds duration) described earlier were used. Tangential, normal, and shear stresses at the crown (back) of the tunnel are shown in Figure 2-10 for two cases. In the first case (Figure 2-10a), tensile failure was not allowed, i.e., the tensile strength of the rock was not limited. In the second case (plotted to an expanded time scale in Figure 2-10b), the rock was assumed to fail in tension under any principal tensile stress, i.e., the tensile strength was conservatively assumed to be zero. In each case the applied internal pressure is superimposed as a straight line on the stress plot.

Two significant differences in behavior are discernible in Figure 2-10. For the case of no tensile failure, the tangential stress is initially compressive but "unloads" rapidly to a significant tensile stress before returning to a net compressive stress. In the case where tensile failure is allowed, however, significant tensile stresses are precluded from developing because tensile cracks form. As a result, the residual compression is reduced significantly. Small tensile tangential stresses may be seen in Figure 2-10b. This is attributed to the fact that the tensile failure model described above introduces a tensile strain component to make the principal stress zero. Theoretically, the tangential stress at the crown is a principal stress and should be zero in this case. However, the stresses shown in Figure 2-10b are computed at the center of the element next to the

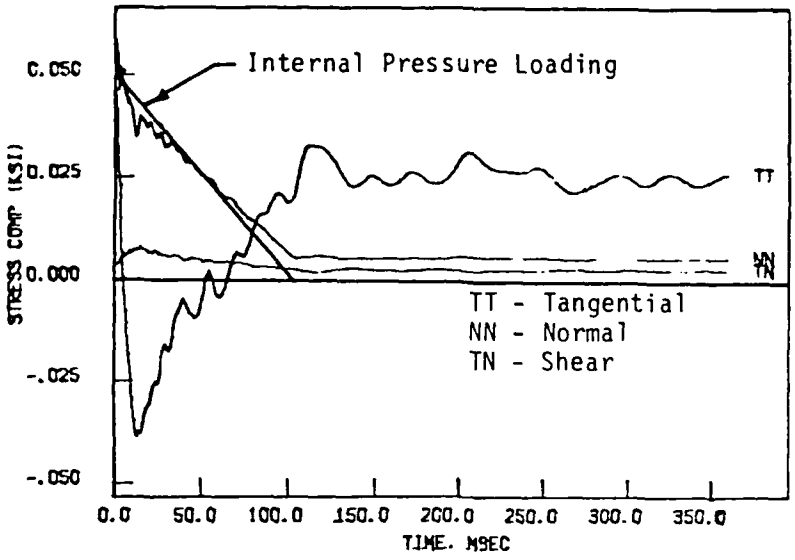

a. Tensile failure not allowed.

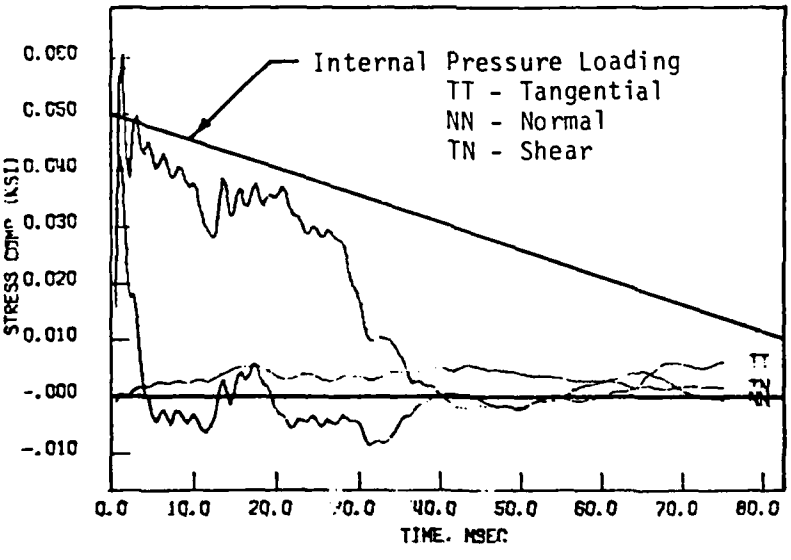

b. Tensile failure allowed.

Figure 2-10. Stresses at crown, 50 psi peak pressure, 20 feet of overburden.

plane of symmetry (e.g., see Figure 2-4). Consequently, the tangential stress is not a principal stress, as may be seen by the fact that the shear stress is not zero, and exhibits a small tensile value.

The other aspect of differing behavior is seen in the normal or radial stress. In Figure 2-10a, as expected, the normal stress follows the applied pressure very closely. The minor difference is due to the reflected wave from the surface (20 feet (6.1 m) above the crown) which reaches the tunnel at about 13 milliseconds. In the case where tensile failure is allowed (Figure 2-10b), the normal stress reduces more rapidly than the internal pressure, beginning at about the time cracking begins. This is due to the fact that enough elements have cracked to reduce the strength of the rock essentially to zero, with the result that the resistance is provided only by inertia. The corresponding vertical displacements at the crown are shown in Figure 2-11. The peak displacement is substantially greater and the decay is much less rapid in the case where tensile failure is allowed. Also, the rise time to peak displacement is somewhat longer.

The extent of tensile cracking at 26 milliseconds is shown by the elements marked with crosses in Figure 2-12. This corresponds to the time of peak vertical displacement shown in Figure 2-11b. Although tensile cracking occurs near the springline, it does not appear to have a significant effect on the computed stresses at this location. Nearly identical behavior is observed with or without tensile failure in the springline stress history plots shown in Figure 2-13.

The effects of tensile cracking could be significant under certain combinations of internal pressure and overburden. Therefore, the approaches to modeling both gravitational stresses and tensile failure described above were included in all subsequent calculations, regardless of the depth of overburden.

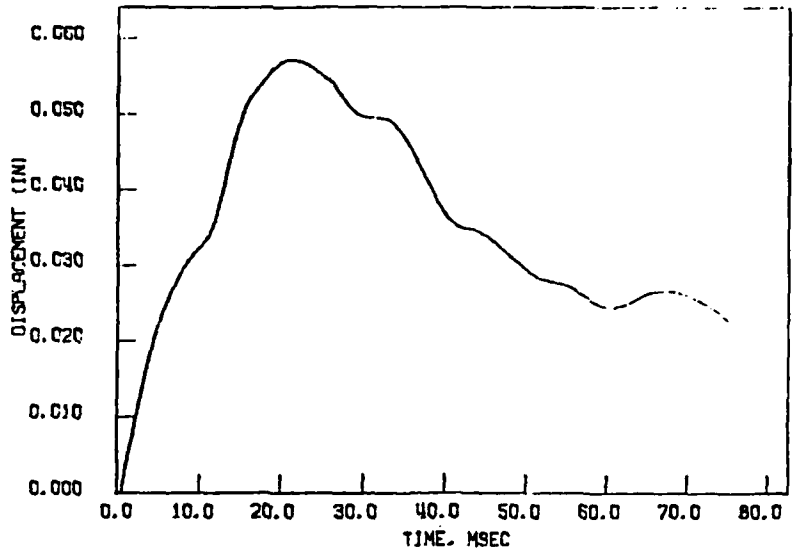

a. Tensile failure not allowed.

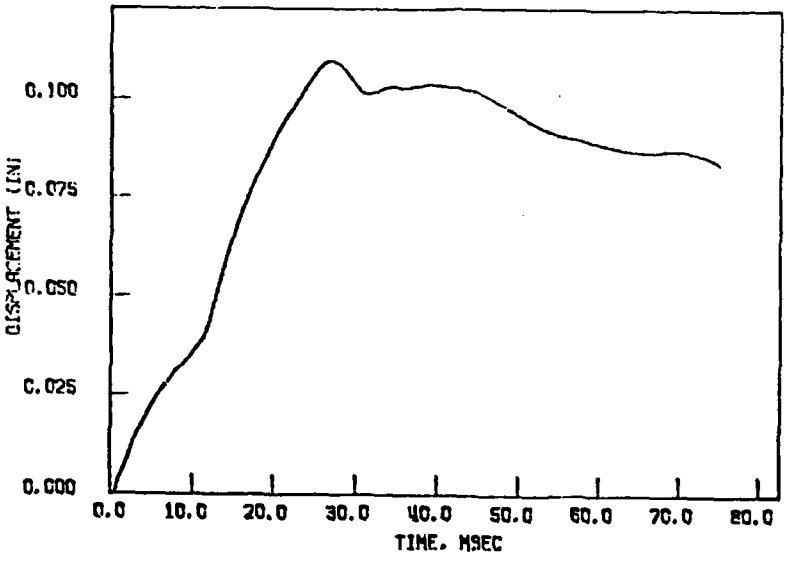

b. Tensile failure allowed.

Figure 2-11. Vertical displacements at crown, 50 psi peak pressure, 20 feet of overburden.

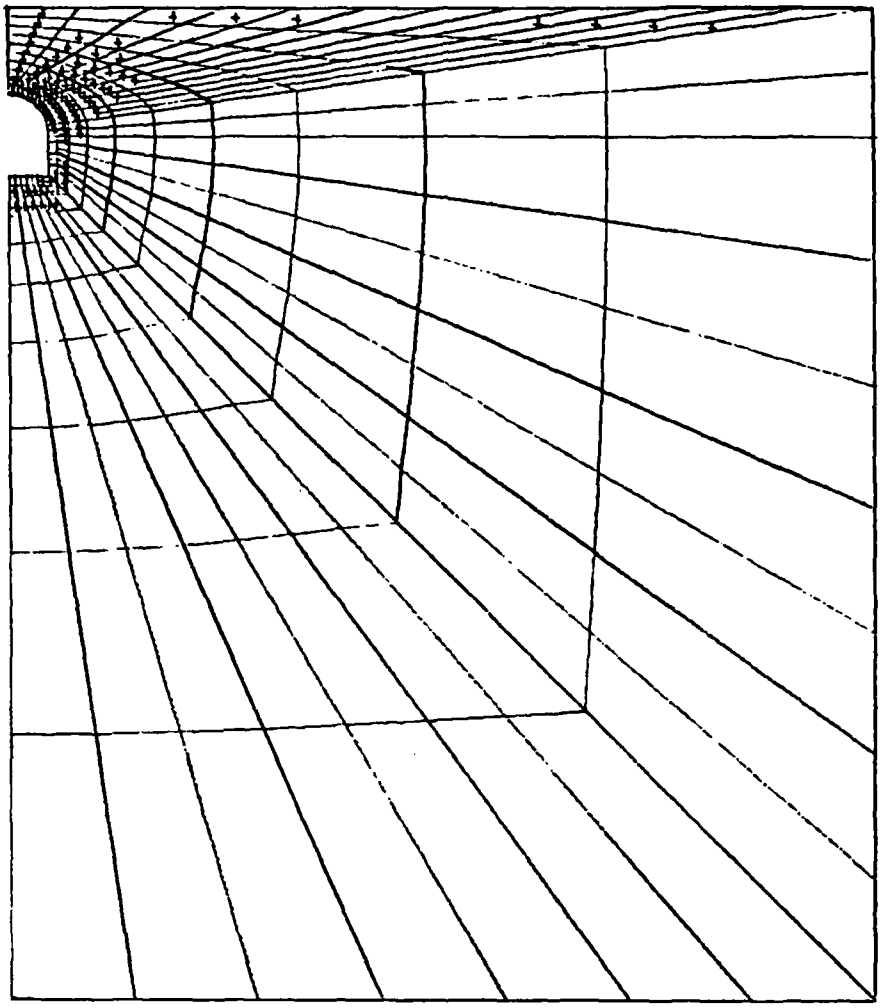

Figure 2-12. Tensile cracking at 26 milliseconds, 50 psi peak pressure, 20 feet of overburden.

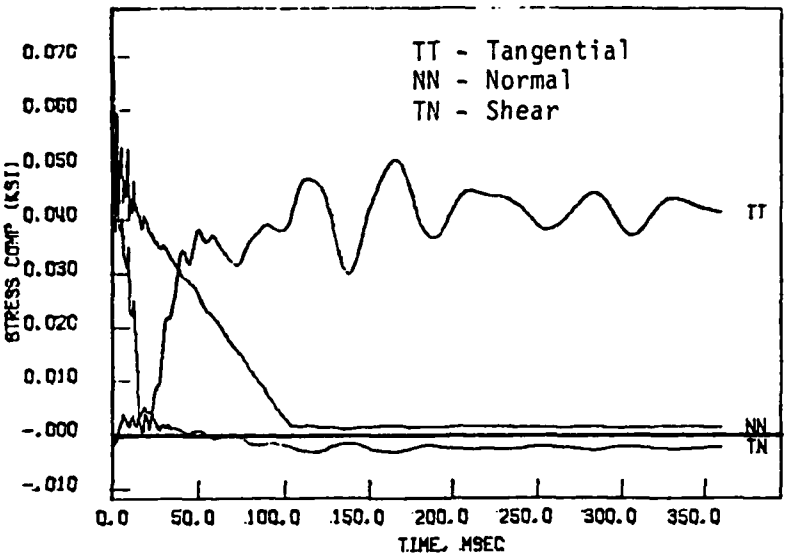

a. Tensile failure not allowed.

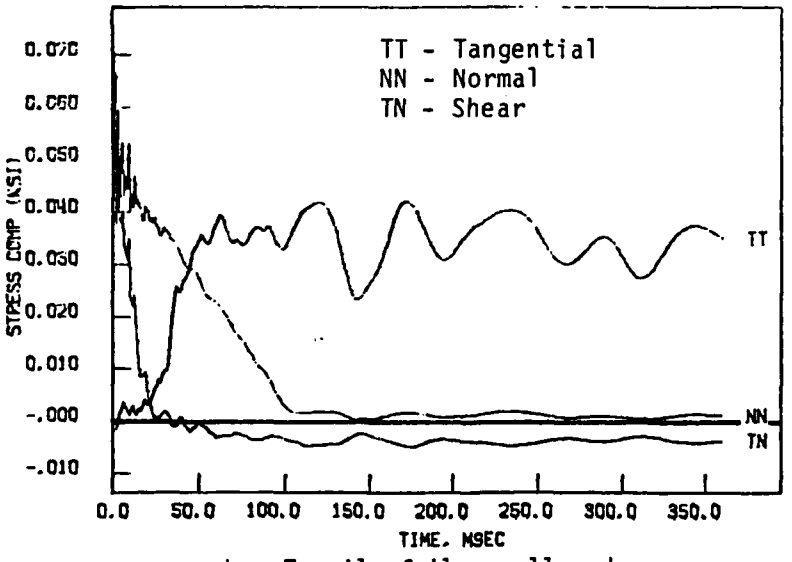

b. Tensile failure allowed.

Figure 2-13. Stresses at springline, 50 psi peak pressure, 20 feet of overburden.

2.2 ROCK DEFORMATION MEASUREMENTS

2.2.1 Measurement Objectives

Early in the tunnel response test program it was agreed that both active and passive measurements of rock deformation should be made at selected locations in the tunnel. The primary objective of the active measurements was to obtain displacement-time histories which could be used to confirm or calibrate our finite element calculations of tunnel response for later use in designing a one-half scale underground simulator and in predicting its behavior.

The primary objective of the passive measurements was to supplement the active data by providing detailed residual tangential and "diametral" rock strain measurements of the tunnel cross-section in the event significant (general or local) inelastic behavior occurred. The passive measurements also aid in interpreting active gage behavior, allowing a comparison between active residual and passive measurements. Residual rock strains and displacements were expected to be very small, as described later. It was recognized that these strains and displacements might be smaller than the expected accuracy of the measurement technique if the tunnel exhibited essentially elastic behavior.

General descriptions of the active and passive measurement techniques are provided in the following two subsections. Details of the techniques and the measurement results are discussed in subsequent sections.

2.2.2 Active Measurements

We investigated several potential methods for measuring dynamic behavior of the tunnel, including stress, acceleration, velocity, and displacement. Because the ground shock environment was expected to be relatively benign (e.g., peak stresses

on the order of 400 psi (2.76 MPa) or less), we concluded that displacement measurements offered the best prospect for obtaining data which would be useful in confirming or calibrating our calculational techniques.

Basically, the displacement gage developed for this program consists of a borehole extensometer which employs a linear variable differential transformer (LVDT) as a transducer. Conceptually, the gage is similar to the gage used to measure soil strains during Phase II of the MISERS BLUFF program (Reference 7), but with a very much longer gage length and different end anchors.

Static measurements of rock displacements using extensometers have been made for many years. To the best of our knowledge, dynamic displacement measurements of the type made during the tunnel response tests had not previously been attempted. Extensometers used for measuring static displacements are normally emplaced with the sensing element located outside the borehole for convenience in recording the displacements periodically. Such an emplacement concept was not considered viable for the tunnel response test measurements because the airblast was expected to destroy any portion of the gage which protruded into the tunnel. It was concluded that the entire gage, including the signal cables, must be recessed into the rock.

The gage may be configured with the LVDT located at either end of the borehole. These two configurations are shown schematically in Figure 2-14. As shown in the figure, each end of the gage is anchored to the rock surrounding the borehole at that point and measures the relative displacement of the rock over the gage length. Although not shown in the figure, the borehole must be plugged at the collar to prevent the airblast wave and explosive products from entering the borehole. Since pressure is applied to the rock at the left side of the figure, the left end of the gage moves first in each case. For the configuration shown in Figure 2-14a, the LVDT core (rigidly attached to the extensometer rod) moves through the body of the

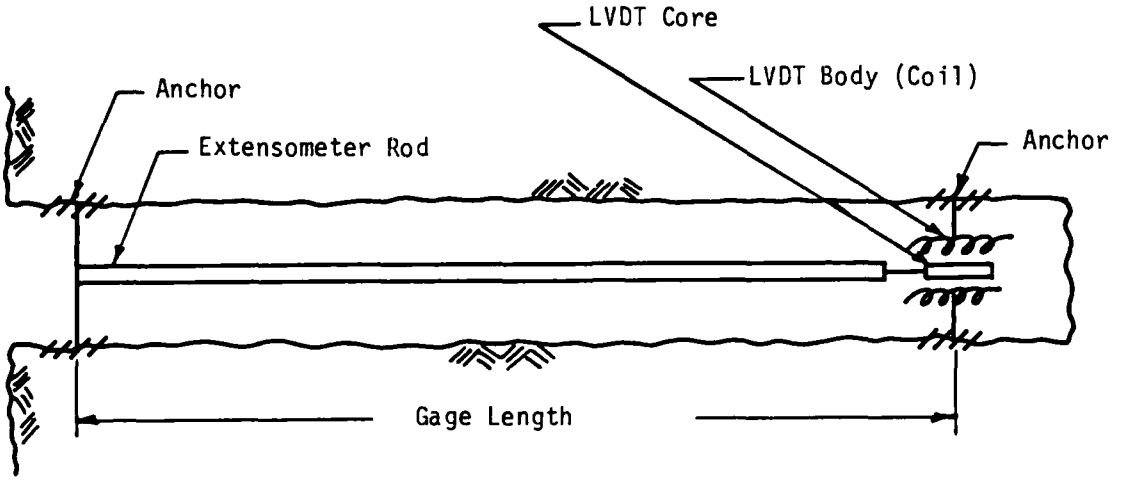

a. Gage configured with transducer at far end of borehole.

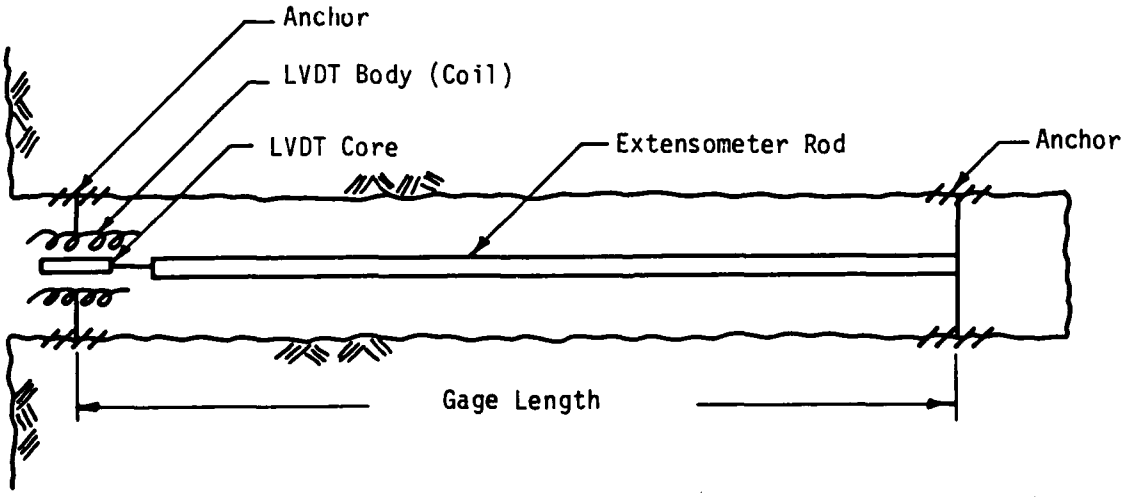

b. Gage configured with transducer near collar of borehole.

Figure 2-14. Schematic representation of dynamic relative displacement gage.

LVDT. For the other configuration (Figure 2-14b), the body of the LVDT begins to move first, while the core remains stationary.

Each of these configurations was judged to have at least one distinct advantage. The configuration shown in Figure 2-14a has the transducer located at the "far end" of the borehole and thus separated from the explosive products and airblast environment in the tunnel by a significant distance. Prior to the tunnel response tests, we believed that this would significantly increase the probability of the gages surviving the three planned tests. Therefore, 20 of the 24 gages were installed in this configuration.

The configuration shown in Figure 2-14b has the transducer located near the collar of the borehole. In this case, as noted above, the body of the LVDT is the first part of the gage to begin moving. This prevents exciting a longitudinal vibration in the extensometer rod (at least until the far end of the gage begins to move) as can happen with the gage configured as shown in Figure 2-14a. This phenomenon is discussed in detail along with the discussion of active measurement results in Section 5. Four gages were installed in the configuration shown in Figure 2-14b.

The dynamic rock displacement gage is inherently a relative displacement gage and, as noted above, measures the relative displacement of the rock between the two end anchors. Of course, it is possible for certain combinations of gage length and ground shock propagation velocity to reach at least the peak absolute displacement of one end of the gage (in this case the tunnel wall) before the other end of the gage begins to move. Ideally, the length of the gage should be sufficient to avoid any motion of the far end. However, there are practical limits to borehole lengths which can be provided.

Based on one of our preliminary calculations of the response of a one-half scale tunnel, we concluded that for the tunnel response tests, a gage length of four tunnel radii (borehole approximately 40 feet (12.2 m) long) should be adequate to obtain a measurement of the peak displacement of the tunnel surface. For this calculation, we used the material properties shown in Table 2-1, the 400 psi (2.76 MPa) pressure-time pulse shown in Figure 2-1a, the finite element grid shown in Figure 2-2, and the approach to modeling gravitational and tensile stresses described above.

Typical calculated rock displacements at various points are shown in Figure 2-15. Vertical displacements along a vertical line through the crown (at the tunnel surface and at one, two, three, and four radii from the tunnel surface) are shown in Figure 2-15a. Horizontal displacements along a horizontal line through the springline are shown in Figure 2-15b. It is apparent from Figure 2-15 that in order for the peak displacement of the tunnel surface to occur before the far end of the extensometer begins to move, the far end must be more than three radii from the tunnel surface; hence, the conclusion that the extensometer should have a length of four tunnel radii.

As discussed above, the transducer will actually measure the relative displacement which occurs between the ends of the gage. These relative displacements have been computed (always assuming one end of the gage is fixed at the tunnel surface) from the data plotted in Figure 2-15 and are shown in Figure 2-16. As an example, the difference between the curves labeled zero and 4R in Figure 2-15a is plotted as the curve labeled 4R in Figure 2-16a. A comparison of Figure 2-15a with Figure 2-16a indicates that the calculated absolute displacements of the tunnel surface at the crown are identical with the calculated tunnel surface displacements relative to a point four tunnel radii above the crown to a time of

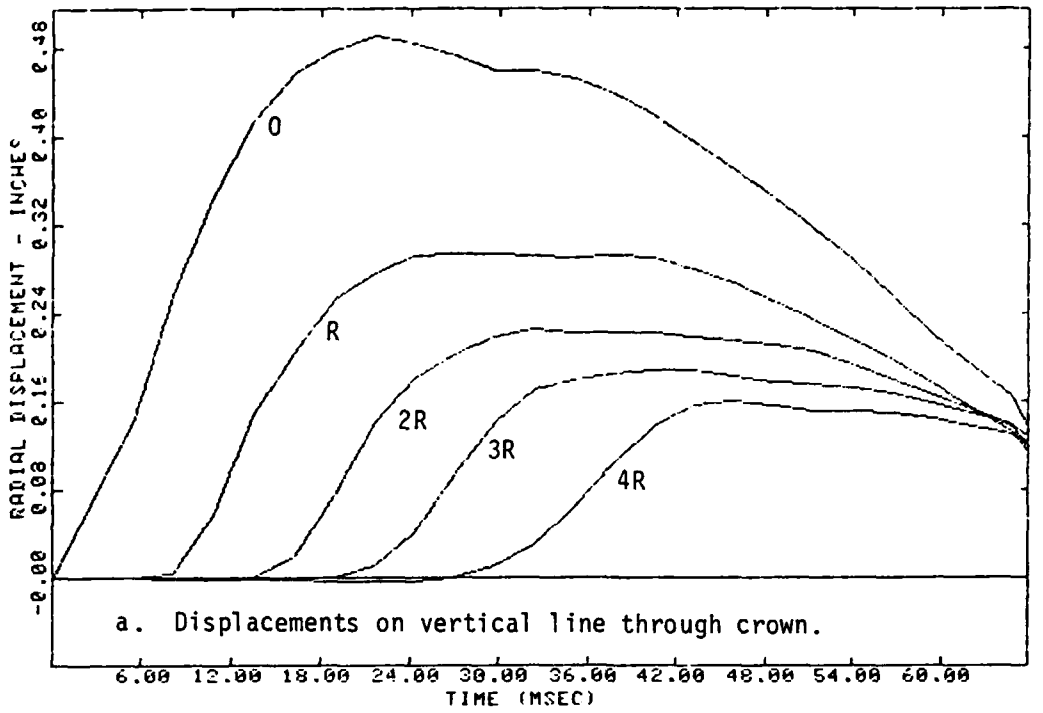

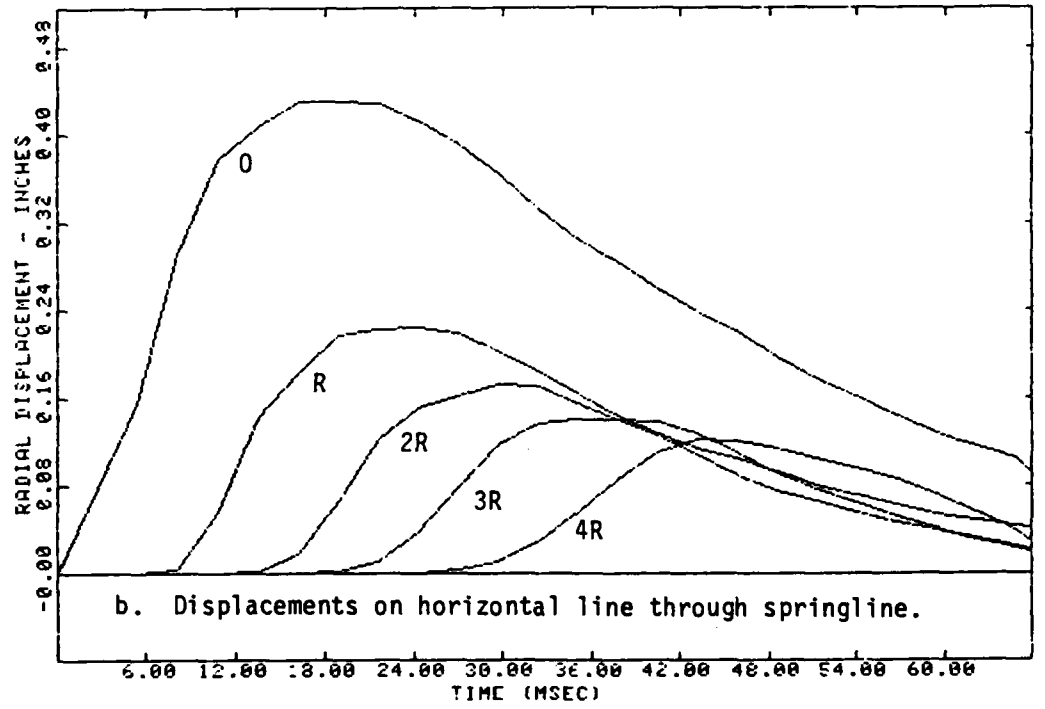

Figure 2-15. Calculated rock displacements at various points. Location of points indicated as multiples of tunnel radius (R) from tunnel surface.

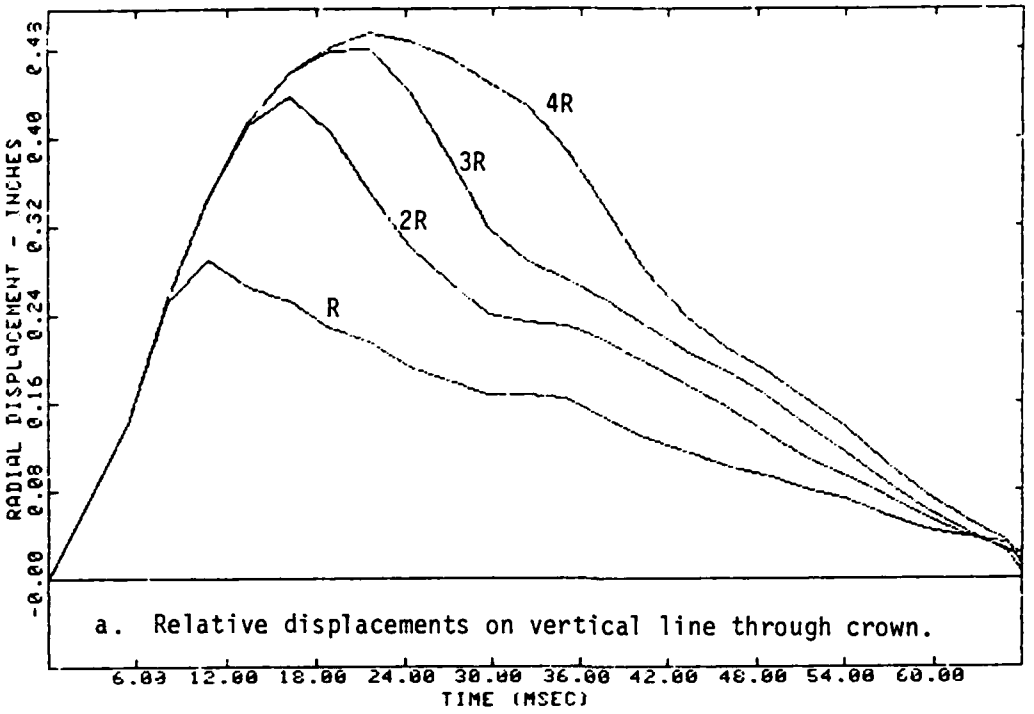

a. Relative displacements on vertical line through crown.

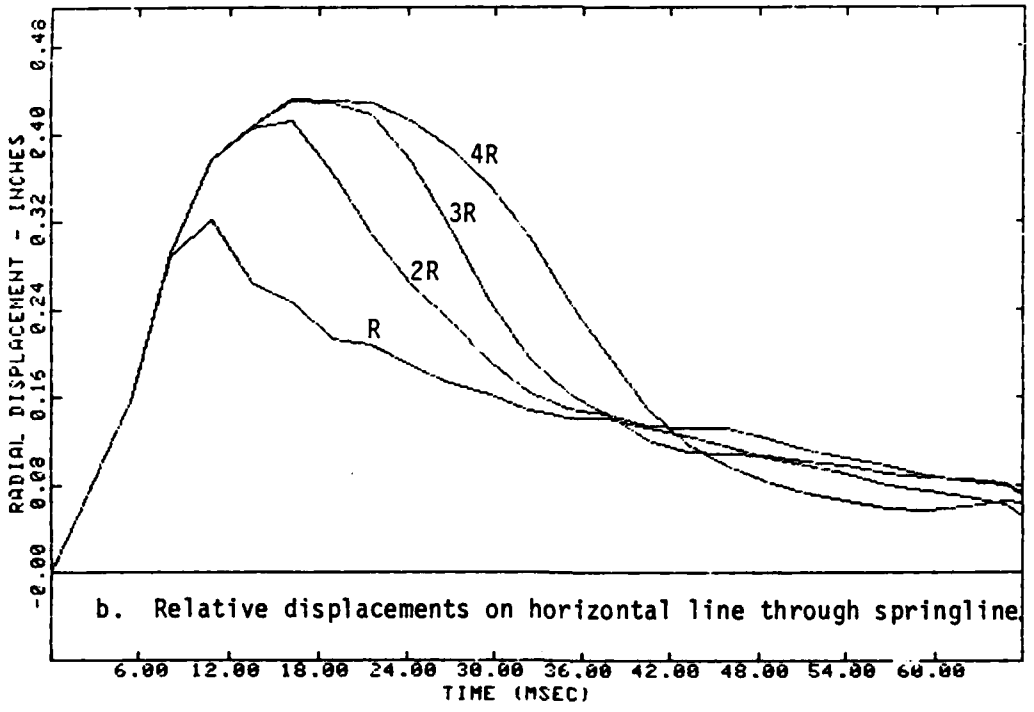

b. Relative displacements on horizontal line through springline.

Figure 2-16. Calculated rock displacements of tunnel surface relative to various points. Location of points indicated as multiples of tunnel radius (R) from tunnel surface.

approximately 27 milliseconds, which is well beyond the time of peak absolute displacement. Absolute and relative displacements at the springline show a similar pattern, except that the curves begin to diverge approximately two milliseconds earlier. It should be emphasized that the curves shown in Figure 2-15 and 2-16 are not presented as pre-test predictions of tunnel response but were used only for the determination of required gage lengths.

Based on the above discussion, we requested boreholes 40 feet (12.2 m) in length and designed the gage with a gage length of 37 feet-two inches (11.3 m), i.e., four tunnel radii. Because of the extremely compressed construction schedule, the Test Group staff requested that we consider reducing the borehole length to 20 feet (6.1 m). Since the required length of the gage is a function of shock propagation velocity through the rock, it was decided to postpone the decision on gage length until rock cores had been tested. Eventually, it was agreed (16 days before the first test) that borehole lengths would be 30 feet (9.1 m), except for two vertical gages in the back of the tunnel near the portal which were limited to 20 feet (6.1 m) because of the shallow depth of cover at that location. The original gage design was modified by merely removing one 10 foot (3.05 m) length of extensometer rod from each gage, resulting in gage lengths of 27 feet-two inches (8.3 m) and 17 feet-two inches (5.2 m), i.e., approximately three and two tunnel radii, respectively.

Dynamic displacement gages were fielded at three locations in the tunnel which were judged to be most significant from the standpoint of tunnel behavior. Gage array locations are shown in Figure 2-17. The bottom part of the figure is a plan view of the tunnel complex. Active gages are located at Sections A-A (in the shotcreted driver section), B-B, and C-C. Passive measurement locations are shown by the circled numbers. The driver is shown as having a length of 100 feet (30.5 m)

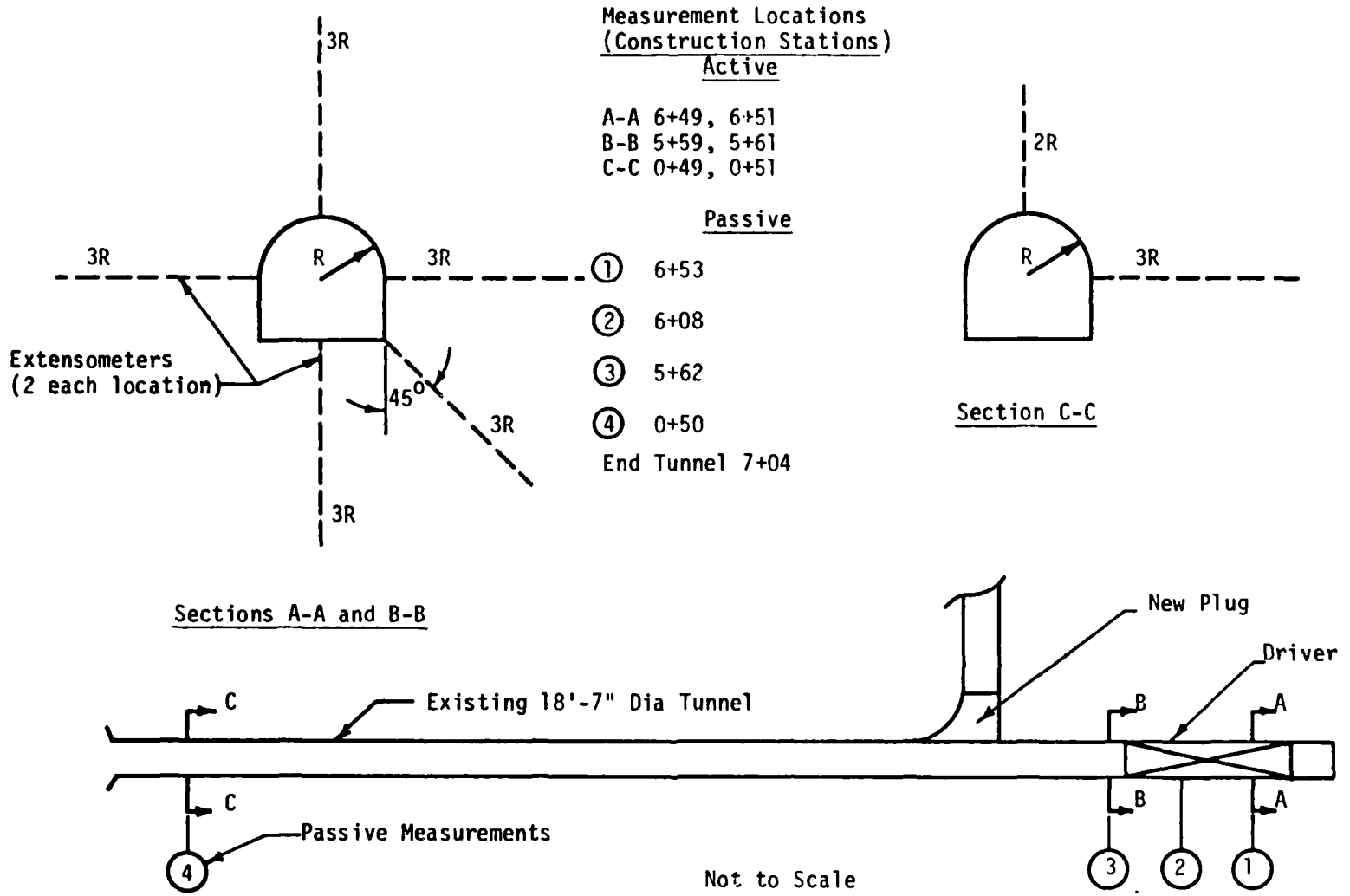

Figure 2-17. Locations for active and passive deformation measurements.

(Construction Stations 5+75 to 6+75), although it was decided after completion of our gage installation to shorten the driver to 75 feet (22.9 m) (Construction Stations 6+00 to 6+75). This change resulted in the gage array shown at Section B-B being approximately 40 feet (12.2 m) from the end of the driver rather than 15 feet (4.6 m) as originally planned. The orientations of the active gages are shown in the sections at the top of Figure 2-17 and construction stations for each gage array are identified in the center of the figure. The two active gages in each pair are located nominally two feet (0.61 m) apart, measured parallel to the axis of the tunnel. This has the effect of providing two "identical" measurements at each location, or a total of 24 measurements, as noted above. There were two reasons for this redundancy:

a. The system was designed to obtain data from multiple tests and it was anticipated that there would not be sufficient time between tests to replace any gages if they failed.

b. Making "identical" measurements would provide an indication of the variability of the experimental data.

Each active gage was checked and calibrated following installation. However, prior to the first test (after grouting the gages and pouring the mud slab), three gages were found to be inoperative. We have been unable to determine the cause. Fortunately, at least one gage in each pair remained functional. As discussed later, each of the remaining 21 gages provided a displacement record on each of the two tunnel response tests. Two of the inoperative gages were in the driver (Section A-A in Figure 2-17), one vertical gage in the center of the invert and one gage oriented at 45 degrees from the vertical. The third inoperative gage was one of the vertical gages in the center of the invert at Section B-B. In all three cases, the inoperative gage was the one nearest the portal.

One pretest prediction calculation was performed for the driver section prior to the first tunnel response test. The results of this calculation were used for setting ranges for the active gages. The material properties shown in Table 2-1 and the finite element grid shown in Figure 2-9 (with 570 feet (173.7 m) of overburden) were used. Figure 2-18 is a direct copy of a calculated pressure-time history received from New Mexico Engineering Research Institute (NMERI) and used as the loading for our pretest prediction.

The one-dimensional NMERI calculation was for an Iremite-driven shock tube with a cross sectional area equal to that of the Little Skull Mountain tunnel. A driver length of 100 feet (30.5 m) and 1,500 pounds (680.4 kg) of Iremite were assumed. The pressure-time history shown in Figure 2-18 is for a station located 75 feet (22.9 m) from the upstream end of the driver.

The prediction calculation differed from our earlier analyses only in the input pressure-time history. The predicted displacements of the tunnel surface at three locations are shown in Figure 2-19. The peak displacement of about 0.09 inches (0.23 cm) occurs at the center of the invert. This corresponds to a maximum diametral strain of 0.0008 inches per inch (0.08 percent) and indicated that no damage should occur in the driver section. The predicted maximum displacement at the rib was nearly equal to that at the invert, while that at the back of the tunnel was about 0.07 inches (0.18 cm). The calculation indicated essentially elastic response and hence residual displacements were expected to be very much smaller than the predicted maximum values. A separate pretest prediction calculation was not performed for the second tunnel response test but maximum displacements were expected to be about twice as large since the driver pressure was approximately doubled.

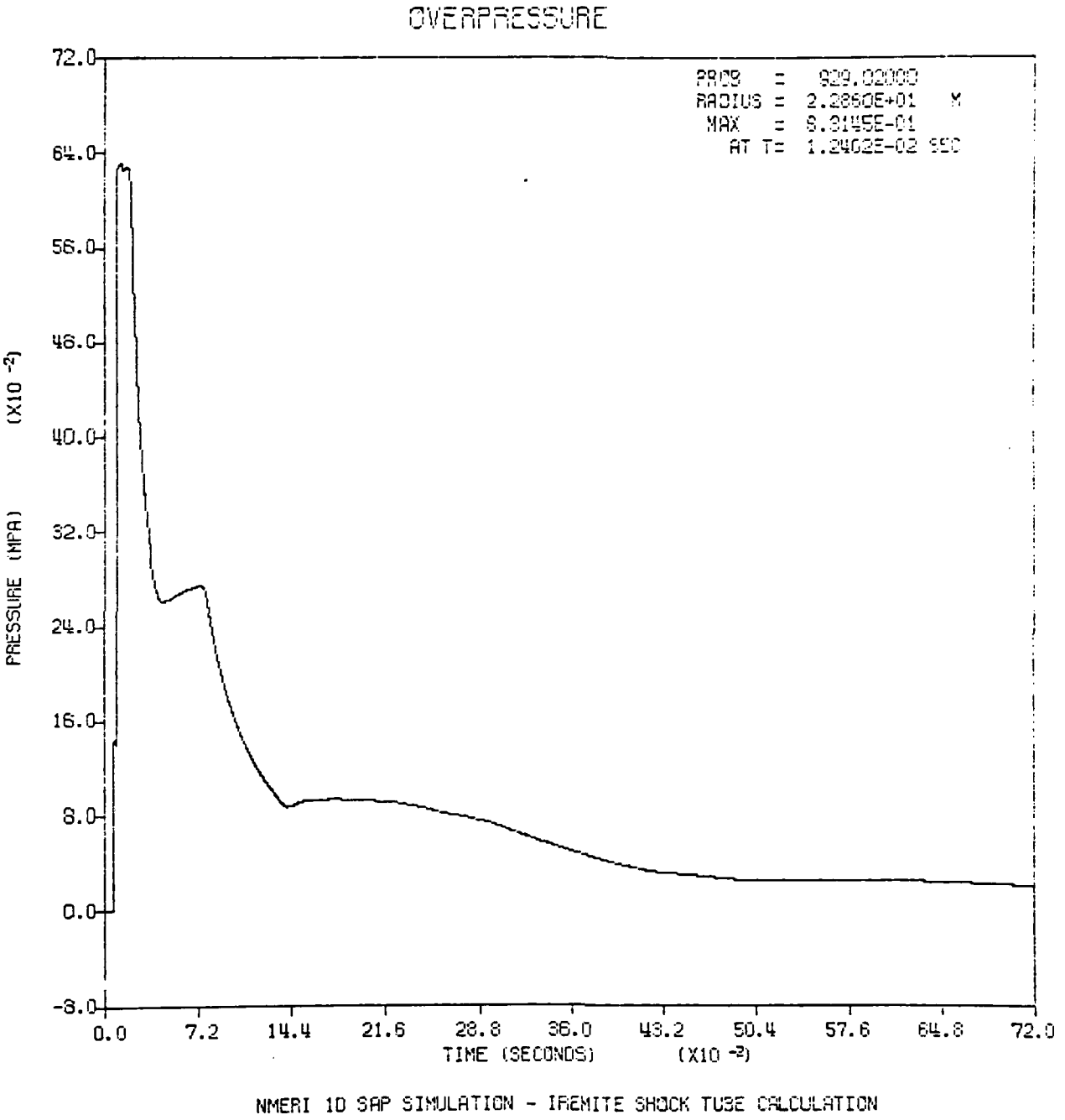

Figure 2-18. Calculated driver pressure-time history used in the prediction calculation.

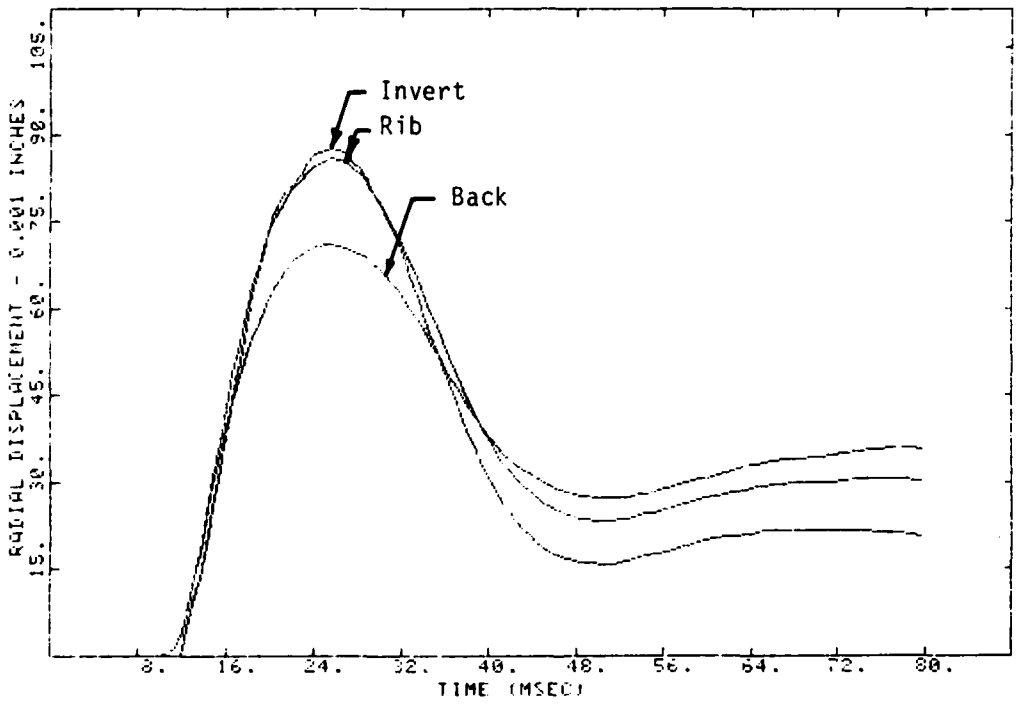

Figure 2-19. Displacement histories from pretest prediction calculation.

2.2.3 Passive Measurements

Passive measurements of residual rock deformations were made using the H-Gage (similar in principal to a Whittemore gage) developed by CASES and used previously on the "add-on" structures experiment fielded on the HURON LANDING underground nuclear test. This instrument accurately measures the distance between gage points (predrilled lag screws) installed in the rock around the tunnel perimeter prior to a test. Passive measurements were made at four different locations along the tunnel, as shown in Figure 2-17. Three of these locations (Construction Stations 0+50, 5+62, and 6+53) were adjacent to active gage locations. The fourth location was at Construction Station 6+08. In general, gage points were installed at 20 inch (50.8 cm) intervals around the tunnel perimeter. Tangential displacement measurements were made between each pair of adjacent gage points. "Diametral" measurements were made as near as possible to the vertical and horizontal centerlines and generally by rotating the gage a minimum of three gage points in either direction from those lines as shown schematically in Figure 2-20. It should be noted that it was not possible both to maintain the 20 inch (50.8 cm) spacing and also locate gage points exactly at each end of each centerline.

As noted above, the H-Gage was previously used to make passive measurements in the HURON LANDING structures experiment drifts. In that case, the nominal gage lengths were 10 inches (25.4 cm) and nine feet (2.74 m) in the tangential and diametral measurement configurations, respectively. For the diametral measurements at Little Skull Mountain, it was necessary (because of the larger tunnel size) to increase the nominal gage length to 18 feet-seven inches (5.66 m) by fitting the gage with an extension. Because of the extremely compressed schedule, it was also decided to increase the nominal gage length to 20 inches (50.8 cm) in the tangential measurement configuration. This reduced the number of tangential measurements at

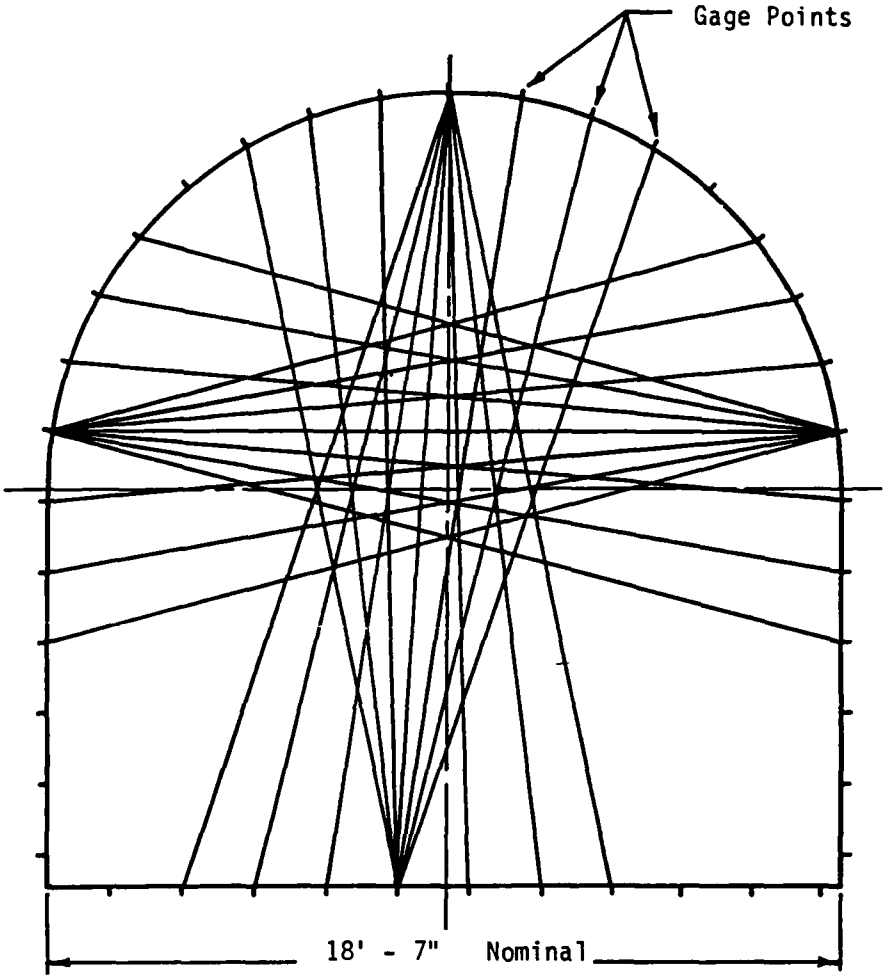

Figure 2-20. Passive measurement locations.

each station to approximately 40 compared to approximately 80 which would have been required with the 10 inch (25.4 cm) gage length.

SECTION 3

ACTIVE INSTRUMENTATION

3.1 PLANNING AND PREPARATIONS

The technique employed for making active (dynamic) rock displacement measurements during the tunnel response tests is described in general terms in Section 2. The measurement plan included 24 dynamic displacement gages. Gage locations are shown in Figure 2-17.

The active measurements required the use of a displacement transducer with adequate frequency response and one which would not be affected by the shock and vibration occurring during the tunnel response tests. In addition, as described in Section 2, it was agreed that we should attempt to measure the peak absolute displacement of the tunnel surface which would require a gage length of a few tens of feet. To our knowledge, a gage capable of satisfying these two requirements (a dynamic displacement over a relatively long span) did not exist. A further complication stemming from the extremely compressed schedule (less than two months between notice to proceed and the first test) required the use of commercially available gages or components. Two proven concepts were available which, in combination, offered a solution.

As described in Section 2, static measurements of rock displacements over long spans have been made for many years, e.g., using extensometers marketed by the Slope Indicator Company (SINCO) of Seattle, Washington. Static displacements are normally recorded through the use of potentiometers, dial indicators, or micrometers. A linear variable differential transformer (LVDT) manufactured by Trans-Tek, Inc. of Ellington, Connecticut, had been used successfully during Phase II of the MISERS

BLUFF program (Reference 7) to measure dynamic soil displacements with a nominal gage length of 12.5 inches (31.8 cm). It was decided to combine the dynamic capabilities of the LVDT with the long span measurement capability of the Slope Indicator system to create a device which would be capable of recording dynamic rock displacements over a span of at least several tens of feet.

After evaluating several of the available Slope Indicator extensometer systems, we decided to use the basic concept of the single position borehole extensometer. This concept consists of a one-quarter inch stainless steel rod which moves inside a one-quarter inch PVC pipe. Some modifications to this system were required. We also evaluated several LVDTs and decided to use the Trans-Tek Model 0244-0000 with a plus or minus one inch (2.54 cm) linear range, primarily because of its immediate availability and because it had been used successfully to make measurements on the MISERS BLUFF experiment. The Slope Indicator Model 51770 single acting hydraulic soil anchor was selected to anchor one end of the gage. It was selected because it offered the best capability for being remotely set and permanently anchored. The three prongs of the soil anchor were not expected to penetrate the rock to any appreciable depth but the pressure exerted on the walls of the borehole was expected to be sufficient to center the device and hold it firmly in place while the borehole was grouted.

3.2 GAGE DESIGN AND ASSEMBLY

A very general schematic representation of the dynamic relative displacement gage was shown earlier in Figure 2-14. As shown in that figure, both ends of the gage must be anchored to the rock and the extensometer rod must be free to move independently of the rock between the anchor points. The hydraulic anchor described above was used at one end of the gage as shown in the more detailed schematic representations in Figure 3-1. Following installation, the anchor was grouted in

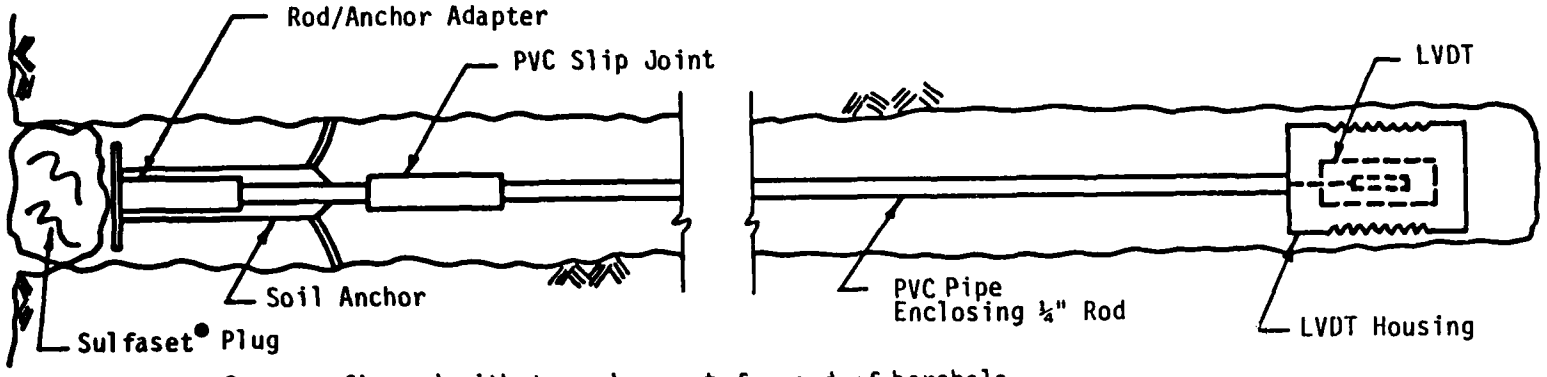

a. Gage configured with transducer at far end of borehole.

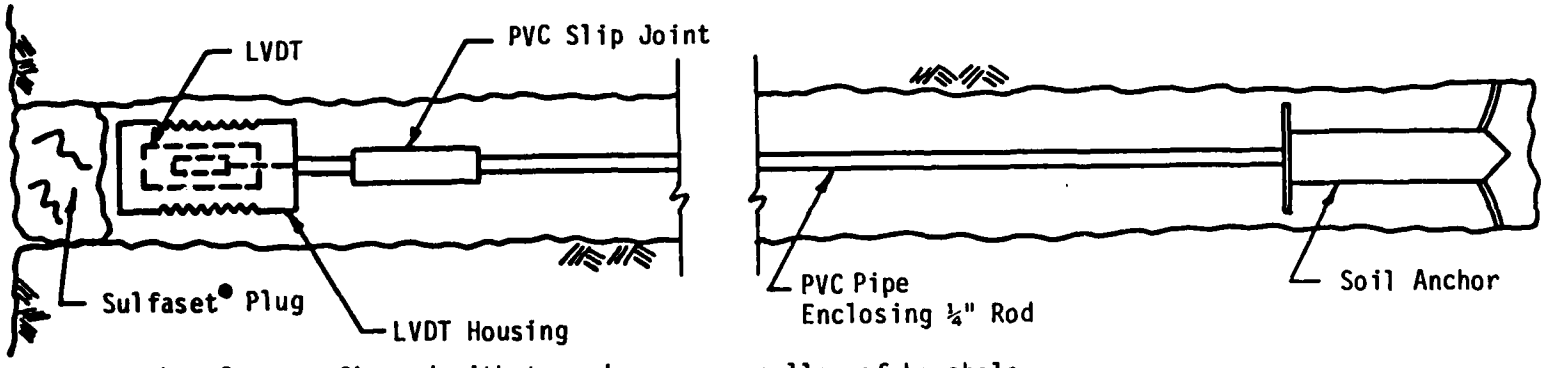

b. Gage configured with transducer near collar of borehole.

Figure 3-1. Schematic representation of dynamic relative displacement gage.

place. The outside of the LVDT housing was grooved and, when grouted in place, served to anchor the other end of the gage.

The completed gage was composed of several subassemblies. A cross sectional view of the gage configured with the transducer at the far end of the borehole is shown in Figure 3-2. Photographs of both ends of one of these gages, following field assembly, are shown in Figure 3-3. The collar end of a partially assembled gage of the other configuration is shown in Figure 3-4. As indicated above, the LVDT, the soil anchor, the extensometer rod, and the PVC pipe were standard commercial items. Subassemblies which were designed and fabricated locally were the LVDT housings, the rod/anchor adapter, and several minor components. Except for potting the LVDTs into their housings (done in the CASES laboratory), all gages were assembled outside the tunnel portal and then carried into the tunnel for installation.

The one-quarter inch PVC pipe was rigidly attached to both ends of the gage. A slip joint was provided in the pipe to isolate longitudinal displacement of the pipe from that of the extensometer rod. The slip joint was located near the collar end of the gage for both configurations, as indicated in Figure 3-1. The slip joint consisted of an 18 inch (45.7 cm) long telescoping section of PVC pipe with O-ring seals at the open end. To provide some temporary rigidity of the gage during installation in the borehole, the slip joint was loosely "locked" in place with a short (about 14 inches (35.6 cm) long) length of one-quarter inch steel tubing taped across the joint with duct tape. The one-quarter inch stainless steel conduit (See Figure 3-2) containing the signal cable also provided some longitudinal rigidity to the gage during installation for the configuration shown in Figure 3-1a.

It was necessary to provide a capability to set the LVDT core at the proper position after the gage was installed in the borehole. This was done for the

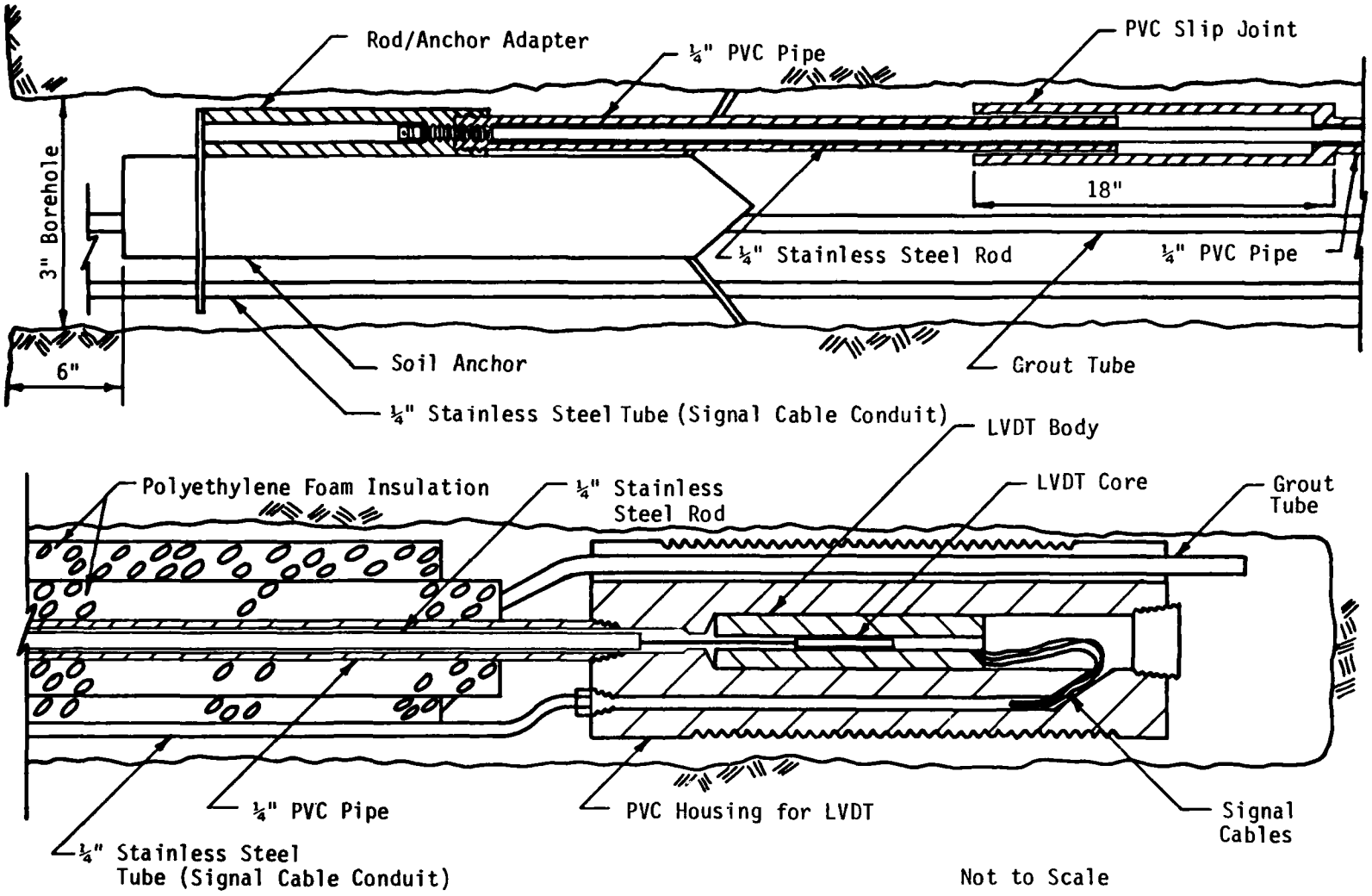

Figure 3-2. Dynamic relative displacement gage configured with transducer at far end of borehole.

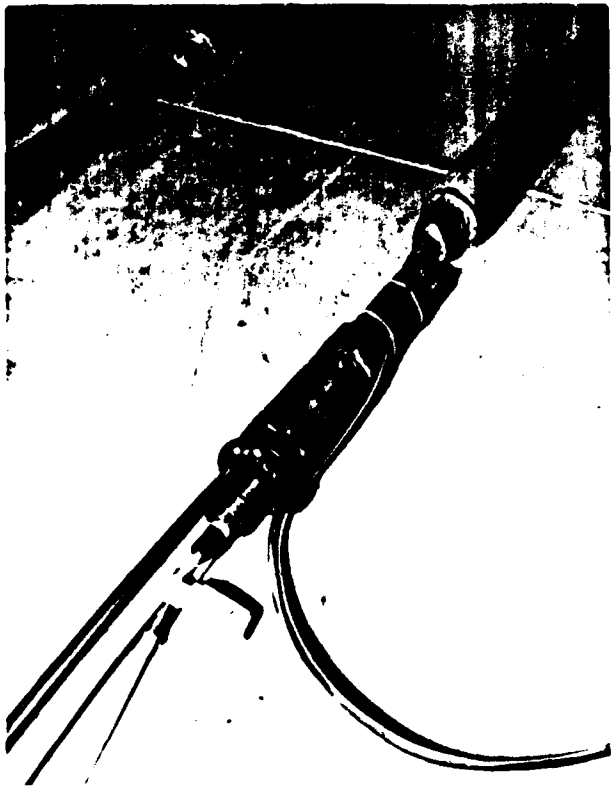

a. Anchor at collar end. Pan Am
Photo CKK-002-12-0U0-20-5-84.

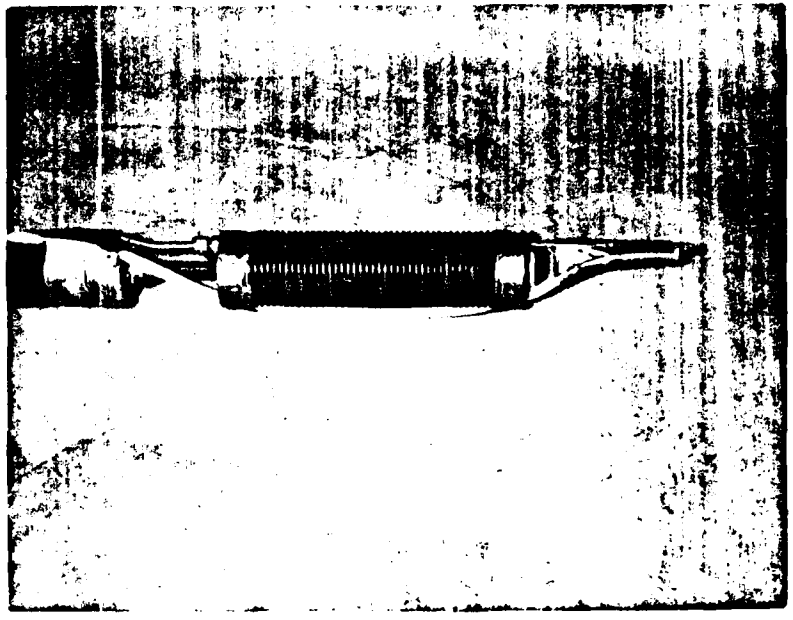

b. Transducer housing. Pan Am
Photo CKK-002-16-0U0-20-5-84.

Figure 3-3. Photographs of both ends of assembled gage configured with transducer at far end of borehole.

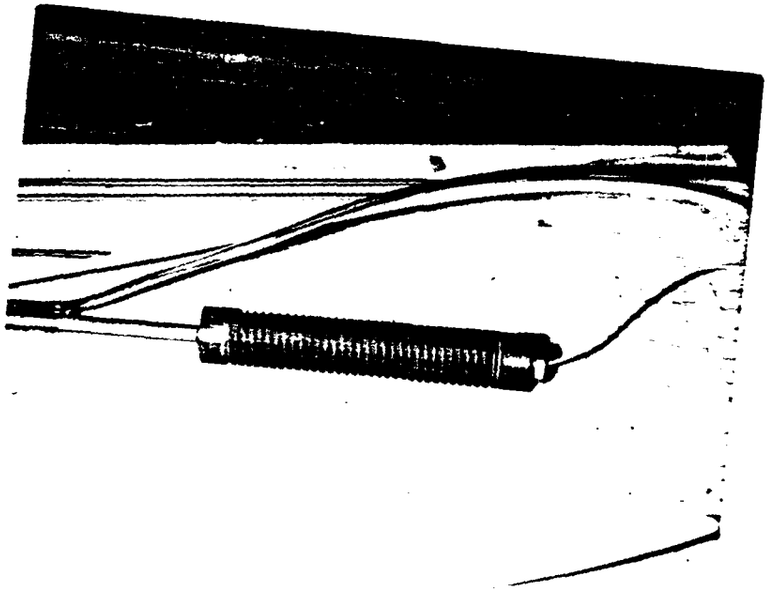

Figure 3-4. Photograph of transducer housing for partially assembled gage configured with transducer at collar. Pan Am Photo CKK-002-17-0U0-20-5-84.

configuration shown in Figure 3-1a by fabricating a threaded rod/anchor adapter and clamping it to the hydraulic anchor as shown in the figure. The adapter permitted a plus or minus two inch (5.08 cm) adjustment of the extensometer rod by turning the slotted rod end with a long screwdriver from outside the borehole. For the configuration shown in Figure 3-1b, gage adjustment was made by moving the LVDT housing and wedging it in place after the hydraulic anchor was set at the far end of the borehole.

The full length of each gage, between the LVDT housing and the anchor, was covered with two layers of polyethylene foam insulation to protect and isolate the gage when the borehole was grouted. The foam insulation is shown in the partial section at the bottom of Figure 3-2 and may be seen in the photographs of the assembled gage in Figure 3-3. A length of Tygon grout tubing which extended past the LVDT housing (See Figure 3-3b) or the anchor was secured to the outside of the polyethylene foam by duct tape wraps every few feet.

3.3 GAGE INSTALLATION

Procedures used for installing the assembled gages in the boreholes, installing and connecting signal cables, and grouting the gages in place are described in this section. The procedures used for both gage types were virtually identical. Therefore, the following discussion generally applies to both gage types, although minor differences are identified.

Construction support was provided by Reynolds Electrical and Engineering Company (REECo). Boreholes were drilled by REECo using a three inch (7.62 cm) carbide rock bit. During the first attempt to install gages it was found that "rifling" of the borehole surface had resulted in an effective hole diameter of less than three inches (7.62 cm). Therefore, the gages could not be inserted into the

borehole. This problem was solved by redrilling the holes with a longer three inch (7.62 cm) bit to even out the bore and produce holes with a minimum three inch (7.62 cm) diameter.

In conjunction with the drilling operation, kerfs were cut by REECo personnel in the tunnel surface from each borehole to the cable trench in the tunnel invert. These kerfs were made just wide and deep enough to hold the one-quarter inch cable conduit, kerf dimensions being approximately one-quarter inch (0.64 cm) wide and one-half to one inch (1.27 to 2.54 cm) deep. Initially cutting the kerfs was attempted with an electric chain saw, but this proved impractical in the particular material encountered. Success was eventually achieved using two abrasive cutting wheels together in a circular saw.

Photographs of gage installation are presented in Figure 3-5. A crew of three people was required to insert the gage into the borehole, with the individual at the collar controlling the operation and guiding the gage placement as shown in the figure. Gages were set so that the end of the gage was six inches (15.24 cm) from the collar to allow space for the Sulfaset® grout plug shown in Figure 3-1. Gages were initially fixed in place by tapping wooden wedges between the end of the gage and the borehole wall. These wedges were set against the soil anchor washer for gages with the transducer at the far end of the borehole and against the LVDT housing for the other gages. Besides serving to center the gage in the borehole, the wedges also held the gage in place in non-horizontal installations until the soil anchor could be set.

The soil anchors operated as one-way hydraulic jacks. That is, the three prongs were forced out of the anchor body and against the borehole walls under hydraulic pressure and, once extended, the prongs could not be retracted. The anchors were pressurized by means of a hydraulic hand pump with pressure gage and

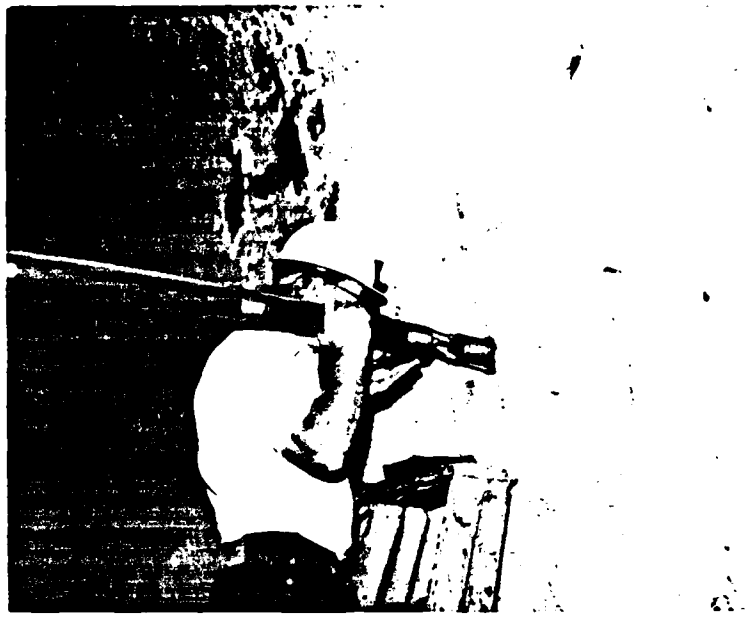

a. Beginning of installation. Pan Am Photo CKK-002-8-0U0-20-5-84.

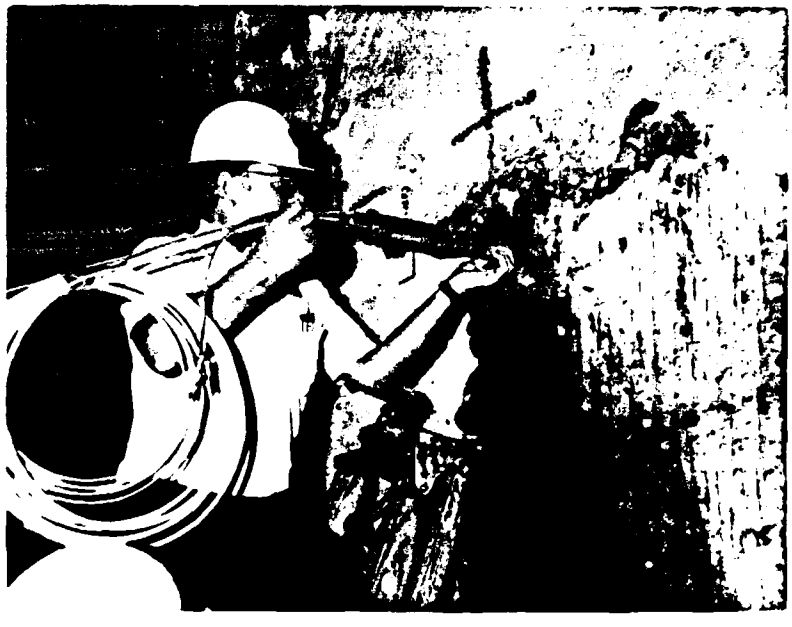

b. Installation nearly complete. Pan Am Photo CKK-002-5-0U0-20-5-84.

Figure 3-5. Installation of gage configured with transducer at far end of borehole.

volumeter. In setting the anchors, a minimum pressure of 1,000 psi (6.89 MPa) and an inflation oil volume of one cubic inch (16.39 cc) were adopted as guidelines. For the 24 gages, setting pressures ranged from 1,200 to 2,100 psi (8.27 to 14.48 MPa) with 22 of them falling in the 1,500 to 2,000 psi (10.34 to 13.79 MPa) range. Oil volumes ranged from 0.8 to 2.1 cubic inches (13.11 to 34.41 cc) with an average of 1.23 cubic inches (20.16 cc). As each anchor was set, the decision to cease jacking was made on the basis of establishing firm anchorage without having the anchor body rotate or cock significantly off of the borehole centerline.

After setting the soil anchor, the adjustment of the LVDT core was checked using a voltmeter. Final adjustment, when required, was made in the same manner as described earlier for the initial settings.

Following final adjustment of the LVDT core, the signal cable conduit was bent as necessary and inserted into the previously cut kerf. The signal cable (which had been cut to approximately the required length and coiled during gage assembly) was routed through the conduit. The required number of lengths of conduit were coupled with Swagelok® fittings and the conduit was eventually terminated at the cable trench. In the tunnel back and ribs, the kerf containing the conduit was covered with a smooth layer of Sulfaset® to provide protection from the airblast wave and detonation products. This was not required in the invert because a concrete mud slab was poured prior to the tunnel response tests. In the driver section, the shotcrete was applied over the Sulfaset®.

REECo personnel installed 22 AWG, four conductor signal cables in the cable trench from each gage array location to the portal and then above ground approximately 1,200 feet (366 m) to the instrumentation van. The 28 AWG Belden YR 15971 cable from each gage was spliced to the 22 AWG cable near the edge of the cable trench. A short length (approximately four feet (1.22 m)) of one inch (2.54

cm) air hose served as the conduit between the end of the one-quarter inch steel conduit and the cable trench. Details of the air hose and splice configuration are shown in Figure 3-6. At the bottom of the trench (not shown in the figure) the air hose was directed toward the portal and the trench was filled with sand, approximately two feet (0.61 m) in depth.

Each gage was grouted over its full length by REECo personnel. Prior to grouting, a Sulfaset® grouting plug was installed on overhead and horizontal gage installations. This plug consisted of foam rubber soaked in Sulfaset® which was then inserted into the borehole at the collar and allowed to set prior to grouting. Along with this plug, a short piece of Tygon tubing was installed as a fill or return (depending on gage position) line for the grouting operation. In a few instances, however, the tube was inadvertently omitted and had to be installed by drilling through the already hardened Sulfaset® For the vertical gages in the back of the tunnel, this short tube was used as the fill line with the return line running to the far end (top) of the borehole. For all other gages, the Tygon tube routed to the far end of the borehole was used as the fill line. Grout was pumped through each fill line and pumping proceeded until competent grout flowed out of the return line (or overflowed at the collar in the case of the invert gages).

3.4 RECORDING AND PLAYBACK

As noted above, the signal cables were routed over the ground surface from the tunnel portal to the instrumentation van, a distance of approximately 1,200 feet (366 m). At the van the cables entered through an open port, without a connector interface, and terminated at a distribution panel behind the equipment racks. Direct connection to the signal conditioners was made from this panel. All equipment in the instrumentation van was set up and operated by Bendix personnel.

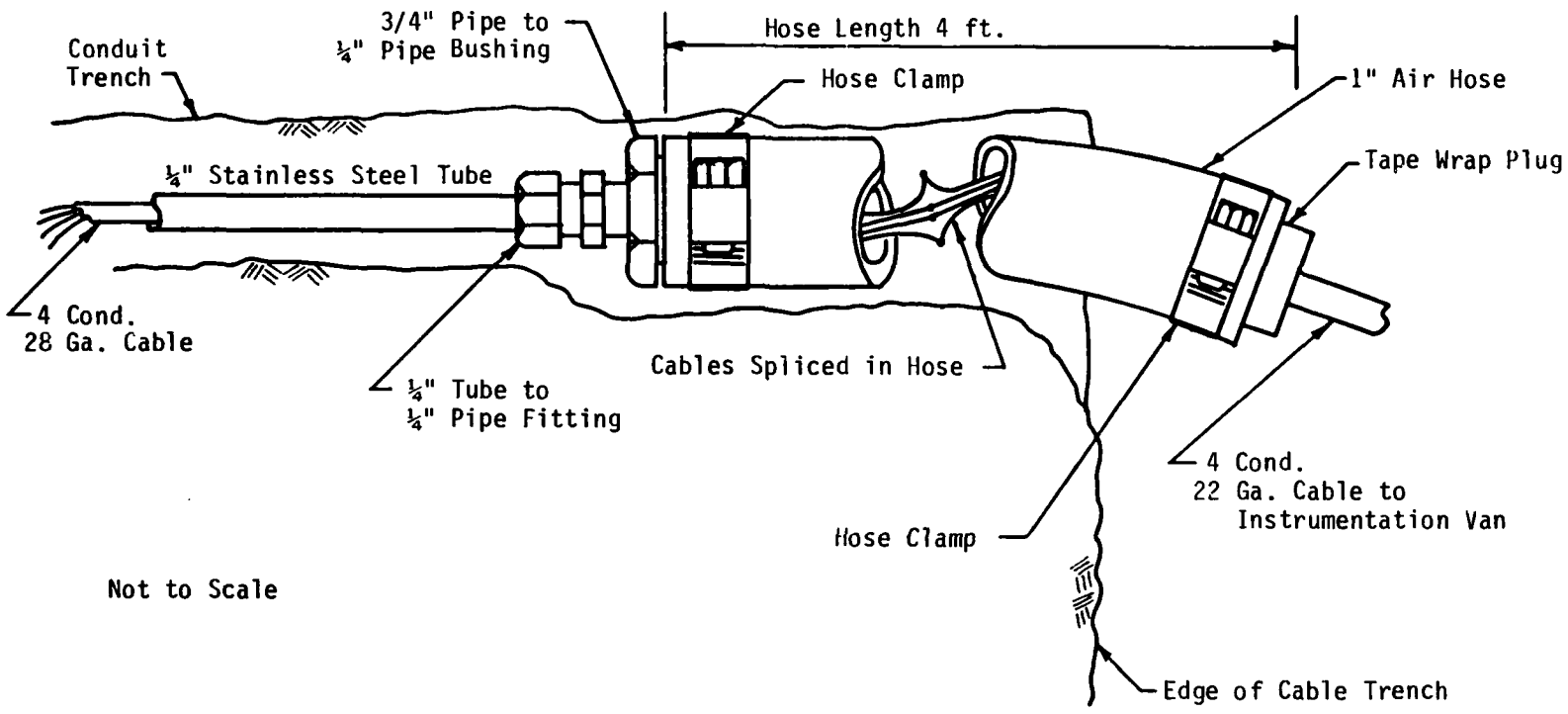

Figure 3-6. Cable splice detail.

The basic instrumentation system consisted of 52 channels of Pacific Instruments Model 8656 signal conditioners which were designed for use with the two Honeywell 101 tape recorders used for the data recording. These conditioners provided individual excitation, attenuation, balancing networks and system calibration. The one-inch 28 track tape recorders were used in the FM mode, one channel per track. The tape speed was 120 inches per second (3.05 mps) with the FM center frequency at 900 kHz using 30 percent deviation. Parallel data channels were set up to provide a 100 percent recording redundancy with the primary channels operating at a higher gain. The excitation voltage was set to provide 10 volts at each transducer. This produced an output signal voltage of approximately plus five volts on each channel.

During the first tunnel response test, the output signal voltages were not balanced to a zero reference level. Consequently, the primary channels were set to record from plus six volts to zero, band-edge to band-edge. The secondary channels were set to record from plus seven to minus seven volts, thereby providing a broader measurement range. Calibration consisted of shorting each channel to produce zero output and using the measured output voltage as the companion data point. Prior to assembling the gages, a voltage versus deflection calibration was performed for each LVDT in the CASES laboratory to verify the factory calibrations provided. This calibration was used for correlation.

For the second test, a balance network was incorporated in each channel to offset the output signal voltage to an initial zero level. The calibration was then applied by substituting a separate voltage source into the circuit. Time was recorded continuously during both tests on one track of each tape recorder in the IRIG-B format. The zero or fire-initiation (FIDU) time was also recorded on individual tracks on each recorder.

After set up and preliminary calibration, recording was accomplished in the following sequence. Tape recorders were turned on three minutes prior to firing to allow time for operational checks. At minus one minute, the calibrations were applied to all channels simultaneously and held for 30 seconds. After the test was complete, at approximately plus one minute, the calibrations were again applied for 30 seconds and the recorders were then stopped.

Playback of the FM tape for "quicklook" data was accomplished by Bendix personnel using a Honeywell Model 1912 oscillograph. No amplifiers were used for this operation and the galvanometer displacements tended to be quite low. Bendix personnel prepared duplicate FM tapes for use in the CASES laboratory where amplified oscillographic playbacks and digitization of all data channels were accomplished.

All tape channels were played back using the equipment depicted schematically in Figure 3-7. This system was used to produce an oscillograph strip chart for each channel and to digitize each record. Digitizing was done using an Analog Devices AD574A 12 bit analog-to-digital converter interfaced to an Apple II+ microcomputer.

The analog signal was sampled at 250 microsecond intervals. The analog signals contained high frequency noise (approximately 6400 hertz) originating from the LVDT oscillator circuits. Therefore a " π " filter was used to assure that only the actual displacement-time data were digitized. All digitized data were recorded on floppy disk and subsequently transmitted to a Prime minicomputer for plotting.

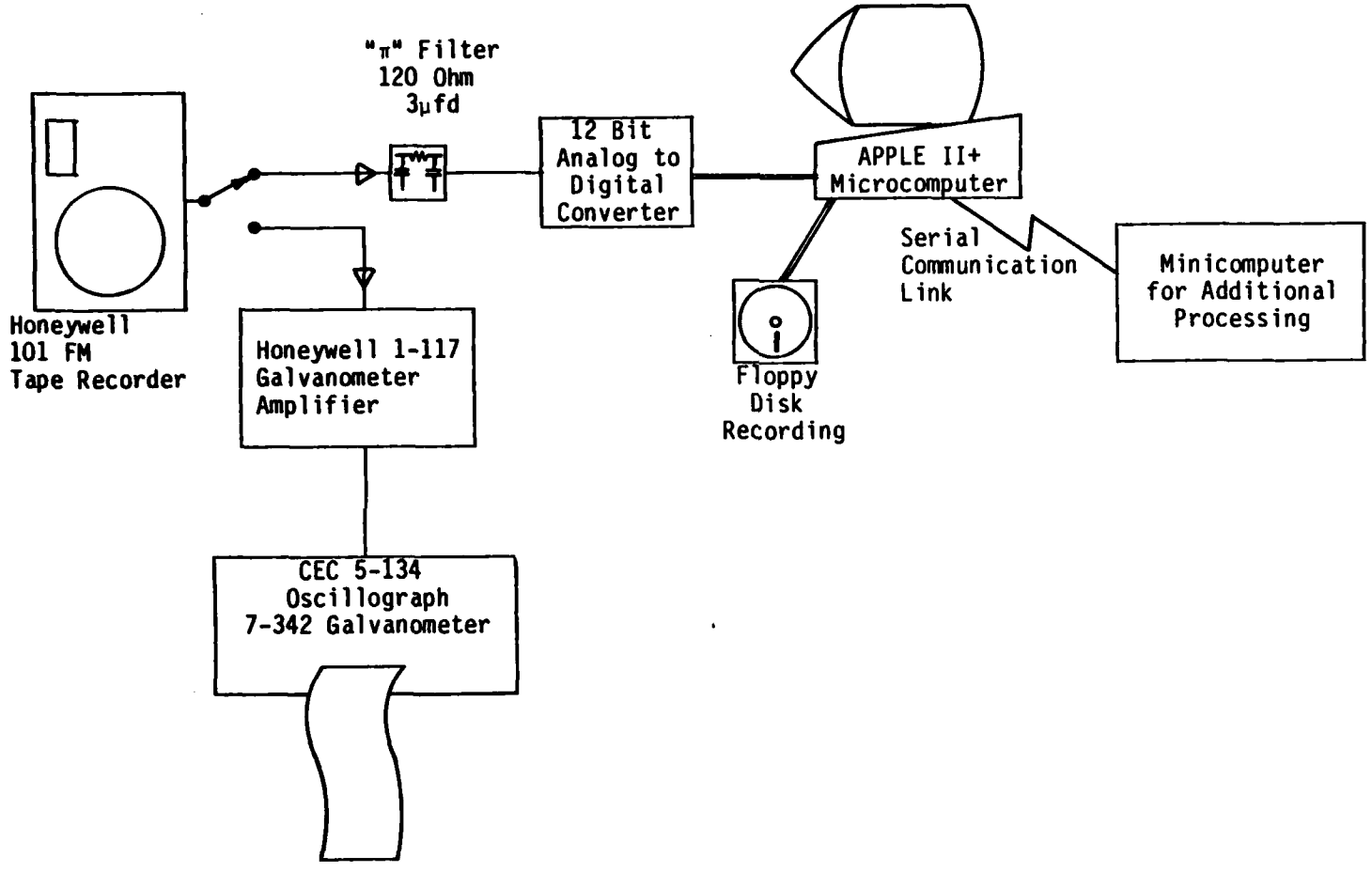

Figure 3-7. Playback and digitizing system.

SECTION 4

PASSIVE INSTRUMENTATION

4.1 GENERAL APPROACH

As described briefly in Section 2, passive measurements of residual rock deformation were made at four tunnel cross sections. These were located at Construction Stations 0+50, 5+62, 6+08, and 6+53 as shown in Figure 2-17. The distances between gage points were measured both before and after each test, with the differences between measurements being the residual deformations.

In general, gage points were installed at intervals of 20 inches (50.8 cm) around the perimeter of the tunnel at each cross section. Tangential measurements were made between each pair of adjacent gage points. "Diametral" measurements were made as near as possible to the vertical and horizontal centerlines and generally by rotating the gage a minimum of three gage points in either direction as shown schematically in Figure 2-20.

4.2 PASSIVE MEASUREMENT EQUIPMENT

As noted earlier, passive measurements of residual rock deformation result from finding the differences between pretest and posttest measurements of the distance between gage points. In order to make accurate measurements, it is necessary to establish accurately located and readily identifiable gage points prior to the test. Furthermore, the gage points must be integral with the rock without significantly weakening it. We used the three inch (7.62 cm) lag screw assembly shown in Figure 4-1 as gage points. Preparation and installation procedures are described later but it is useful to note here the #54 hole drilled in the head of the lag screw which served as the receptacle for the index point of the gage described in the following

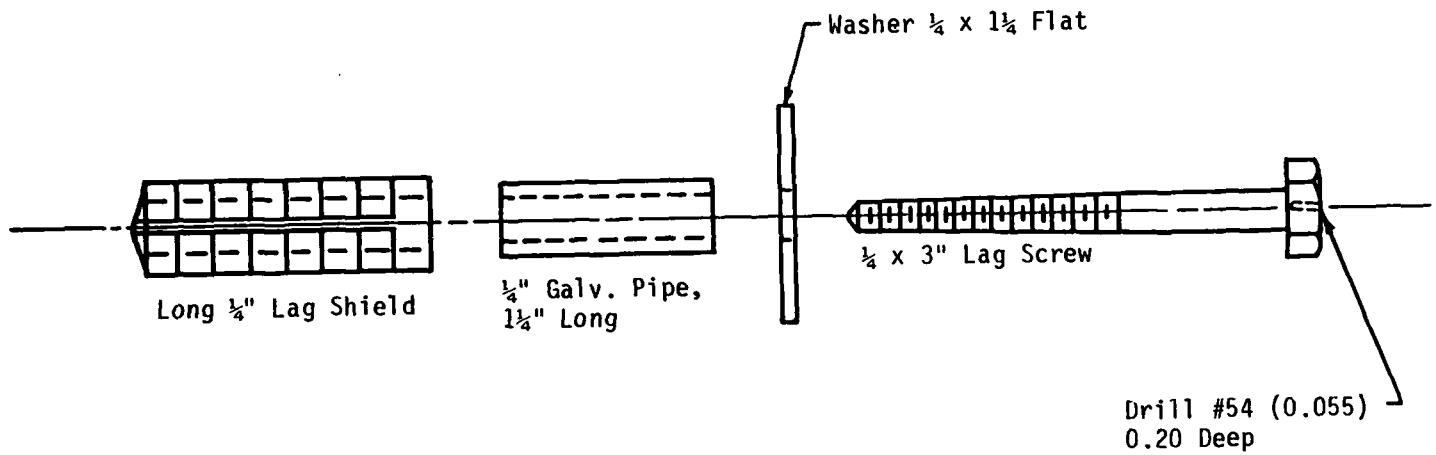

Not to Scale

Figure 4-1. Passive measurement gage point assembly.

paragraphs. The washer shown in the figure was stamped, prior to installation, with a three digit number to allow each gage point to be easily identified.

The H-Gage (similar in principal to the Whittemore gage) was developed by CASES for making residual deformation measurements. The gage is suitable for measuring either tangential or diametral deformations, although changing from one type measurement to the other requires changing the assembled components. As noted earlier, the gage was originally used to make tunnel measurements on the HURON LANDING structures experiment. The original configuration used to make tangential measurements on that experiment had a nominal gage length of 10 inches (25.4 cm) and is shown in Figures 4-2a and 4-2b.

In the tangential configuration, the index points are threaded into the gage in holes drilled perpendicular to the axis of the gage. A linear potentiometer, located in the transducer housing shown at the right end of the gage in Figure 4-2, is used to obtain a differential measurement from a reference dimension established by the basic gage length. As shown in the figure, the gage is spring-loaded and the transducer housing can move longitudinally with respect to the tube at the left end of the gage. Precise calibration of the potentiometer is obtained by the use of a 10.000 inch (25.40 cm) Invar bar. The linear range of the potentiometer is $\pm$0.2 inches (0.51 cm) which yields a measurement range, in the configuration shown in Figures 4-2a and 4-2b, of 10.0 $\pm$0.2 inches (25.4 $\pm$0.51 cm). Also, as shown in Figure 4-2a, two additional index point holes, 0.2 inches (0.51 cm) either side of the basic center hole, are provided in the transducer housing. The index point may be installed in these alternative locations which changes the gage length and provides a measurement range of 9.6 to 10.4 inches (24.38 to 26.42 cm).

As noted in Section 2, it was decided to increase the nominal gage length to 20 inches (50.8 cm) in the tangential measurement configuration because of the

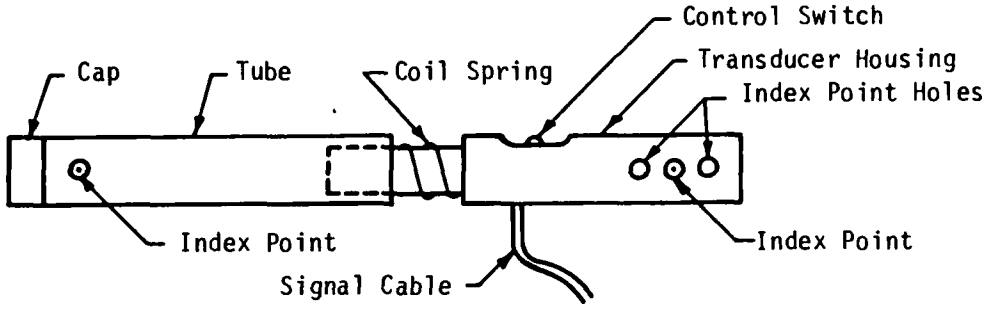

a. Top view, 10 inch nominal gage length.

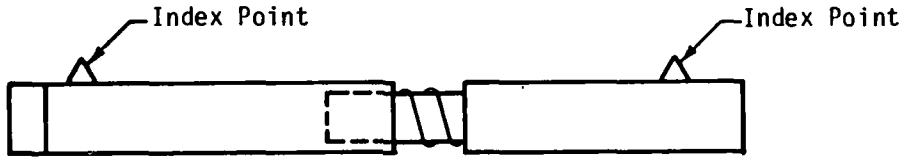

b. Side view, 10 inch nominal gage length.

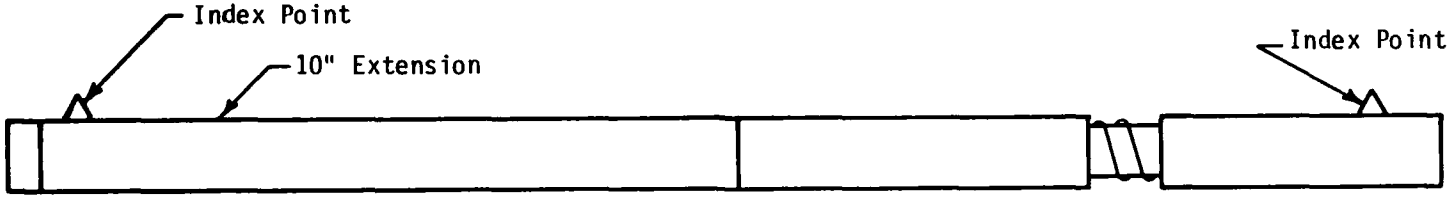

c. Side view, 20 inch nominal gage length.

Not to Scale

Figure 4-2. H-Gage, configured for tangential measurements.

extremely compressed schedule. Doubling the gage length reduced the number of tangential measurements at each station to approximately 40 compared to approximately 80 measurements which would have been required with the 10 inch (25.4 cm) gage length. The gage length was increased by providing a 10 inch (25.4 cm) extension tube as shown in Figure 4-2c. With the extension in place, the measurement range is from 19.6 to 20.4 inches (49.78 to 51.82 cm).

Two types of index point are available. One type of point is approximately 5/8 inch (1.59 cm) long and may be used for either tangential or diametral measurements. The other type of point is approximately 1½ inches (3.81 cm) long. When used for making tangential measurements, the longer points provide greater clearance over irregularities in the tunnel surface. The H-Gage in the tangential measurement configuration, with 20 inch (50.8 cm) nominal gage length and 1½ inch (3.81 cm) index points is shown in Figure 4-3.

The original configuration of the H-Gage used to make diametral measurements on the HURON LANDING structures experiment is shown schematically in Figure 4-4a. It consists of the basic gage as shown in Figures 4-2a and 4-2b, to which the basic extension tube containing a telescoping rod has been attached. Also, the index points are inserted in the ends of the gage as shown in the figure. The telescoping rod was drilled with 84 holes. These holes are nominally 0.4 inches (1.02 cm) apart but their precise spacing has been measured and is used for the actual measurement. The rod is extended to the approximate distance between gage points and the restraining pin is inserted into the appropriate hole in the rod. Deviation from this approximate dimension is then determined precisely by the potentiometer.

The nominal gage length range for the configuration shown in Figure 4-4a is from 102 to 150 inches (2.59 to 3.81 m). Since this range is not large enough to measure the tunnel (nominally 18 feet-seven inches (5.66 m) in diameter), it was

09268413

Figure 4-3. H-Gage in tangential measurement configuration, with 20 inch nominal gage length and 1½ inch index points.

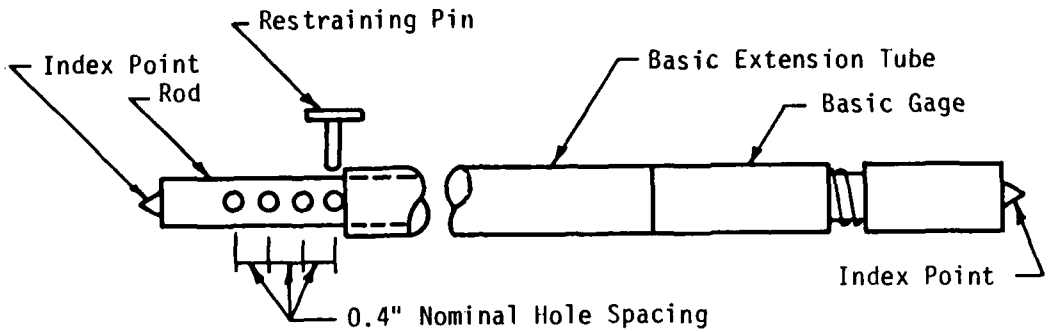

a. Gage length range: 102-150 inches.

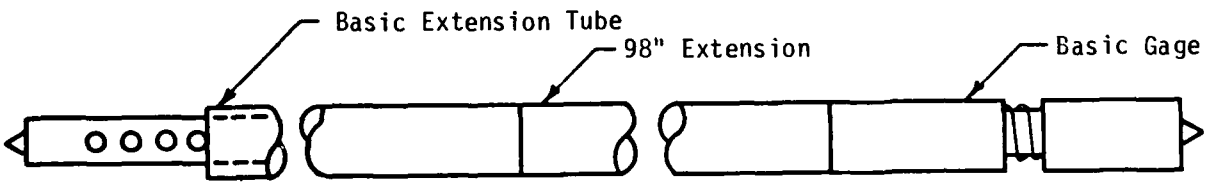

b. Gage length range: 200-248 inches.

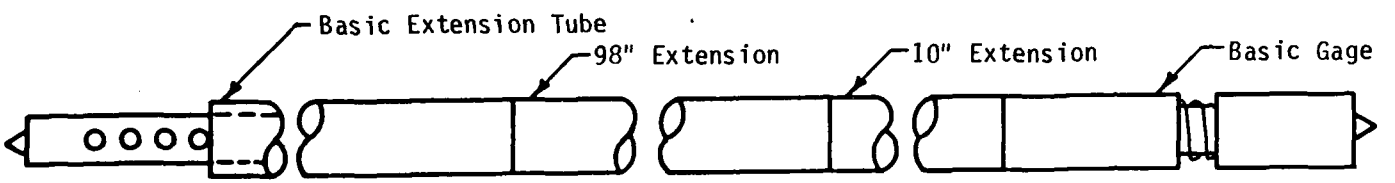

c. Gage length range: 210-258 inches.

Not to Scale

Figure 4-4. H-Gage, configured for diametral measurements.

necessary to add a 98 inch (2.49 m) extension to the gage as shown in Figure 4-4b, which provided a nominal gage length range from 200 to 248 inches (5.08 to 6.30 m). The maximum gage length can be extended to 258 inches (6.55 m) by inserting the 10 inch (25.4 cm) extension, described earlier, as shown in Figure 4-4c.

Since several variables are involved, integration of a microcomputer into the measuring apparatus has proven convenient. An Apple II+ (shown with the H-Gage in Figure 4-3) was used for this purpose because of the relative simplicity with which the analog to digital signal conversion equipment could be interfaced with the microcomputer's native components. Using the microcomputer, the various gage assembly configurations (including precise dimensions thereof), and calibration factors, the measurement voltages can be assimilated in seconds to produce a measurement in convenient engineering units in the field. The use of a floppy disk data recording system allows the data to be easily preserved in machine readable form for further analysis later.

A remote ten-key data pad (also shown in Figure 4-3) was developed for this project to allow the pin identification numbers and gage configuration data to be remotely entered into the microcomputer. This device resembles a hand calculator on a 30 foot (9.1 m) cord and proved invaluable in permitting diametral measurements to be made by two people. The success of the device and the overall measurement process was partially dependent on software routines which allowed these data and the measurement results to be displayed on the microcomputer screen in a large digit format (see Figure 4-3). These special routines allowed four lines of six digit numbers to be displayed on the screen in a size easily readable from a distance of 30 feet (9.1 m).

4.3 PASSIVE MEASUREMENT PROCEDURES

Three separate operations were involved in making passive measurements of residual rock deformations. These are (a) installation of gage points, (b) making tangential measurements, and (c) making diametral measurements. The procedures employed in each of these operations are described below.

The first step in the installation of a gage point was to drill a hole in the rock using a one-half inch (1.27 cm) diameter masonry bit. Each hole was drilled just deep enough to accommodate the gage point assembly shown in Figure 4-1. The lag screw, washer, spacer, and lag shield were then assembled and inserted in the hole. It was usually necessary to drive the assembly into the hole with a hammer to almost the full depth. Final setting of the gage point was done by tightening the lag screw in the lag shield with a wrench.

As described earlier, the measurement range of the H-Gage, configured for tangential measurements, was from 19.6 to 20.4 inches (49.78 to 51.82 cm). Therefore, it was necessary to install the gage points at a relatively accurate and uniform spacing. This was accomplished by setting each gage point, in sequence, by using the previously set gage point as a reference for the nominal 20 inch (50.8 cm) spacing. Using a drilling jig fabricated for this purpose, it was possible for a two person crew to install the gage points at each station in approximately two hours. Despite the care exercised in drilling the holes, there were a few instances where the final positions of adjacent gage points were such that the distance between them was not within the measurement range because the drill tended to "wander" on the rough rock surface. At each station, gage point installation began at the base of the right rib, and worked up the rib, over the back, and down the left rib. Installation of gage points in the invert was delayed until after the mud slab was poured.

As noted earlier, the gage points were identified prior to installation by stamping a number on a washer under the head of the lag screw. The numbers and locations of the gage points are shown for the four measurement locations in Figures 4-5 through 4-8. These figures are idealized representations of the real tunnel cross sections. As such they are intended to show the approximate locations of the gage points. Due to variations in the actual tunnel geometry, the number of gage points and their precise locations vary from one cross section to another. Gage point 130 (Figure 4-5) was not firmly anchored in the mud slab because the slab at that point was only about two inches (5.08 cm) thick and was underlain by loose material. Gage point 182 (Figure 4-6) was lost during construction. Two washers were inadvertently stamped with the number 190. These were identified as 190a and 190b when measurements were made and are identified as such in Figure 4-7.

Many aspects of the procedures for making tangential and diametral measurements were identical. Measurements of each type were made at each of the four stations prior to the first tunnel response test, during the two week interval between the two tests, and following the second test. Our original plan was to repeat each of these three sets of measurements in order to identify and correct possible reading errors and to provide data with which to assess the accuracy (based on repeatibility) of the measurements. Unfortunately, schedule constraints did not permit us to make any repetitive measurements until after the second test. At that time, most tangential measurements were repeated once and selected diametral measurements were repeated twice at Construction Stations 0+50 and 5+62.

Tangential measurements were made in a straightforward manner, usually beginning at the base of the right rib and working up the rib, over the back, down the left rib, and across the invert. In the few cases where the distance between adjacent gage points was not within the measurement range of the H-Gage, the

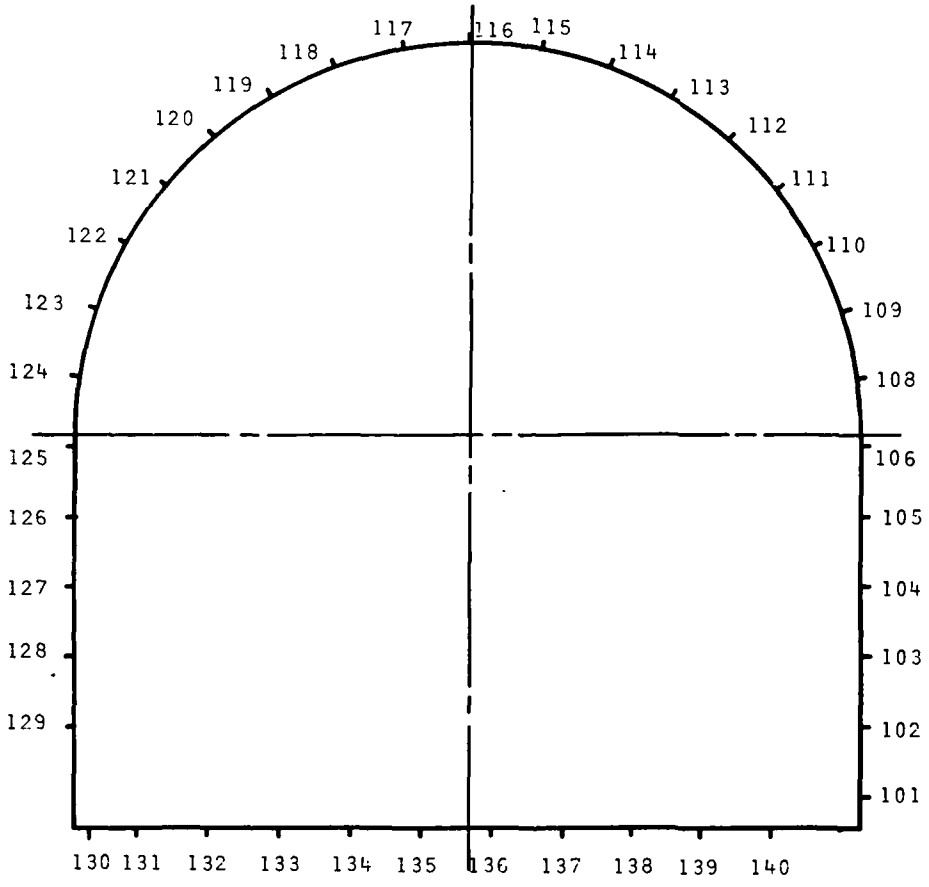

Figure 4-5. Passive gage point identification at Construction Station 0+50.

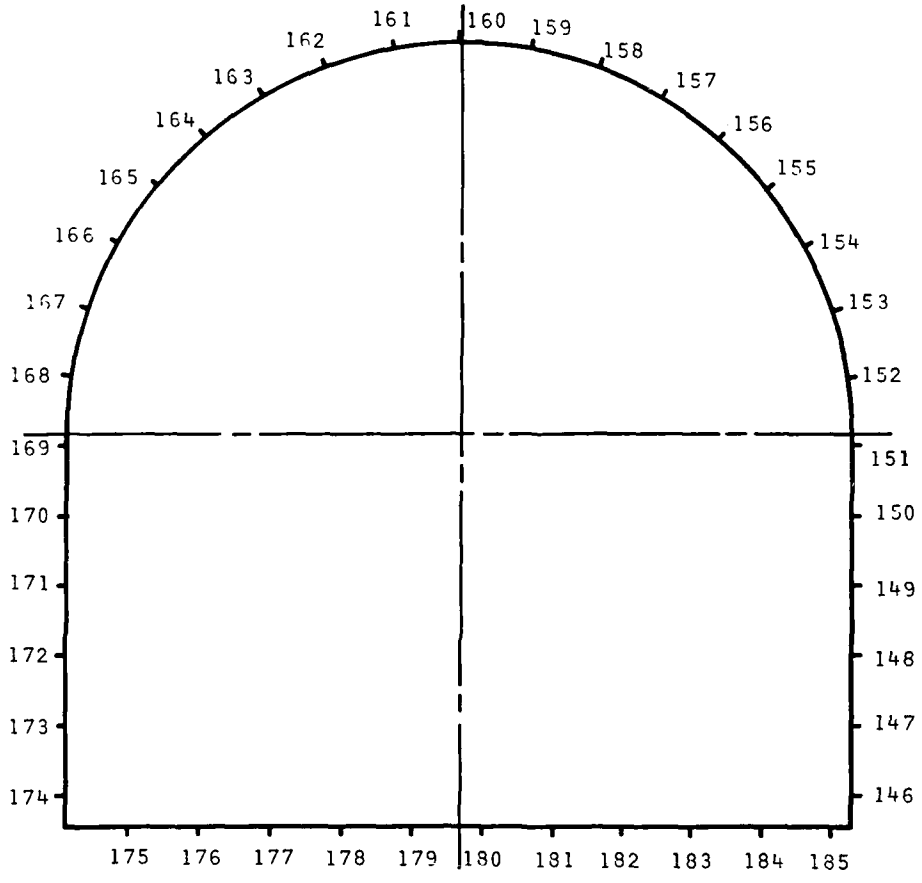

Figure 4-6. Passive gage point identification at Construction Station 5+62.

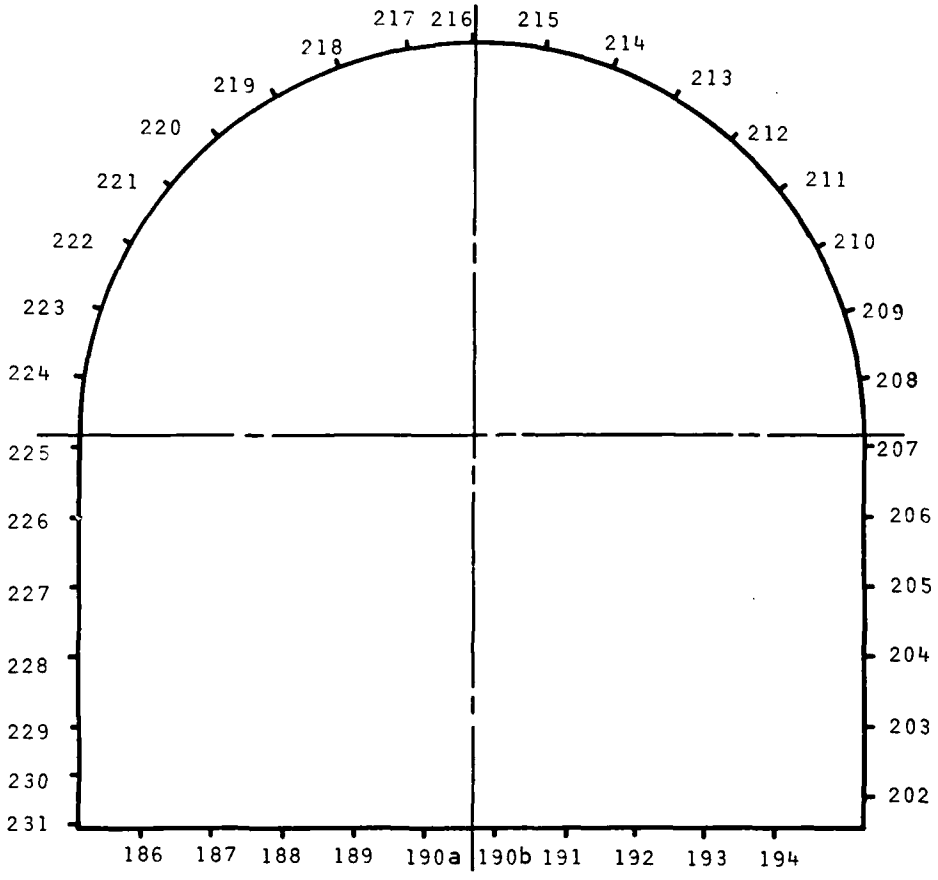

Figure 4-7. Passive gage point identification at Construction Station 6+08.

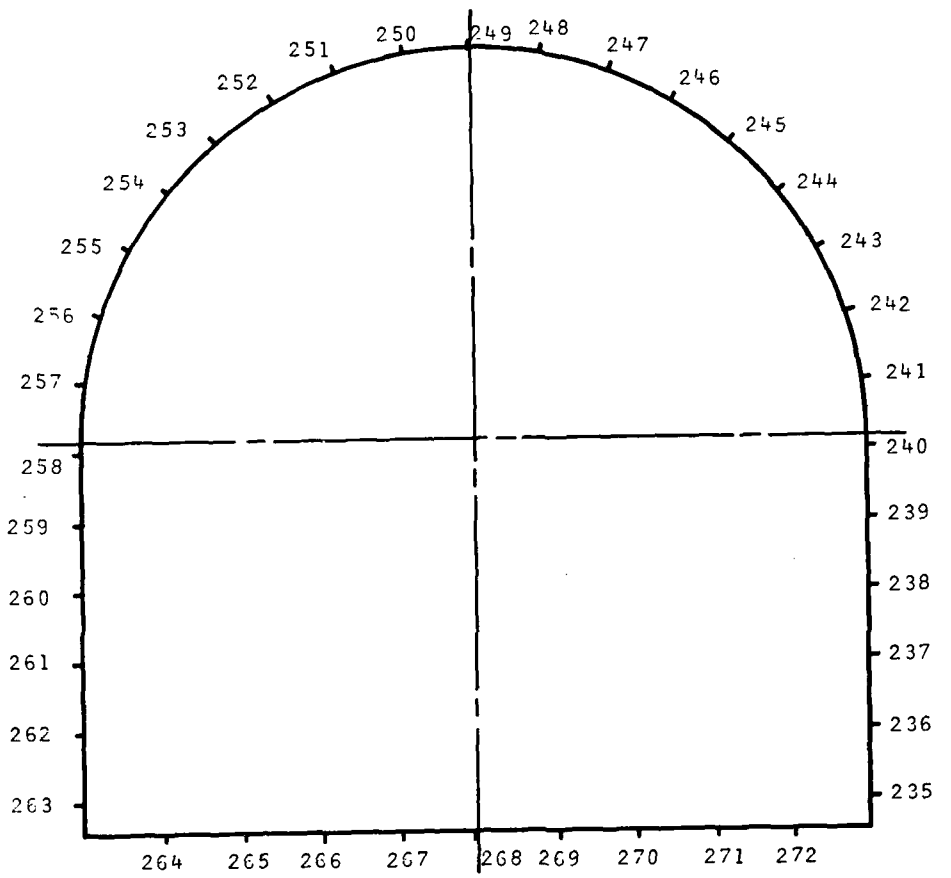

Figure 4-8. Passive gage point identification at Construction Station 6+53.

measurements were necessarily omitted. Because of the rough surface on the lower ribs, some measurements required the use of the long index points. Consequently, the long points were used for all the tangential measurements to avoid the necessity for changing index points.

As discussed in Section 2, diametral measurements were made as near as possible to the vertical and horizontal centerlines of the tunnel and generally by rotating the gage a minimum of three gage points in either direction from those lines as shown schematically in Figure 2-20. All diametral measurements were made with the H-Gage configured as shown in Figure 4-4c.

SECTION 5

ACTIVE MEASUREMENT RESULTS

5.1 RELATIVE DISPLACEMENT RECORDS

The dynamic relative displacement gages fielded at Little Skull Mountain are described in Section 3. Locations of the gages were shown in Figure 2-17, which is repeated here, for convenience, as Figure 5-1. The bottom part of the figure is a plan view of the tunnel complex. Active gages were located at Sections A-A (in the shotcreted driver section), B-B, and C-C. The positions around the tunnel and the orientations of the gages are shown at the top of the figure and the construction station for each gage array is identified in the center of the figure. The two active gages in each pair were located nominally two feet (0.61 m) apart, measured parallel to the axis of the tunnel.

Gage numbers, locations, and orientations are summarized in Table 5-1. The peak measured relative displacements are also provided for both tests for each operational gage. The three gages found to be inoperative prior to the first test (A-3-P, A-4-P, and B-4-P) are indicated by "No Record" in the right-hand columns of Table 5-1.

As discussed in Sections 2 and 3, 20 of the 24 gages were installed with the transducer at the "far end" of the borehole. The other four gages (A-1-X, A-2-X, B-2-X, and C-2-X) were reversed, i.e., with the transducer at the collar of the borehole. These gages are identified by an asterisk in Table 5-1.

Relative displacement records from gages located at Section A-A (Figure 5-1) for both tunnel response tests are shown in Figures 5-2 through 5-6. Outward displacements (away from the centerline of the tunnel) are positive. All of these

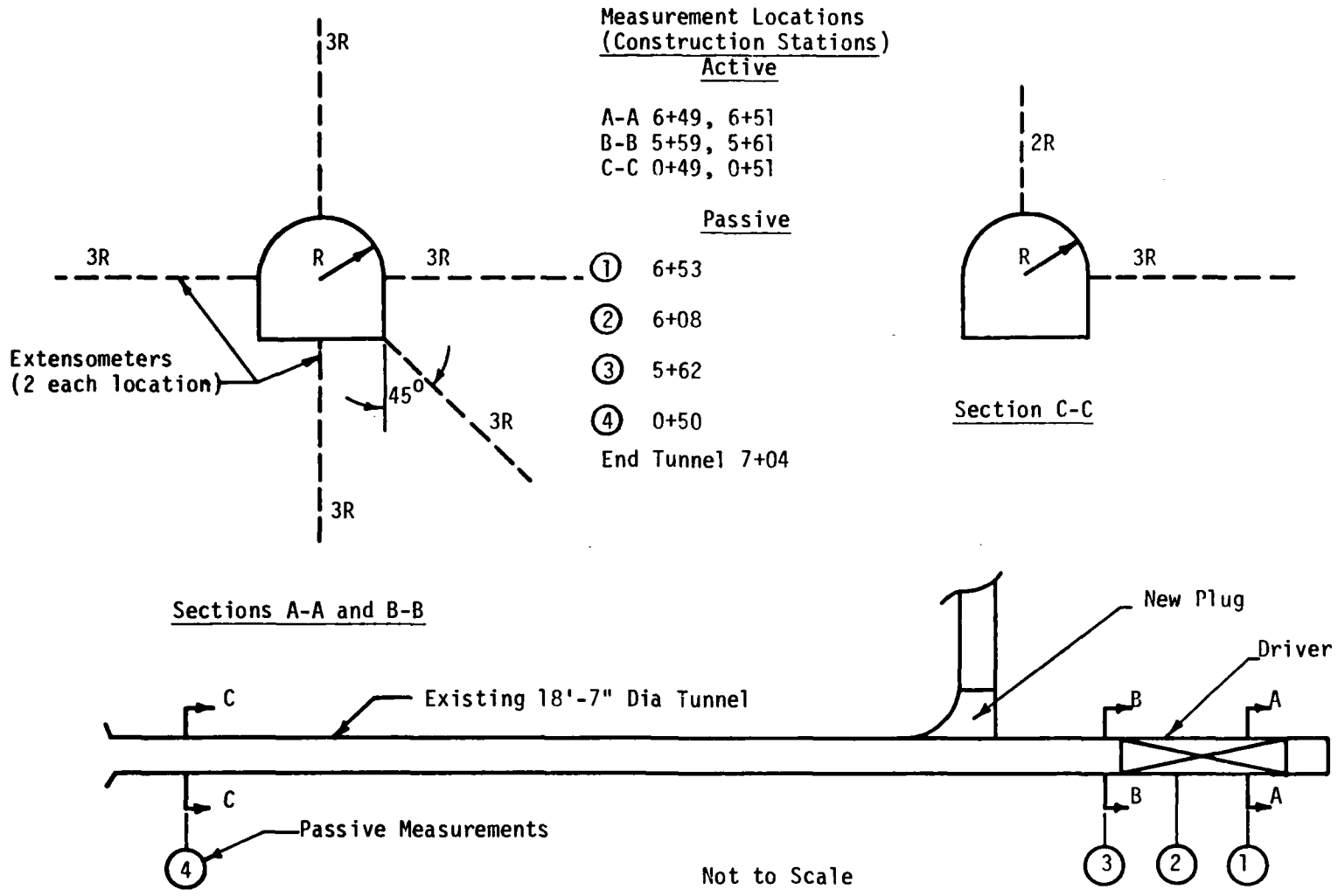

Figure 5-1. Locations for active and passive deformation measurements.

Table 5-1. Active displacement gage summary.

Gage Number	Construction Station	Location	Orientation	Peak Measured Relative Displacement (inches)	
				Test 1	Test 2
A-1-P	6+49	Back	Vertical	0.0391	0.0748
*A-1-X	6+51			0.0384	0.0663
A-2-P	6+49	Right	Horizontal	0.0438	0.0726
*A-2-X	6+51	Rib		0.0395	0.0631
A-3-P	6+49	Right	45 Degrees	No Record	
A-3-X	6+51	Abutment		0.0326	0.0440
A-4-P	6+49	Invert	Vertical	No Record	
A-4-X	6+51			0.3270	0.4128
A-5-P	6+49	Left	Horizontal	0.0126	0.0179
A-5-X	6+51	Rib		0.0369	0.0629
B-1-P	5+59	Back	Vertical	0.0111	0.0238
B-1-X	5+61			0.0123	0.0223
B-2-P	5+59	Right	Horizontal	0.0199	0.0357
*B-2-X	5+61	Rib		0.0109	0.0212
B-3-P	5+59	Right	45 Degrees	0.0094	0.0173
B-3-X	5+61	Abutment		0.0100	0.0174
B-4-P	5+59	Invert	Vertical	No Record	
B-4-X	5+61			0.0297	0.0537
B-5-P	5+59	Left	Horizontal	0.0120	0.0246
B-5-X	5+61	Rib		0.0139	0.0264
C-1-P	0+49	Back	Vertical	0.0047	0.0062
C-1-X	0+51			0.0052	†0.0098
C-2-P	0+49	Right	Horizontal	0.0330	0.0451
*C-2-X	0+51	Rib		0.0336	0.0486

* Gage sensor located at collar of borehole.

† Ignores spike (0.0150) which occurs at 275 milliseconds.

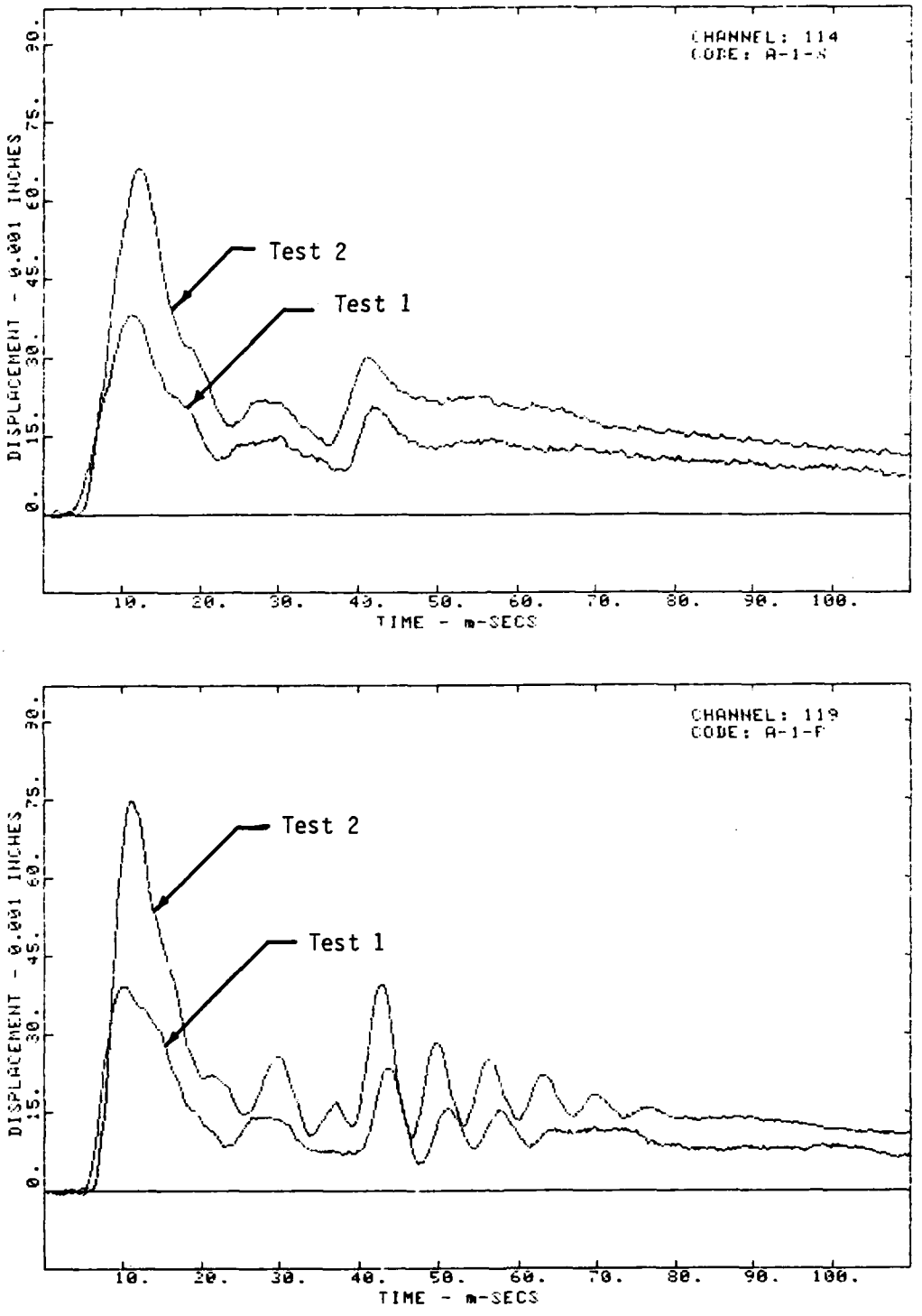

Figure 5-2. Relative displacement records, comparison between tests, back of tunnel, gages A-1-X and A-1-P.

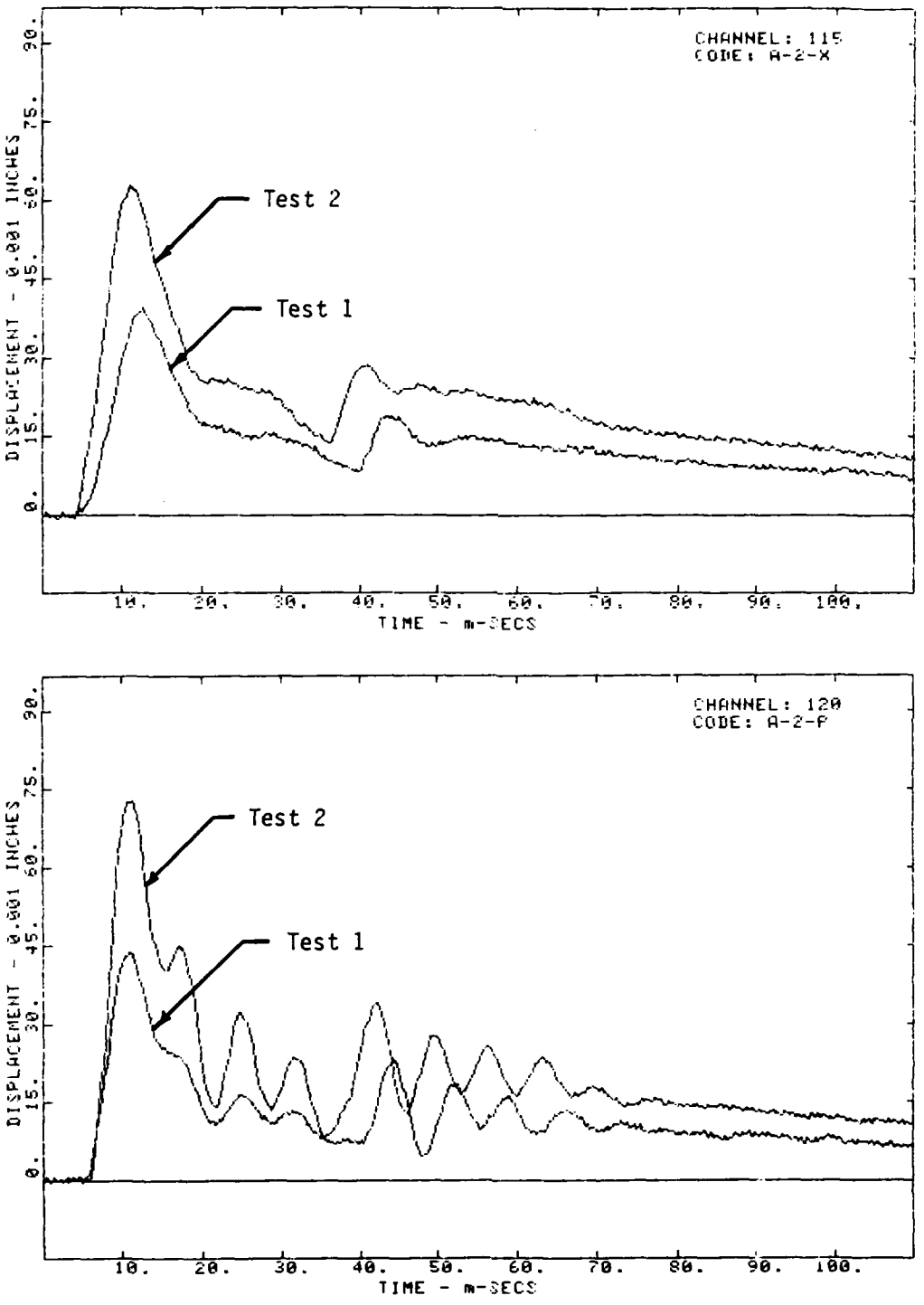

Figure 5-3. Relative displacement records, comparison between tests, right rib, gages A-2-X and A-2-P.

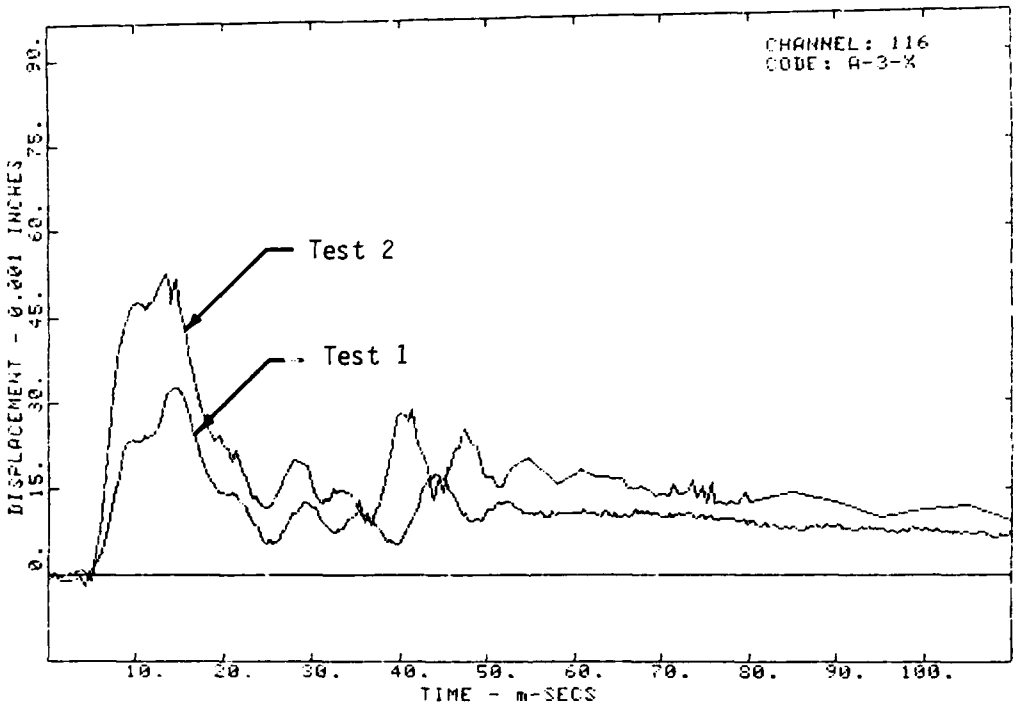

Figure 5-4. Relative displacement records, comparison between tests, right abutment, gage A-3-X.

AD-A165 442 UNDERGROUND DYNAMIC AIRBLAST SIMULATOR INVESTIGATIONS 2/2
TUNNEL RESPONSE MEA..(U) MERRITT CASES INC REDLANDS CA
D N BURGESS ET AL. 31 OCT 84 84-015-T1 DNA-TR-84-404
UNCLASSIFIED DNA001-84-C-0005 F/G 19/4 NL

END
FILMED
DTIC

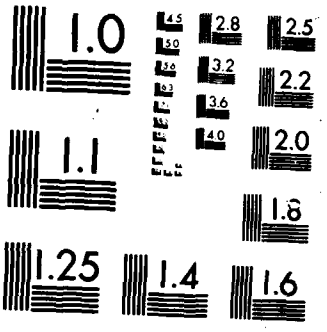

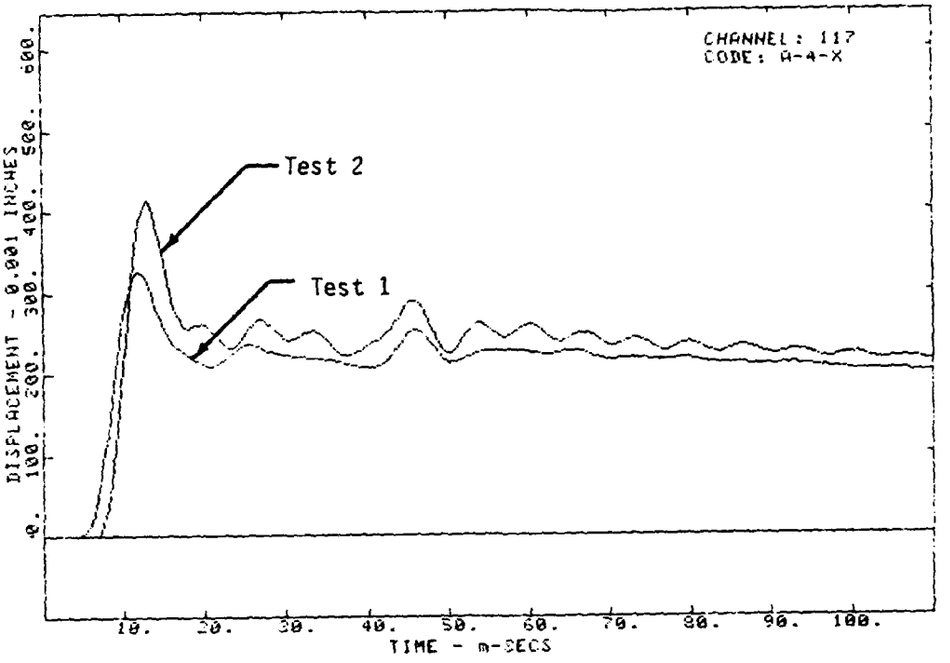

Figure 5-5. Relative displacement records, comparison between tests, invert, gage A-4-X.

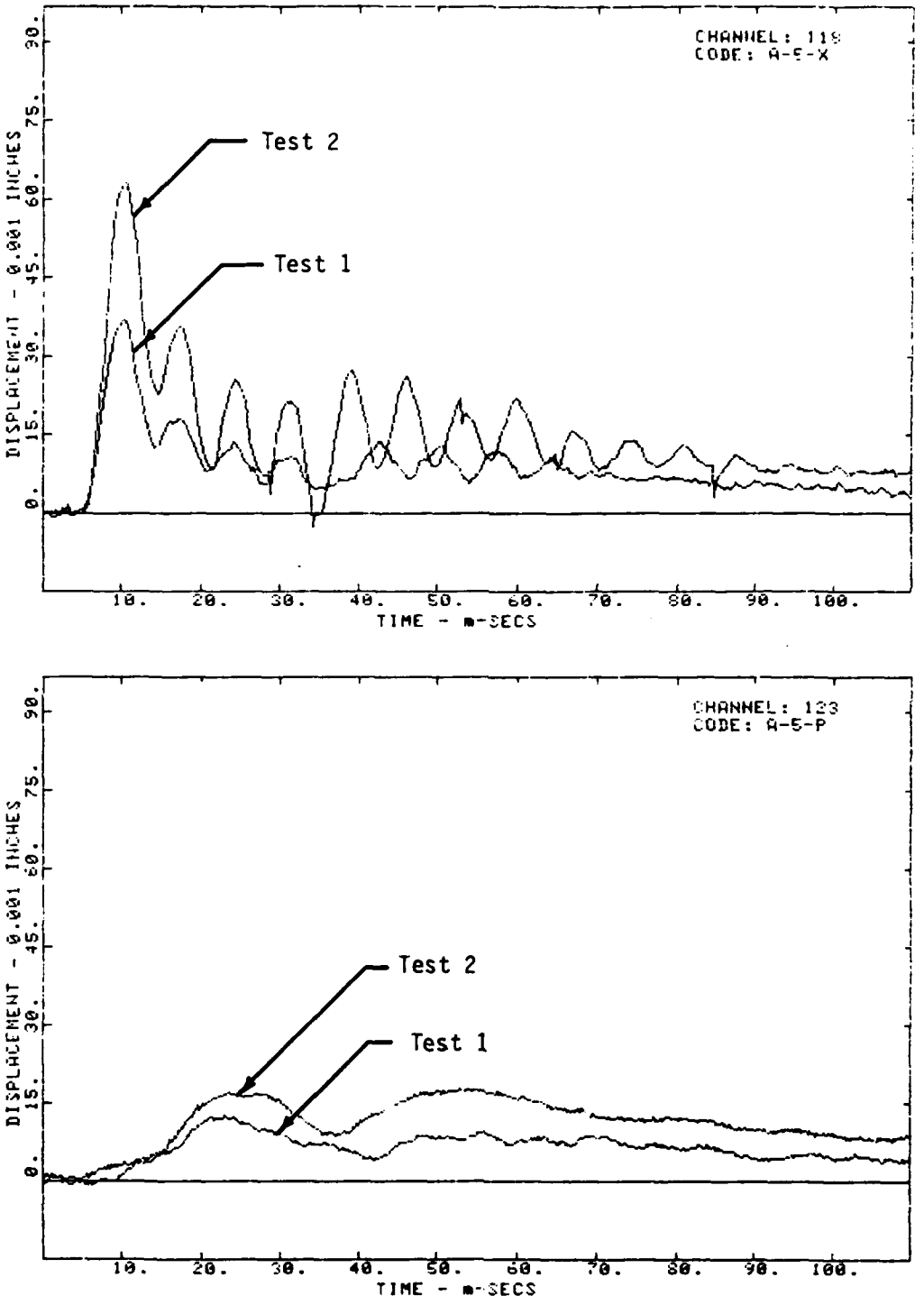

Figure 5-6. Relative displacement records, comparison between tests, left rib, gages A-5-X and A-5-P.

records, except for gage A-4-X (Figure 5-5), are plotted to the same scale for convenience in making comparisons between gages. In each case, the records for "companion" gages (those located two feet apart) are presented on the same page, with the "X" gage (farthest from the portal) at the top of the figure. Records for gages A-3-X and A-4-X are shown alone in Figures 5-4 and 5-5, respectively, because the companion gages A-3-P and A-4-P were found to be inoperative prior to the first test. The recording channel and gage number are shown at the upper right corner of each plot.

The dubbed tape for the second test which we received from Bendix contained no usable record for gage A-3-X from either the primary or backup recorder. Therefore, the second test record shown in Figure 5-4 was obtained by manually digitizing a strip chart record provided by Bendix.

Relative displacement records from gages located at Section B-B (Figure 5-1) for both tunnel response tests are shown in Figures 5-7 through 5-11. These records are all plotted to the same scale (different from the scale used for Figures 5-2 through 5-6). Again, the records for companion gages are shown on the same page, except for Figure 5-10 where one of the two gages (B-4-P) was inoperative prior to the first test. It was also necessary to manually digitize the first test record for gage B-2-X (Figure 5-8) from the backup strip chart record provided by Bendix.

Relative displacement records from gages located at Section C-C (Figure 5-1) for both tunnel response tests are shown in Figures 5-12 and 5-13. As discussed in Section 3, the gage length for gages C-1-X and C-1-P was only 17 feet-two inches (5.2 m), whereas all others had a gage length of 27 feet-two inches (8.3 m).

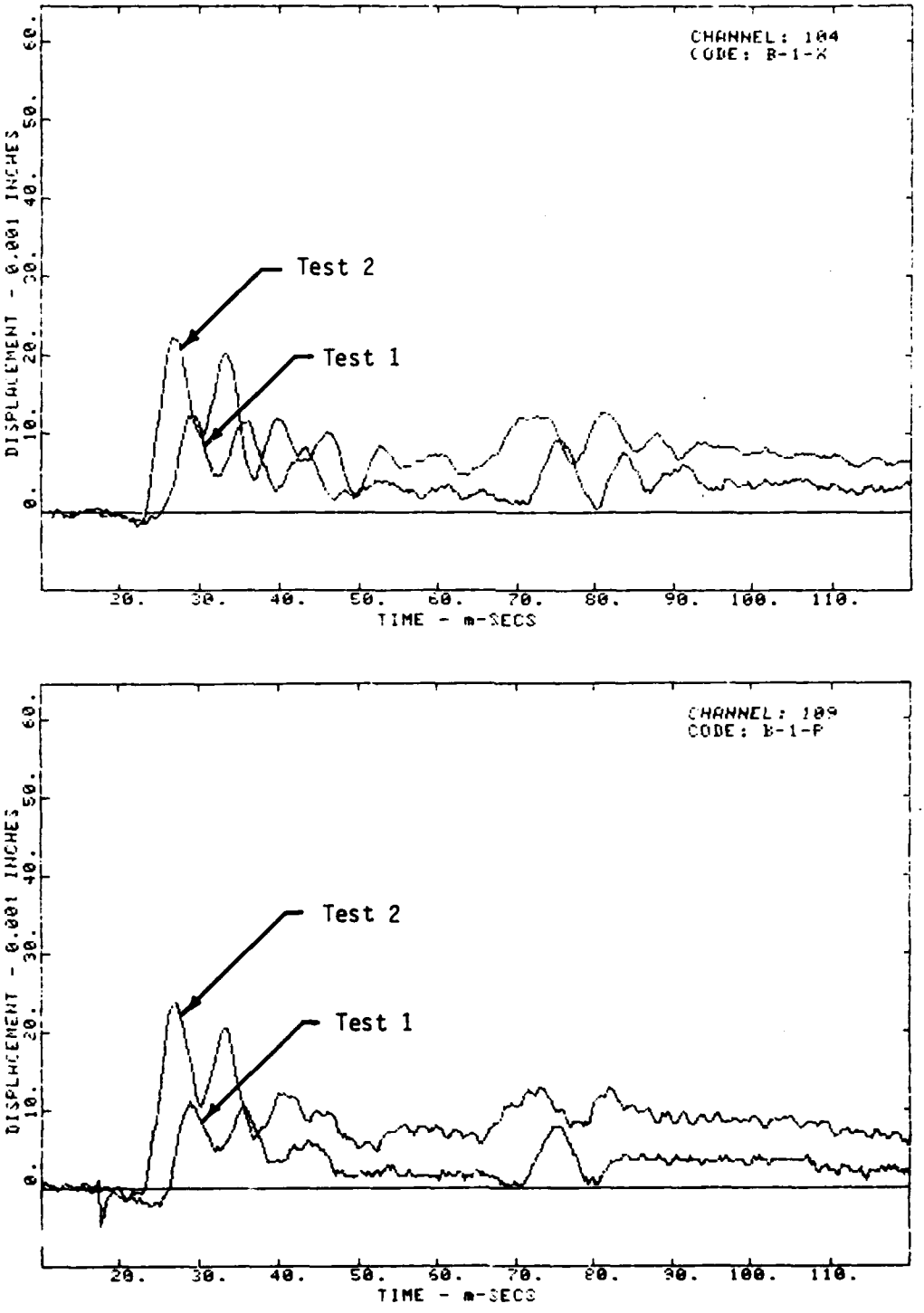

Figure 5-7. Relative displacement records, comparison between tests, back of tunnel, gages B-1-X and B-1-P.

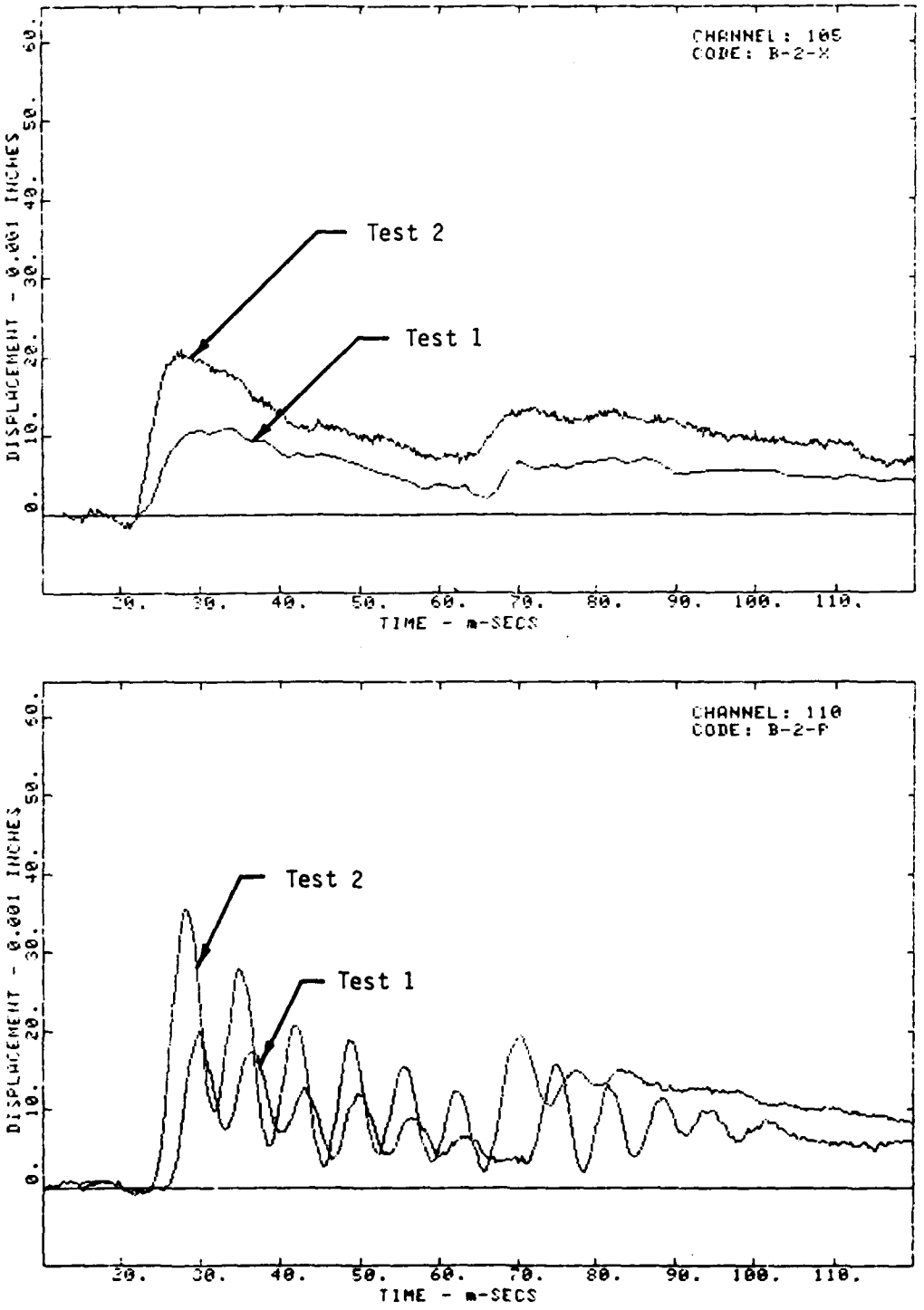

Figure 5-8. Relative displacement records, comparison between tests, right rib, gages B-2-X and B-2-P.

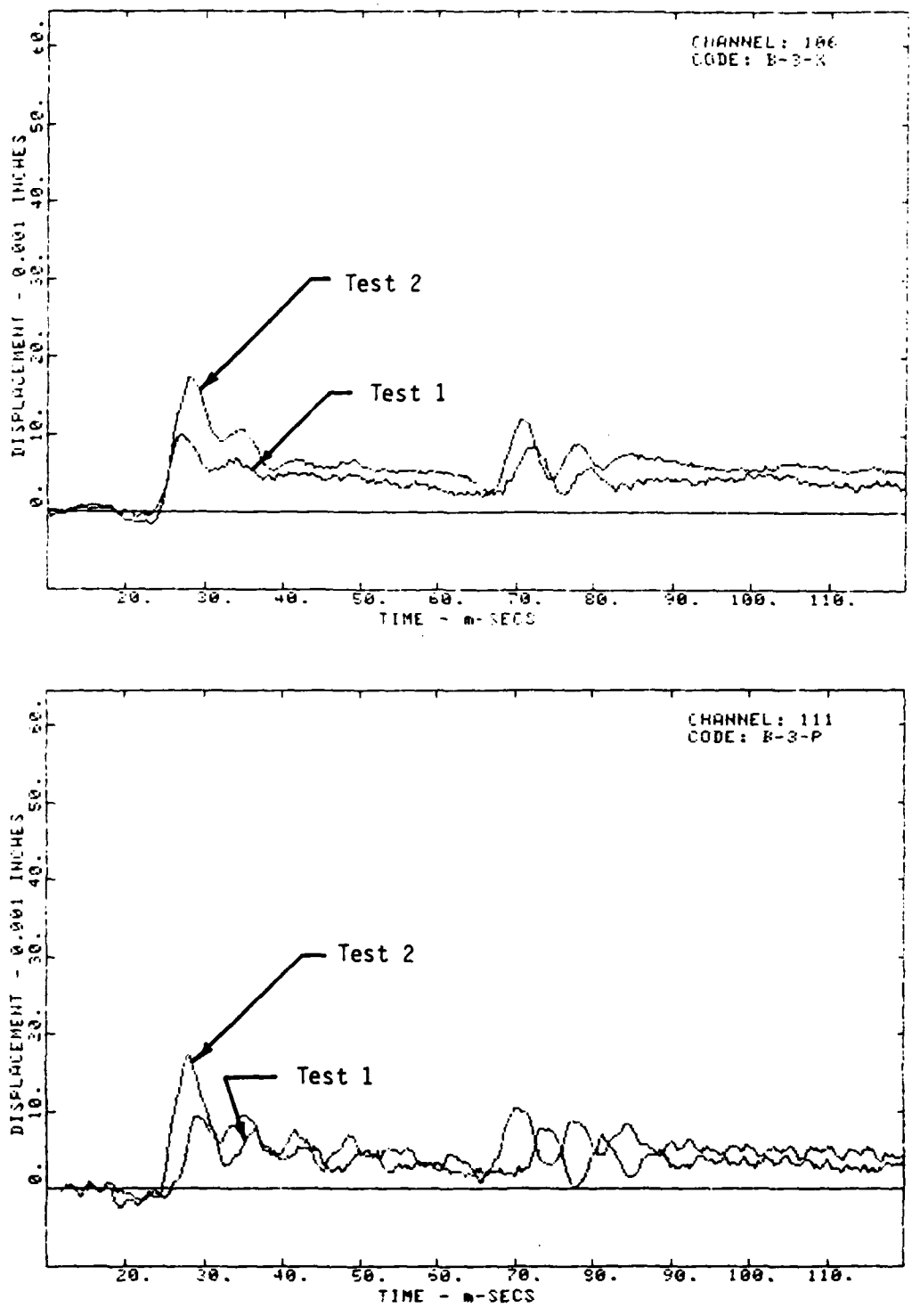

Figure 5-9. Relative displacement records, comparison between tests, right abutment, gages B-3-X and B-3-P.

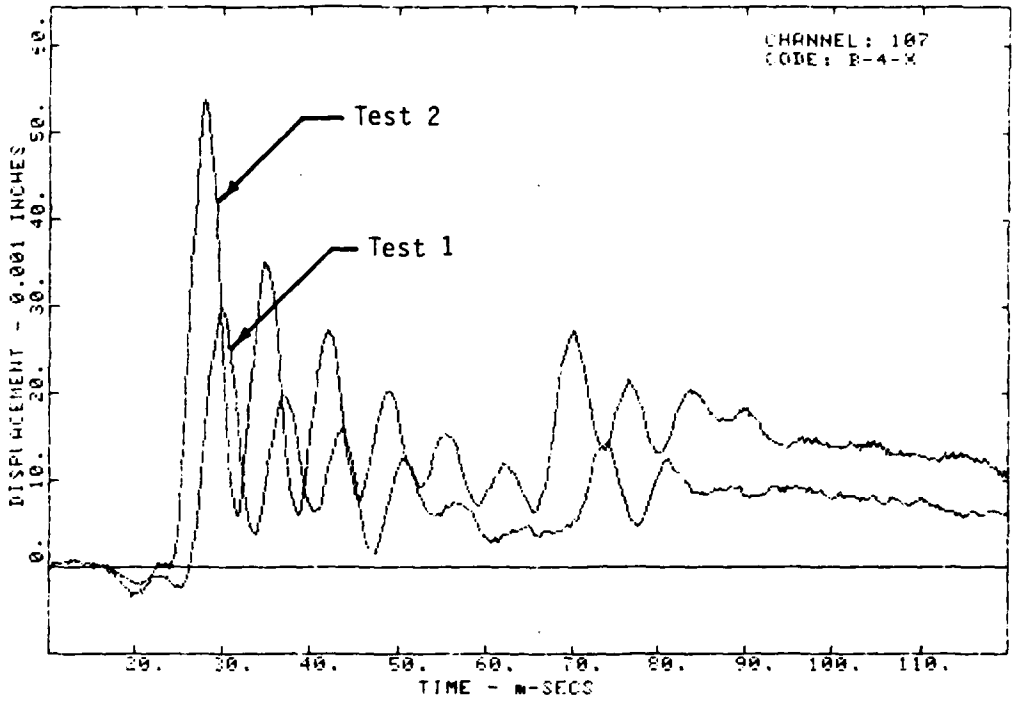

Figure 5-10. Relative displacement records, comparison between tests, invert, gage B-4-X.

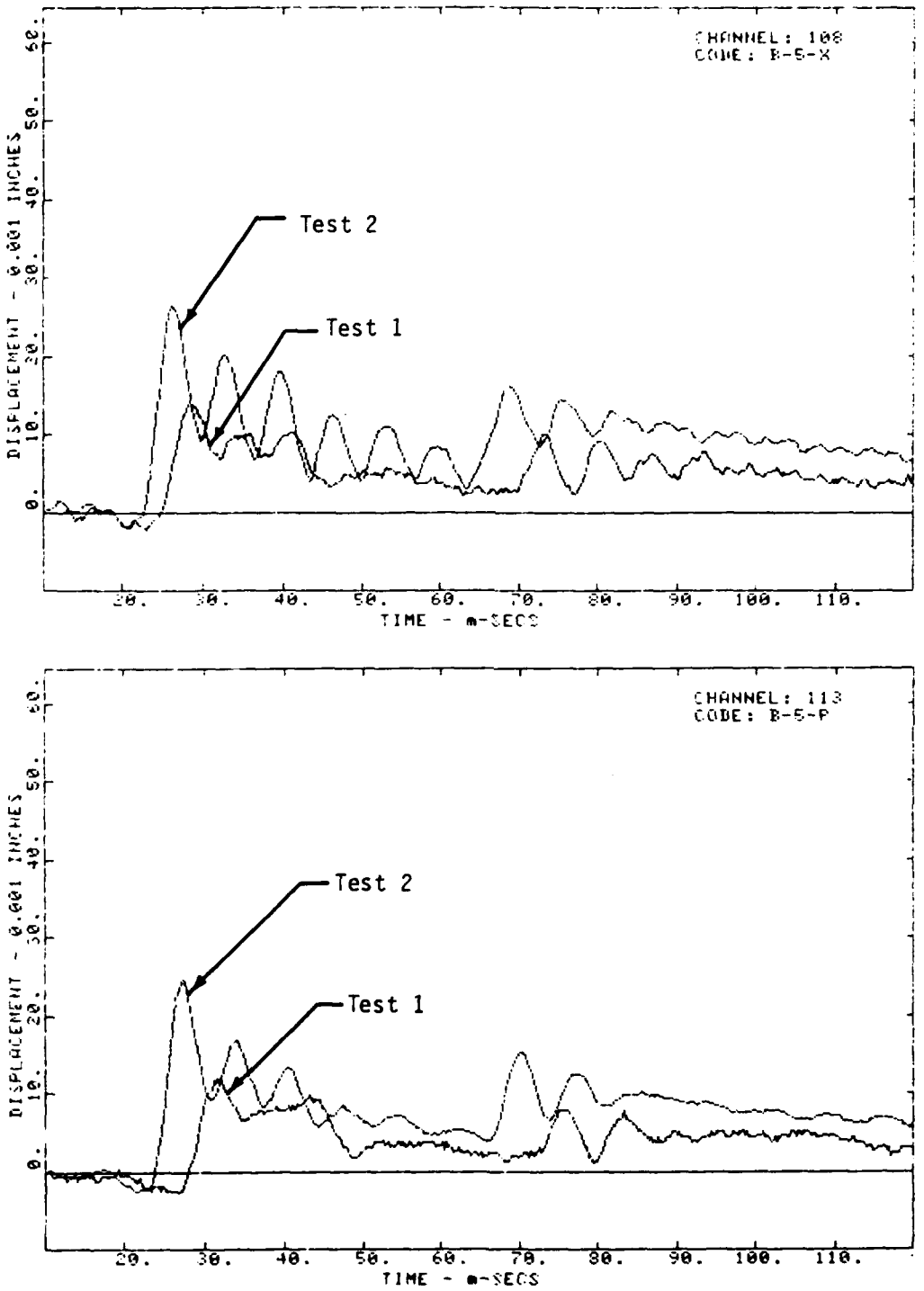

Figure 5-11. Relative displacement records, comparison between tests, left rib, gages B-5-X and B-5-P.

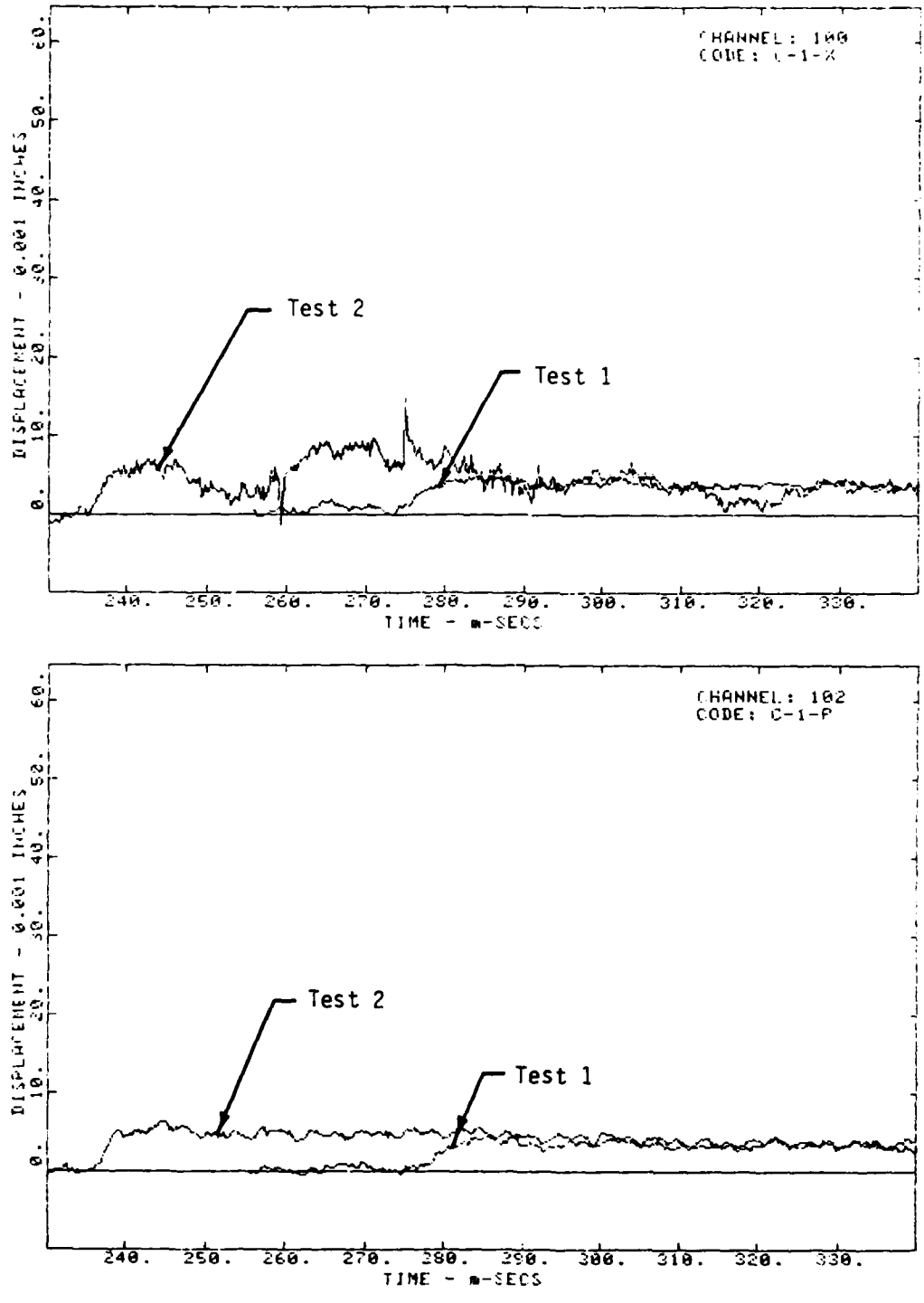

Figure 5-12. Relative displacement records, comparison between tests, back of tunnel, gages C-1-X and C-1-P.

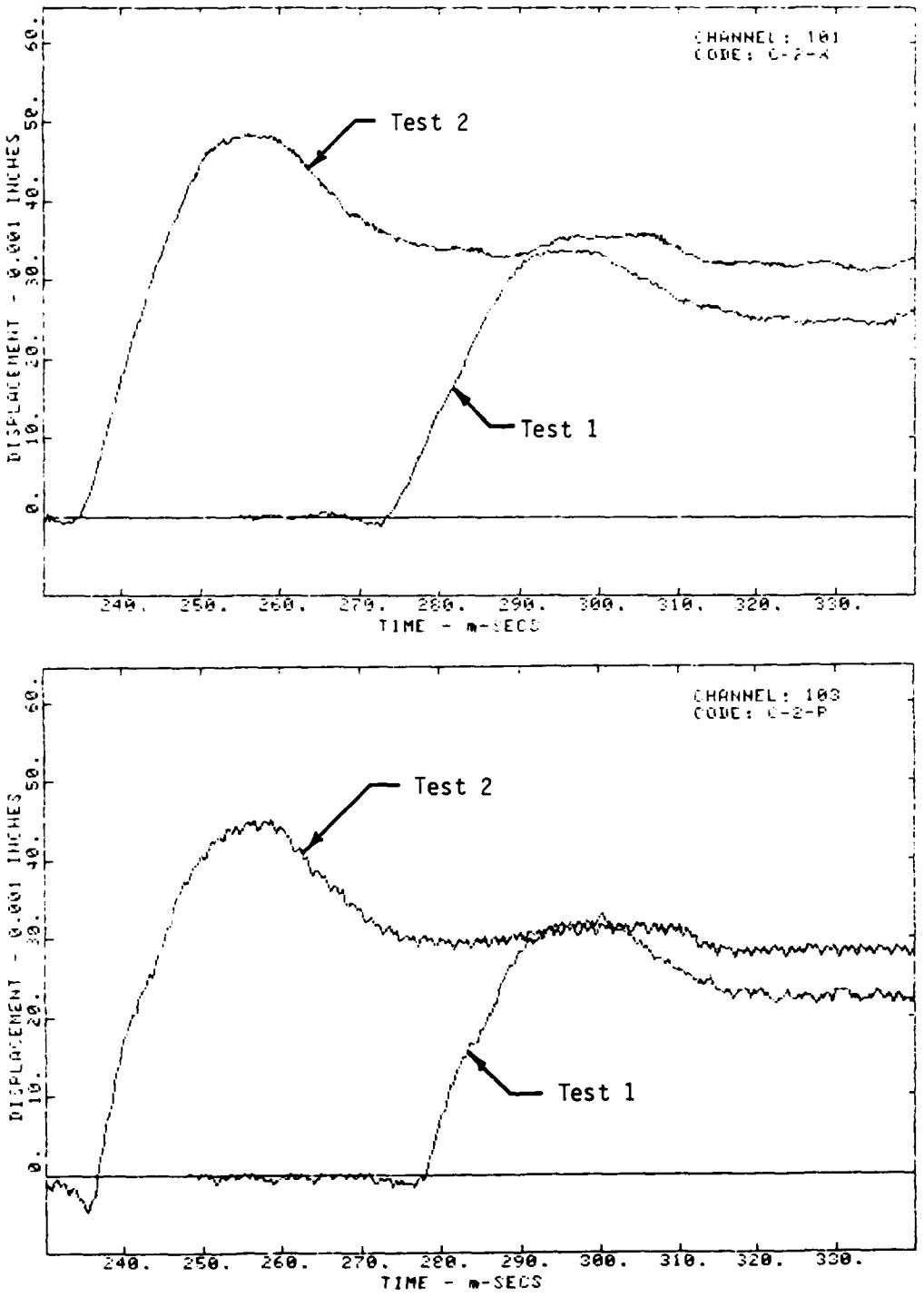

Figure 5-13. Relative displacement records, comparison between tests, right rib, gages C-2-X and C-2-P.

5.2 DISCUSSION OF GAGE RECORDS

As noted earlier, four of the displacement gages (A-1-X, A-2-X, B-2-X, and C-2-X) were configured with the transducer located at the collar of the borehole. These four gages provided significantly "smoother" records than most of those with the transducer located at the far end of the borehole. This phenomenon is apparent from comparison of the records from gages A-1-X, A-2-X, and B-2-X (Figures 5-2, 5-3, and 5-8, respectively) with the records of the companion gages. The record from gage C-2-X is also quite smooth (Figure 5-13) but the contrast between it and its companion gage is not so significant.

As noted in Section 2, the difference in gage behavior described above was anticipated prior to fielding the gages and was the reason for reversing four of the gages, even though we were concerned that the transducer might not survive the relatively severe environment near the collar of the borehole. In those gages with the transducer located at the far end of the borehole, the ground shock causes the anchor and the extensometer rod to move while the body of the LVDT remains stationary. The motion of the anchor causes a longitudinal oscillation of the extensometer rod which appears as a "ringing" signal in the gage records. On the other hand, when the sensor is placed at the collar of the borehole, the LVDT body moves while the extensometer rod remains stationary and the gage ringing does not occur.

The "ringing" signal has a period of approximately seven milliseconds (e.g., see Figure 5-8). The fundamental period of longitudinal vibration of a bar clamped at one end and free at the other end is given by (Reference 8):

$$T = 4L\sqrt{\rho/E}$$

where T = natural period

L = length

E = Young's Modulus

ρ = density

Using the properties of the steel rod provided by the manufacturer, the period is computed as 6.67 milliseconds, which is very close to the observed value. Consequently, we have concluded that the observed "ringing" signal does, in fact, represent longitudinal oscillation of the extensometer rod.

It is apparent from Figures 5-2 through 5-6 that the general character of each Test 2 record is very similar to that for the same gage in Test 1. Relative displacements from Test 2 are generally higher than those from Test 1 for all these records (also true for the other records discussed below). Furthermore, except for gages A-4-X and A-5-P (discussed later) and the "ringing" signal discussed above, the character of the Section A-A records is very similar from gage to gage.

A second rise in relative displacement may be seen in all of the records shown in Figures 5-2 through 5-6 at a time of about 40 milliseconds. This corresponds in time to the second peak in the airblast pressure measured by NMERI (see Figure 5-14, the test pressure-time history at Construction Station 6+20). The second pressure peak is caused by a reflection of the airblast off the face of the tunnel which was 29 feet (8.8 m) beyond the "upstream" end of the driver.

The records for the gages located at Section B-B exhibit the same similarity in character when Test 2 is compared to Test 1 (Figures 5-7 through 5-11), although the similarities are not quite so obvious because of the difference in shock arrival times between the two tests. When the records of one test are shifted in time so that the arrival times agree, the similarities are obvious. As an example, the records for gage B-1-P are shown in Figure 5-15 with the Test 1 record shifted.

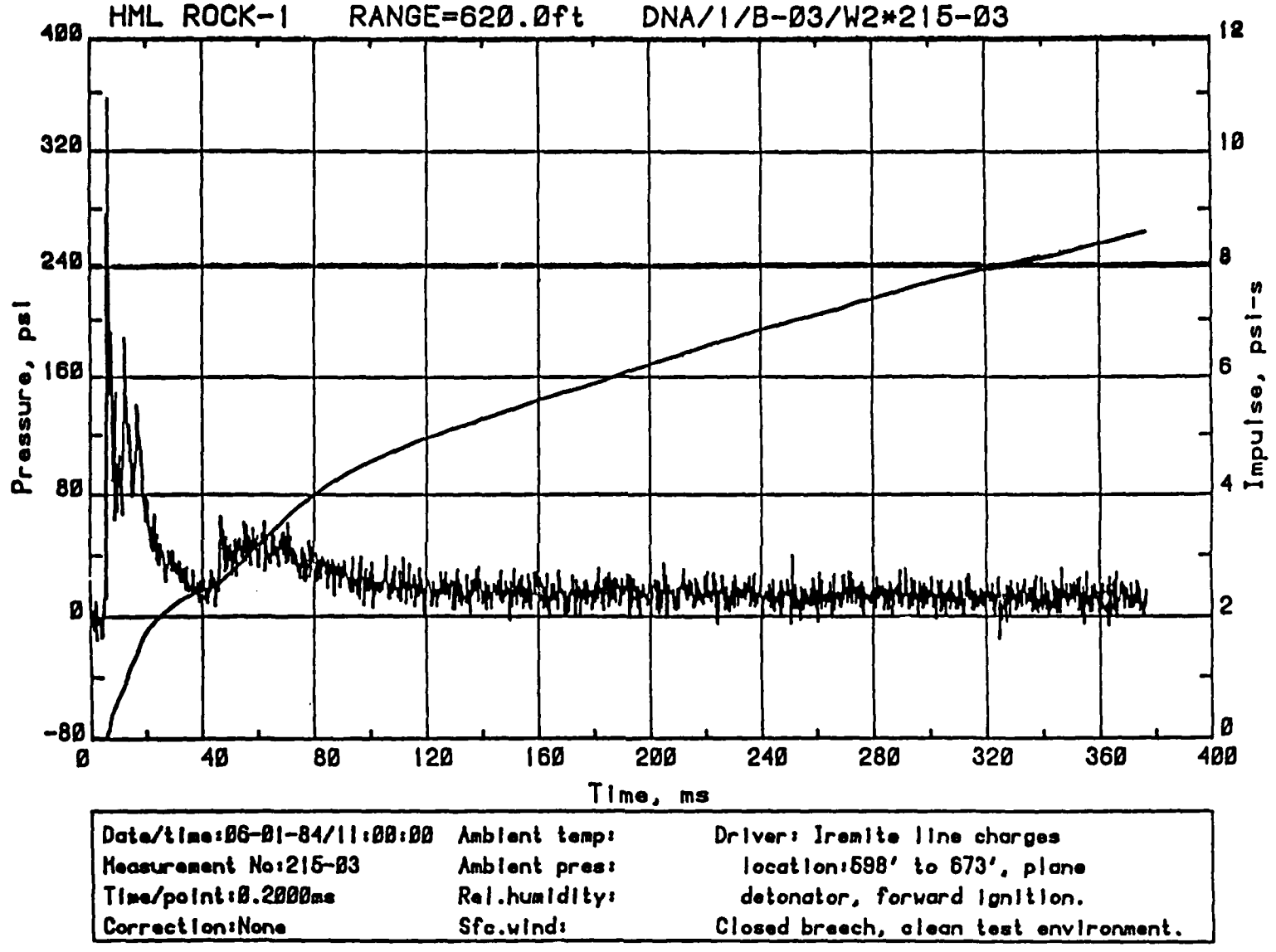

Figure 5-14. Pressure-time history at Construction Station 6+20, Test 1 (from NMERI).

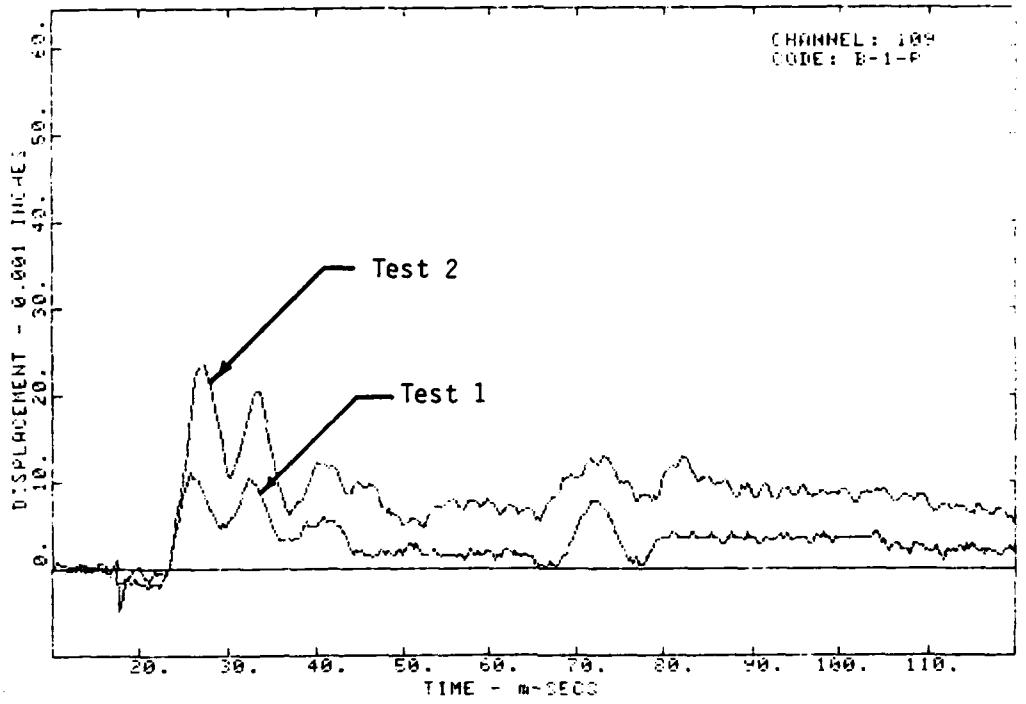

Figure 5-15. Relative displacement records, comparison between tests, back of tunnel, gage B-1-P (Test 1 record shifted so first arrival times agree).

Again, except for gage B-2-P (discussed later) the character of all records at Section B-B is similar from gage to gage.

In all of the records shown in Figures 5-7 through 5-11, very small negative displacements occur prior to the time at which the airblast in the tunnel reaches the gage location. This phenomenon is to be expected because the shock propagation velocity in the rock exceeds the velocity at which the airblast propagates down the tunnel and causes a small inward displacement of the rock near the tunnel surface due to the Poisson effect. We performed a two dimensional calculation of the blast wave propagating down the tunnel. The results of the calculation are consistent with the measured negative displacements.

A second rise in relative displacement may be seen in all the records shown in Figures 5-7 through 5-11 at a time of about 70 milliseconds. Again, this corresponds in time to the second peak in the airblast pressure record.

The records for the gages located at Section C-C also exhibit similar character when comparing Test 2 to Test 1 (Figures 5-12 and 5-13). However, there is a substantial difference in arrival times for the two tests. The Test 2 record for gage C-1-X (Figure 5-12), from the backup recorder, is noisy, but is the best record available. The records for gage C-1-P are shown in Figure 5-16 with the Test 1 record shifted so first arrival times agree. It is quite apparent that the two records are very similar in character.

Five of the gages (A-4-X, A-5-P, B-2-P, C-2-P, and C-2-X) exhibited what appears to be anomalous behavior. The belief that the behavior of these gages is anomalous is based on comparisons with other gage records and with the calculations discussed later. Each of these gages is discussed below.

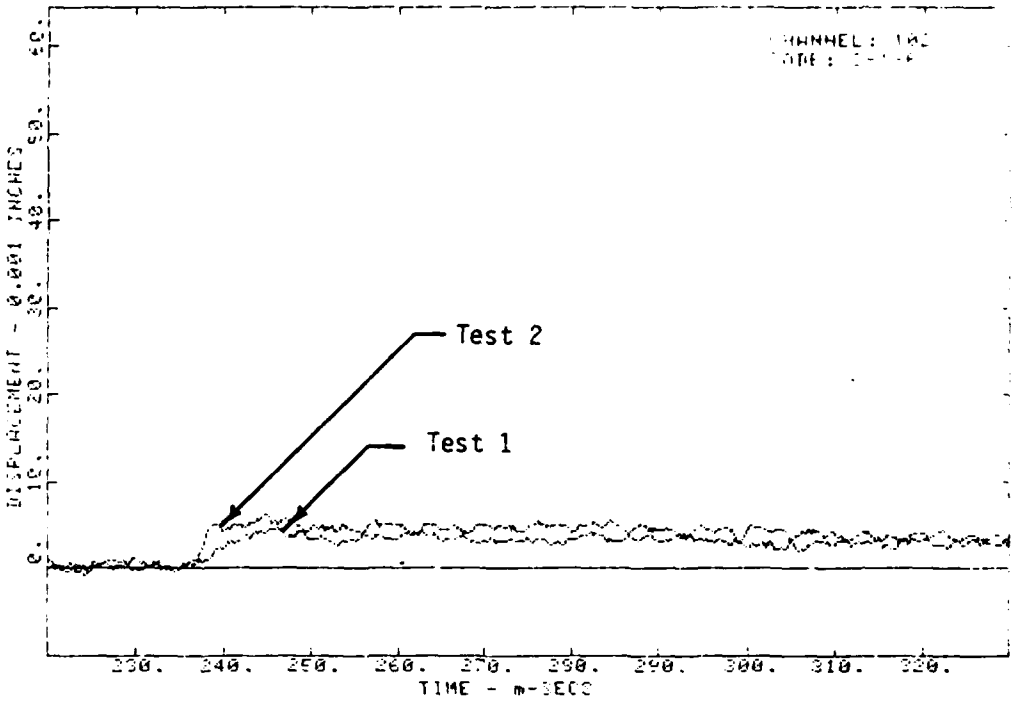

Figure 5-16. Relative displacement records, comparison between tests, back of tunnel, gage C-1-P (Test 1 record shifted so first arrival times agree).

Gage A-4-X (in the invert in the driver section of the tunnel) indicated a peak relative displacement on the order of eight times as large as the peaks measured by all other gages in Section A-A for each test. Also, the general character of these records (Figure 5-5) is substantially different from that of the other records in that the relative displacements at 100 milliseconds after shock arrival are still 61 and 53 percent of the peak values for Test 1 and 2, respectively. Furthermore, voltage measurements made after both tests also indicate much larger residual displacements than for other gages. We are not aware of any problem with either the fabrication or installation of this gage. The calibration has been carefully checked and is believed to be correct. Therefore, it appears there may have been a problem with the transducer and that the only way to determine the cause of the problem is to excavate the gage.

Gage A-5-P (in the left rib in the driver section) indicated considerably lower (more than a factor of two) relative displacements than its companion gage A-5-X and than the two gages directly across the tunnel in the right rib (gages A-2-X and A-2-P). The character of the records from this gage (Figure 5-6) also is completely different from that of the other gage records, including a much longer rise time, but is consistent between tests. While this gage was being grouted in place, the grout pump broke down and the grout line became plugged, although grout flow through the return line was eventually achieved. It is not clear whether the grouting problem contributed to the apparent anomalous behavior of the gage. However, the gage behavior is consistent either with poor anchorage at the collar of the borehole or with grout being forced into the gage and retarding the motion of the extensometer rod within the PVC pipe.

Gage B-2-P (in the right rib at Section B-B) indicates relative displacements somewhat higher than its companion gage (B-2-X) and the two gages directly across

the tunnel in the left rib (gages B-5-X and B-5-P). However, the character of the gage records (Figure 5-8) is quite similar to that for the other gages at this location which have the transducer at the far end of the borehole. We are not aware of any problems with either fabrication or installation of this gage. The higher apparent readings may simply be the result of overshoot caused by "ringing" of the gage.

Gages C-2-X and C-2-P (in the right rib at Section C-C) indicated relative displacements much higher than expected. Also, the general character of the records (Figure 5-13) is different from that of other records in that the relative displacements remain quite high (similar to gage A-4-X discussed above). The Sulfaset® plugs at the collars of the boreholes were installed without inserting grout return lines for both of these gages. This required drilling through the plugs to insert the grout return lines prior to grouting the gages in place. Although we did not observe this grouting operation, it was reported that "they had trouble grouting the gages." It is certainly not obvious that a problem with grouting these gages in place can explain the apparent anomalous behavior of the gages because the records are nearly identical from gage to gage and from test to test even though gage C-2-X had the transducer at the collar and gage C-2-P had the transducer at the far end of the borehole. If improper anchorage occurred, we would expect to see substantial differences in the gage records. It is possible, although not probable, that both transducers malfunctioned in the same way. It is also possible, of course, that these records truely represent the behavior of the rock in the region of shallow overburden near the portal.

5.3 COMPARISON OF GAGE RECORDS AND CALCULATIONS

As described in Section 2, pretest predictions were made using the material properties shown in Table 2-1 and a predicted pressure-time history provided by

NMERI (Figure 2-18). The actual pressure-time histories measured by NMERI (Reference 3) were significantly different from the prediction. The record from a static pressure gage located at Construction Station 6+20 (approximately 30 feet (9.1 m) "downstream" from Section A-A of Figure 5-1) was provided earlier in Figure 5-14. The same record is shown with an expanded time scale for the first 50 milliseconds in Figure 5-17.

After receiving the Test 1 pressure records from NMERI, we recalculated the rock displacements in the driver section and compared the results to our gage records. From this comparison, it was apparent that the rock at the tunnel surface had not reached peak absolute displacement before the far end of the gages began to move.

As discussed in Section 2, the displacement gages actually measure relative displacement over the gage length and will only provide peak absolute displacements for certain combinations of gage length and shock propagation velocity. It appeared that the shock propagation velocity was considerably higher than we initially assumed (3,655 feet per second (1,114 mps)). Our preliminary observations were discussed with DNA personnel following the second test. As a result of this discussion, a hole 60 feet (18.3 m) in length was drilled in the right rib near Section A-A. Sonic velocities were measured at six locations in this borehole by Fenix & Scisson personnel. The highest measured velocity was 6,977 feet per second (2,127 mps), the lowest was 6,316 feet per second (1,925 mps), and the average was 6,475 feet per second (1,974 mps).

Using the above information and the pressure-time history shown in Figures 5-14 and 5-17, we recalculated rock displacements in the driver section using shock propagation velocities of 7,000 and 5,000 feet per second (2,134 and 1,524 mps). The velocity was changed by modifying the assumed value of Young's Modulus for the

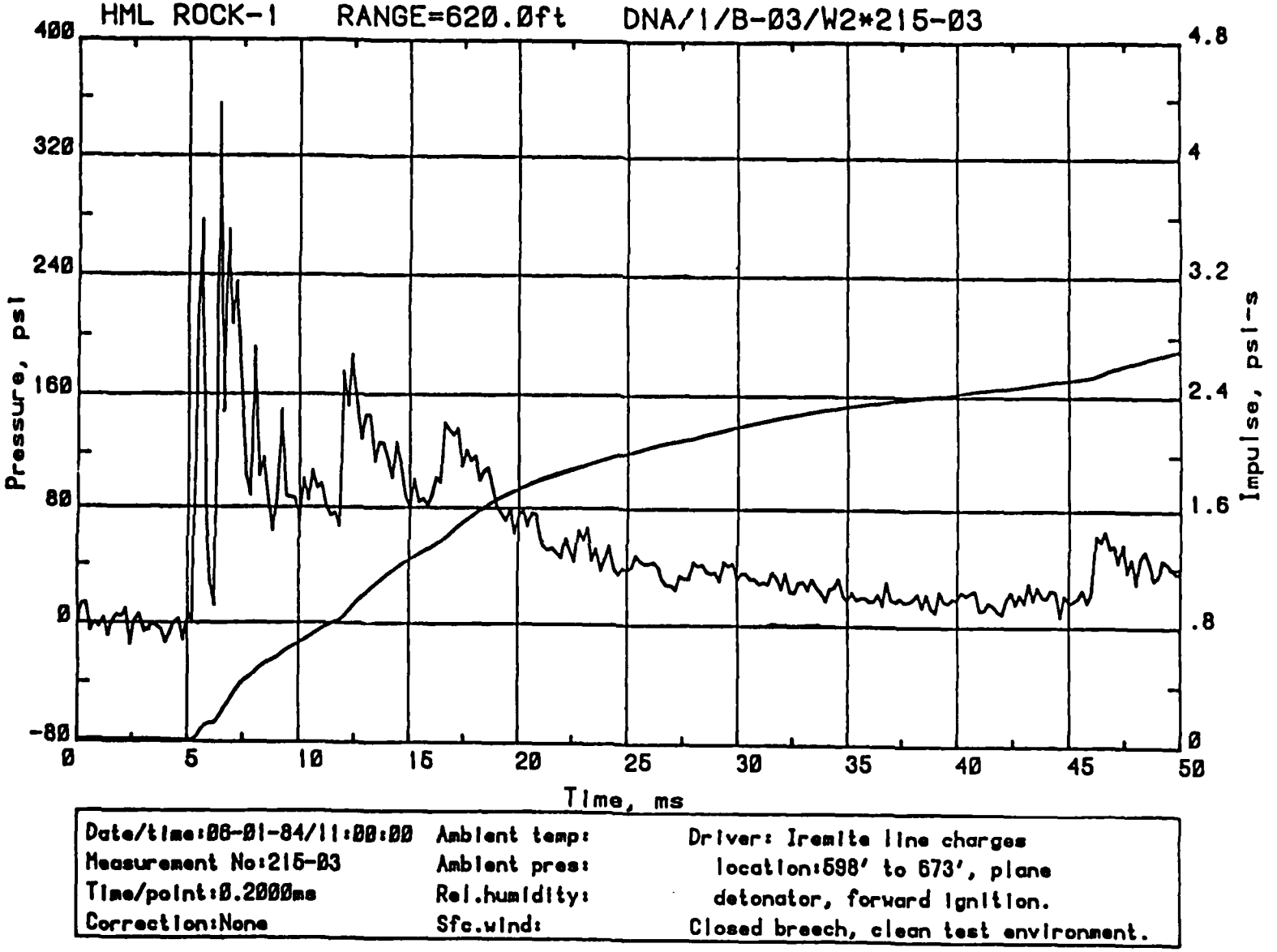

Figure 5-17. Pressure-time history at Construction Station 6+20 with expanded time scale, Test 1 (from NMERI).

rock and keeping all other assumed material properties constant. The assumed values of Young's Modulus were 240,000, 448,150, and 878,500 psi (1,655, 3,090, and 6,057 MPa) corresponding to velocities of 3,655, 5,000, and 7,000 feet per second (1,114, 1,524, and 2,134 mps), respectively. The calculated relative displacements (over a gage length of 27 feet-two inches (8.3 m)) at the back of the tunnel in the driver section are shown in Figure 5-18. Comparison of these calculated relative displacements with the Test 1 record from gage A-1-X indicated that a shock propagation velocity of 5,000 feet per second (1,524 mps) provided a reasonable match. The propagation of a relatively high pressure shock wave at a velocity somewhat less than the very low pressure seismic signal measured by the sonic tests appears to be quite reasonable.

As noted earlier, the pressure gage fielded by NMERI was approximately 30 feet (9.1 m) downstream from our Section A-A gages. Therefore, the Test 1 pressure-time history shown in Figures 5-14 and 5-17 was shifted to the left by 2.5 milliseconds. The magnitude of the time shift was based on 12,000 feet per second (3,658 mps) burn velocity (provided by NMERI) for the Iremite.

The calculated relative displacement at the back of the tunnel (using a shock propagation velocity of 5,000 feet per second (1,524 mps) and the 2.5 millisecond time shift) is compared to the Test 1 record from gage A-1-X in Figure 5-19. The same two records are shown in Figure 5-20, except the calculated record has been shifted to the right so that the peak relative displacements occur at the same time (12 milliseconds). A comparison of calculated absolute and relative displacement for the back of the tunnel is shown in Figure 5-21.

Comparisons of measured and calculated relative displacements are presented below for both tests. All of the calculations were done using a shock propagation velocity of 5,000 feet per second (1,524 mps), corresponding to a Young's Modulus of

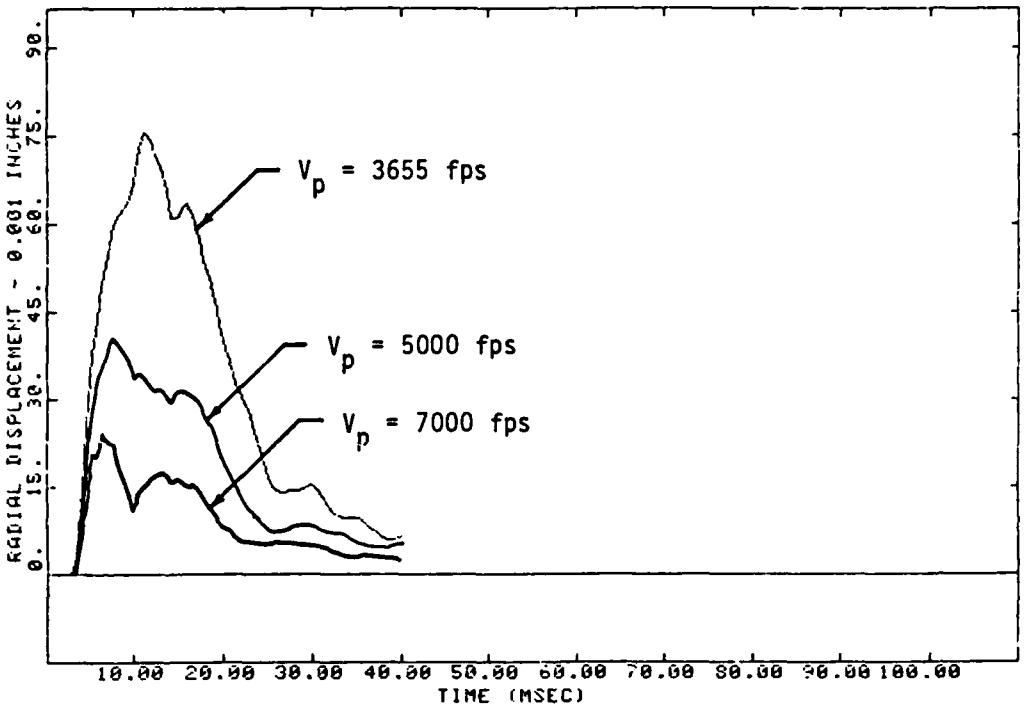

Figure 5-18. Comparison of calculated relative displacement at back, driver section, 27 foot-two inch gage length, Test 1.

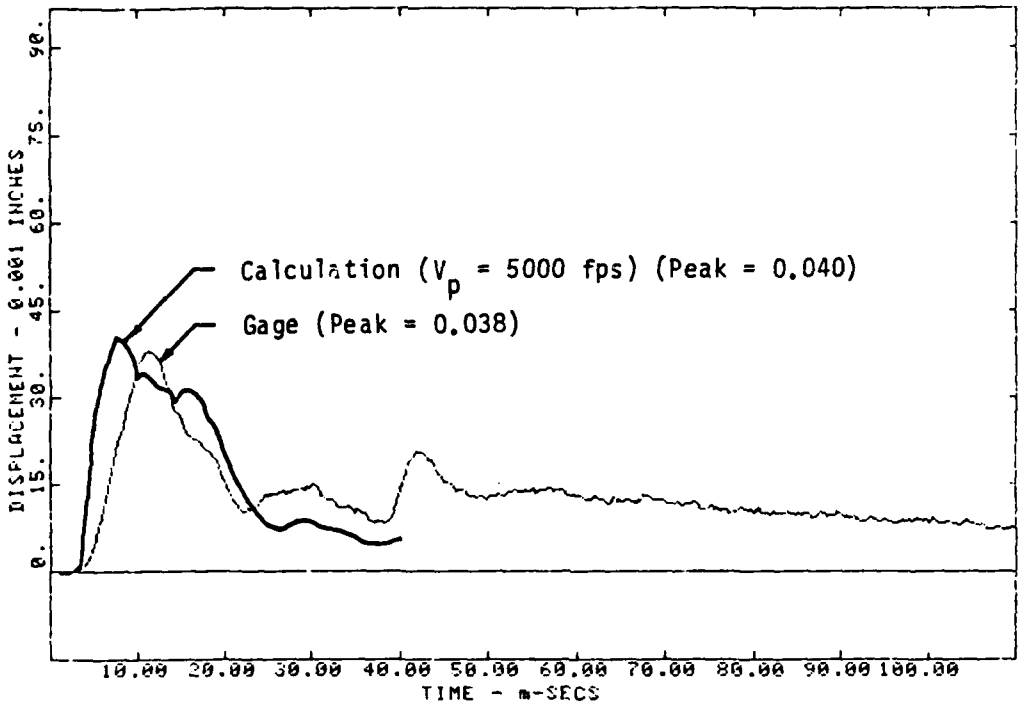

Figure 5-19. Comparison of calculated and measured relative displacement at back of tunnel, 27 foot-two inch gage length, Test 1.

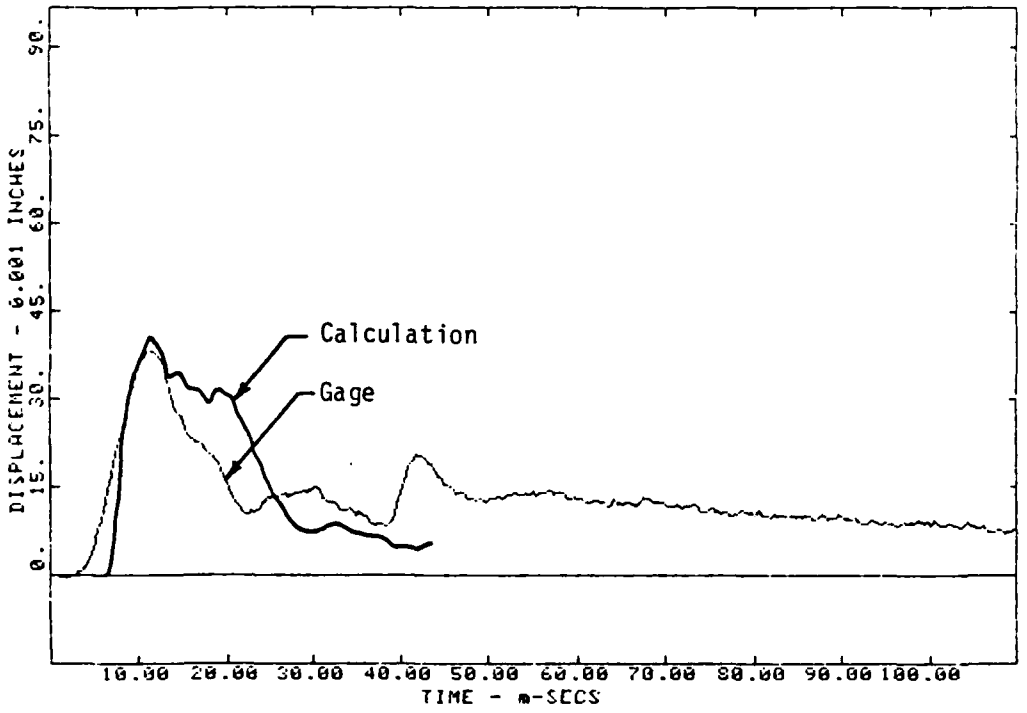

Figure 5-20 Records from Figure 5-19 with calculated record shifted to match time of peak displacements.

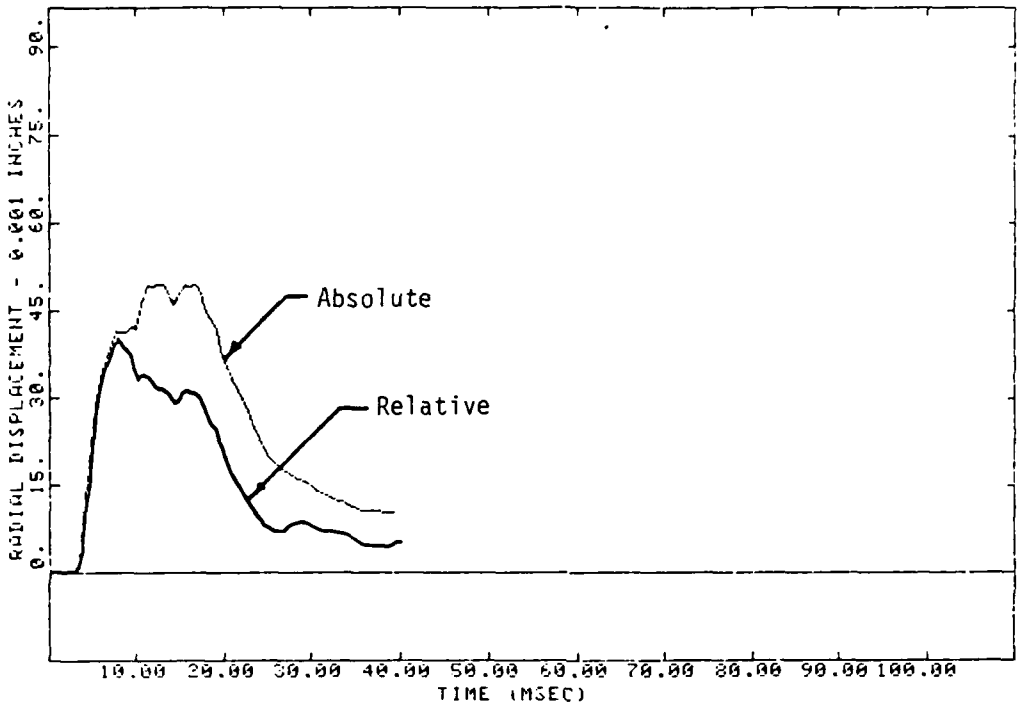

Figure 5-21. Comparison of calculated absolute and relative displacements, back of tunnel, Test 1.

448,150 psi (3,090 MPa). In each case, the input to the calculation was a pressure record provided by NMERI (Reference 3). Since none of the NMERI pressure gages were located at precisely the same construction station as any rock displacement gage, it was necessary to adjust arrival times accordingly. This was accomplished by plotting, for each test, airblast wave arrival time against distance along the tunnel and determining from the appropriate curve the arrival times for each of our gage locations.

Comparisons of gage records and calculated relative displacements for the gages located at Section A-A are shown in Figures 5-22 through 5-26. In each case, the comparison for Test 1 is at the top of the figure and the comparison for Test 2 is at the bottom of the figure. Also, the two companion gage records (where they exist) are shown on the same plot in solid line and are identified by gage number. The calculated relative displacements are shown as dashed lines. For convenience, the two plots from Figure 5-19 are repeated in Figure 5-22.

In each case, the calculated relative displacement slightly leads the measured value. This is not surprising when one considers the manner (described above) in which it was necessary to adjust arrivals from pressure gage locations to displacement gage locations. In the case of Section A-A the pressure gage was located at Construction Station 6+20 and the displacement gages were located at Construction Stations 6+49 and 6+51.

In general, there is reasonable agreement (except for gages A-4-X and A-5-P, discussed earlier) between calculated and measured relative displacements. The best agreement is at the back of the tunnel (Figure 5-22), followed by the right rib (Figure 5-23) and the right abutment (Figure 5-24). We believe it would be possible to obtain a match between calculated and measured values for both ribs and the right abutment similar to that shown for the back of the tunnel by making minor

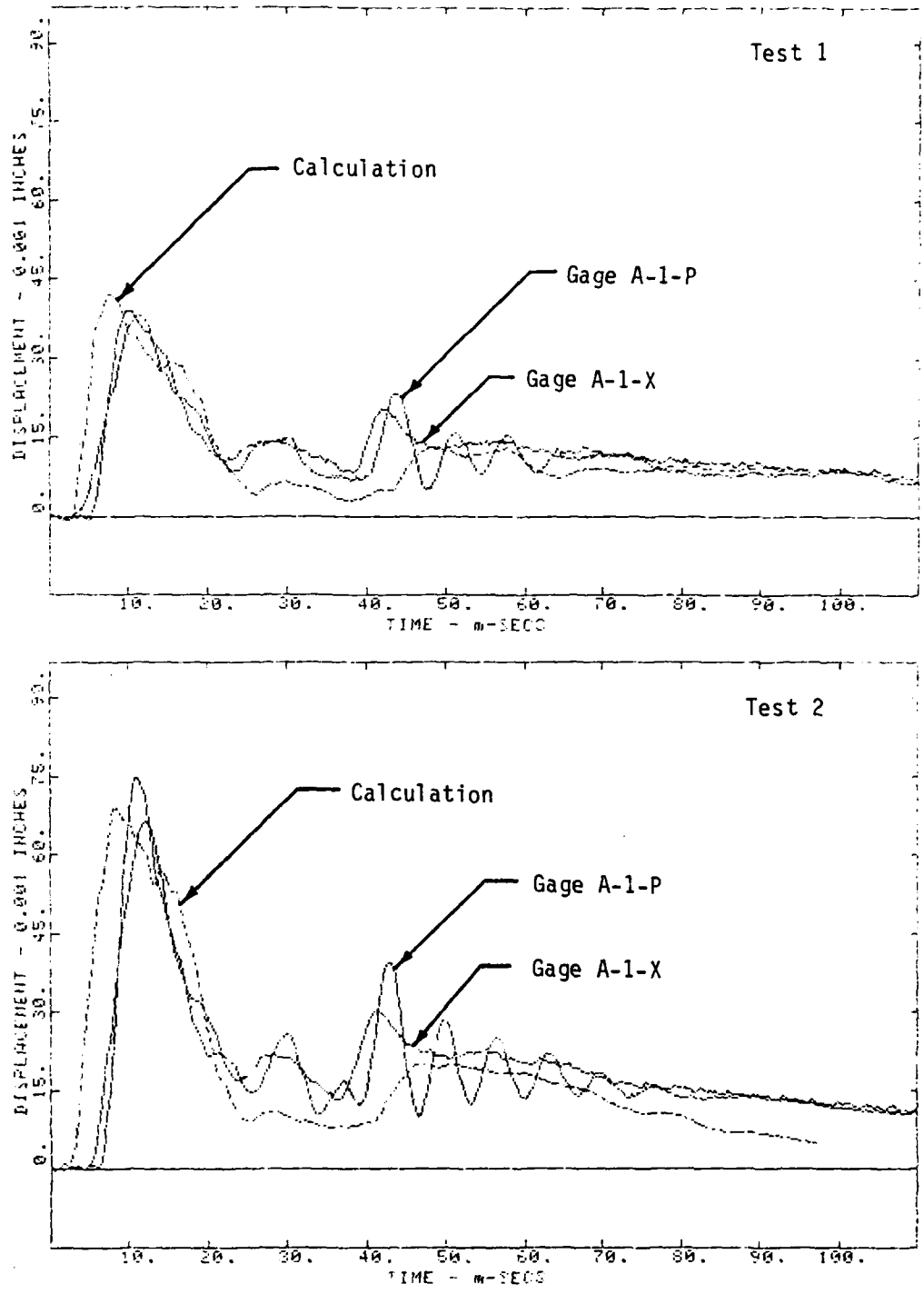

Figure 5-22. Comparison of calculated and measured relative displacements, gages A-1-X and A-1-P.

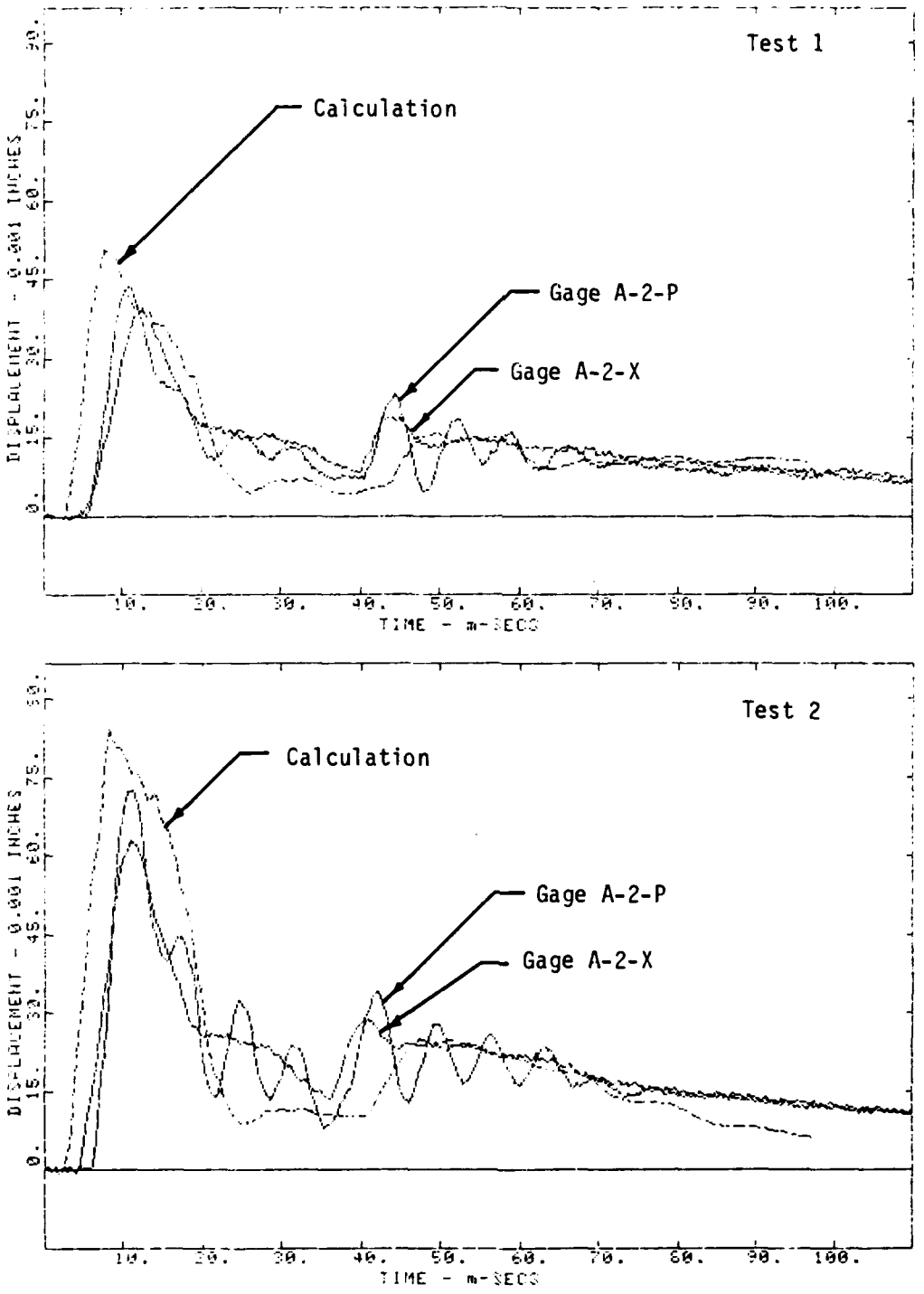

Figure 5-23. Comparison of calculated and measured relative displacements, gages A-2-X and A-2-P.

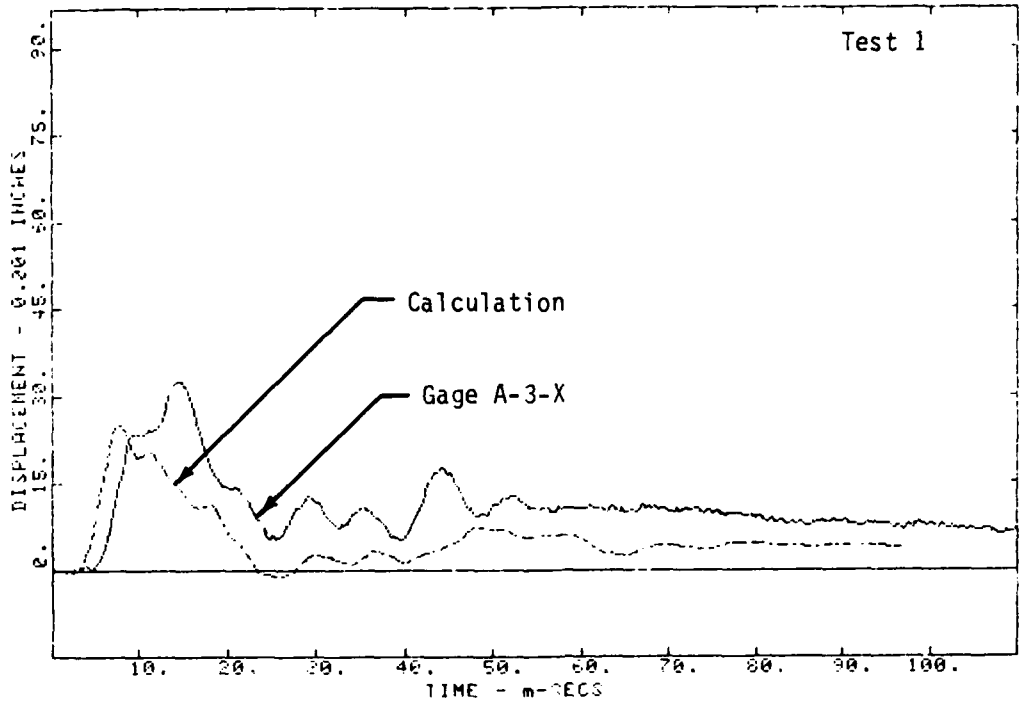

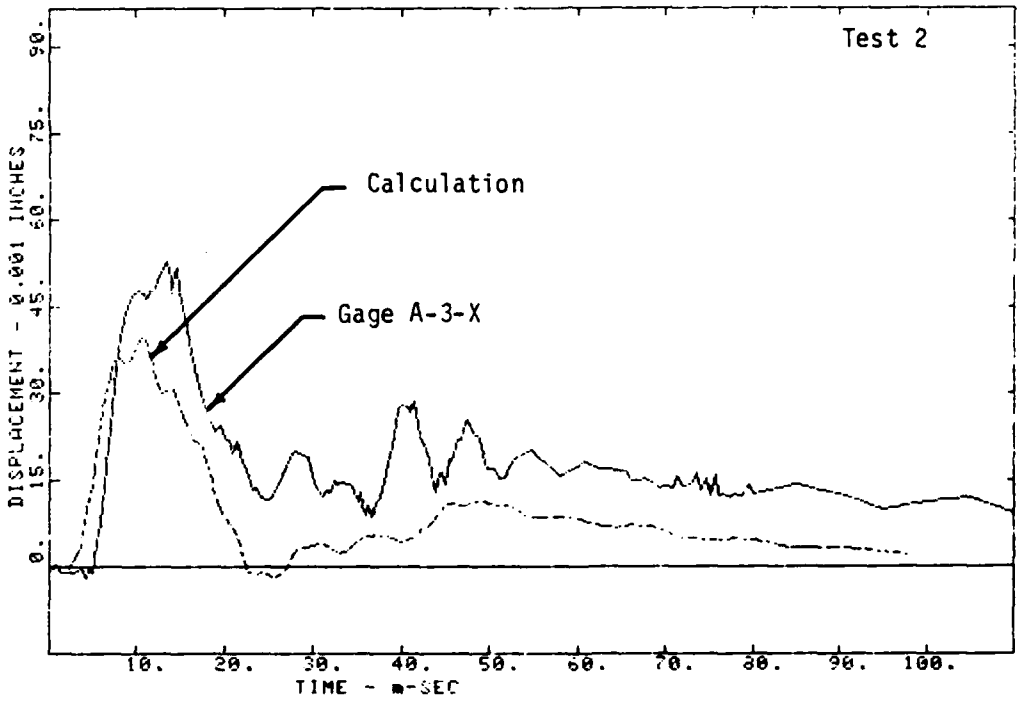

Figure 5-24. Comparison of calculated and measured relative displacements, gage A-3-X.

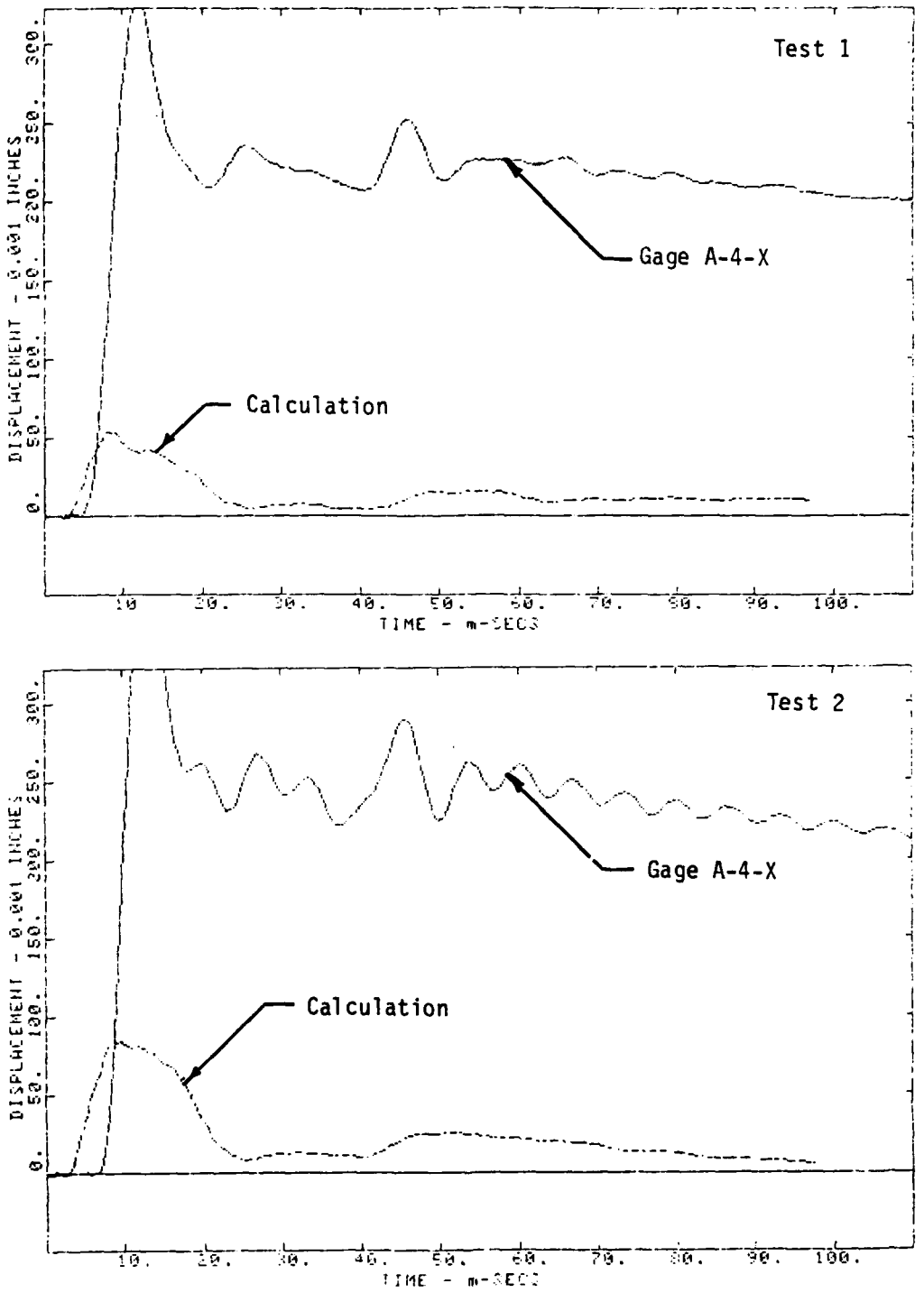

Figure 5-25. Comparison of calculated and measured relative displacements, gage A-4-X.

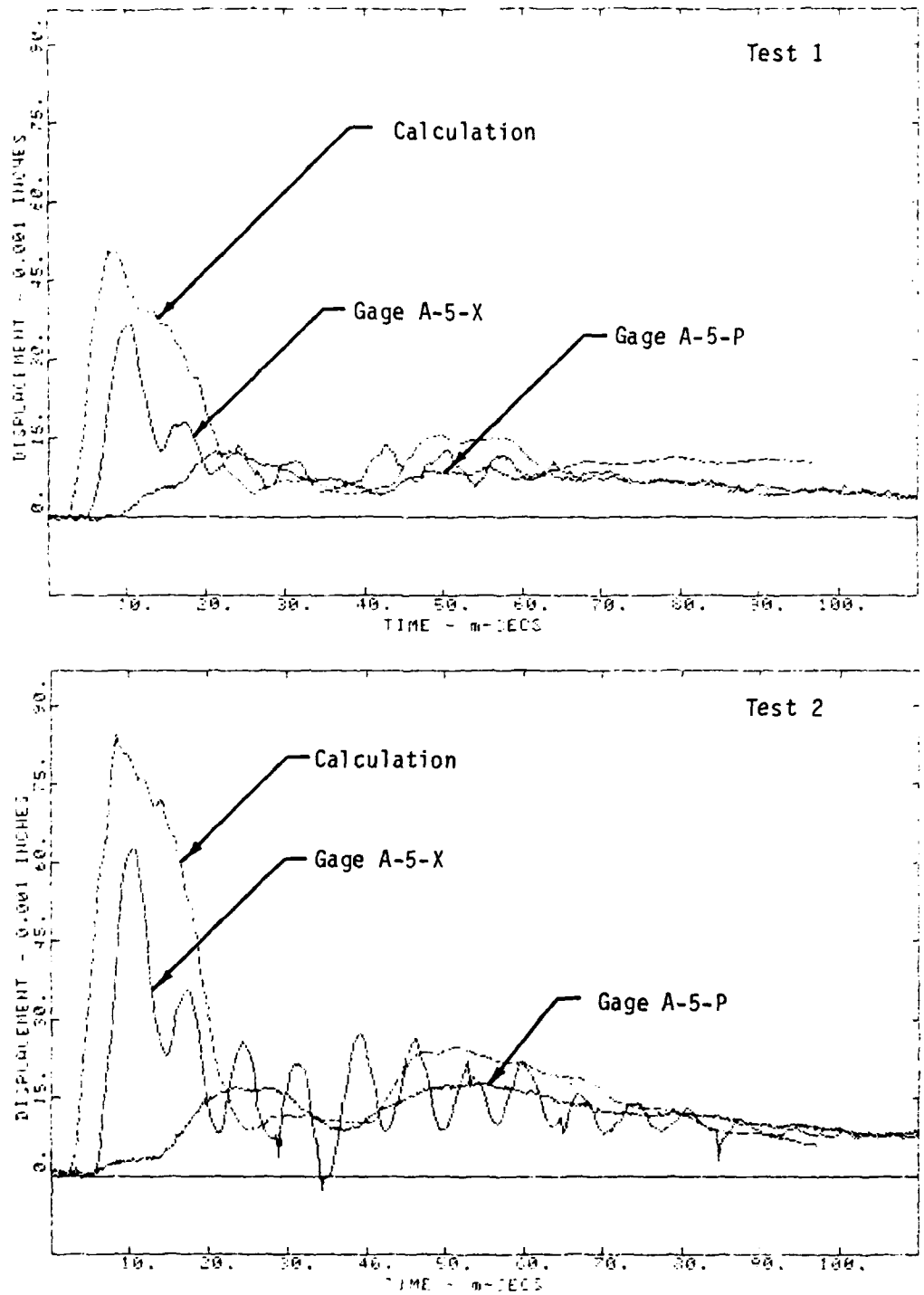

Figure 5-26. Comparison of calculated and measured relative displacements, gages A-5-X and A-5-P.

adjustments in the shock propagation velocity, although we have not attempted to do so.

Comparisons of gage records and calculated relative displacements for the gages located at Section B-B are shown in Figures 5-27 through 5-31. The calculated curves are based on pressure records from gages located at Construction Station 5+75, while the displacement gages were located at Construction Stations 5+59 and 5+61. Again, the calculated values are shown as dashed lines and the gage records as solid lines. In the comparisons for the second test (lower half of each figure), two calculations are shown because the two adjacent pressure gages at station 5+75 registered significantly different pressure records. These calculations are identified by the number of the appropriate NMERI pressure gages as given in Reference 3.

In each case, the calculated relative displacement leads the measured value by up to about five milliseconds. Part of this discrepancy is probably due to inaccuracies in adjusting arrival times between the pressure gage and displacement gage locations. Also, the calculations do not account for the small negative (inward) displacements discussed earlier.

In general there is reasonable agreement between calculated and measured relative displacements, although not as good as at Section A-A. A fundamental assumption underlying the calculations is that the pressure is uniform throughout the tunnel cross section at any particular time. This assumption may very well not be true. In any case, the differences between calculated and measured relative displacements are of the same order as the difference between the pressures recorded by pressure gages 213 and 214.

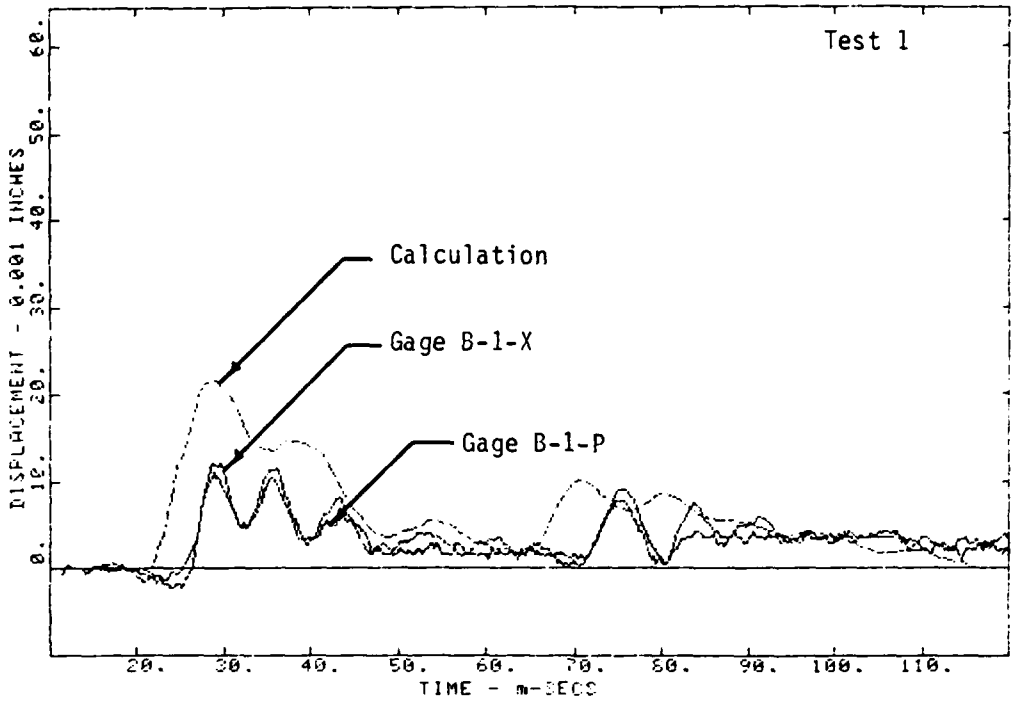

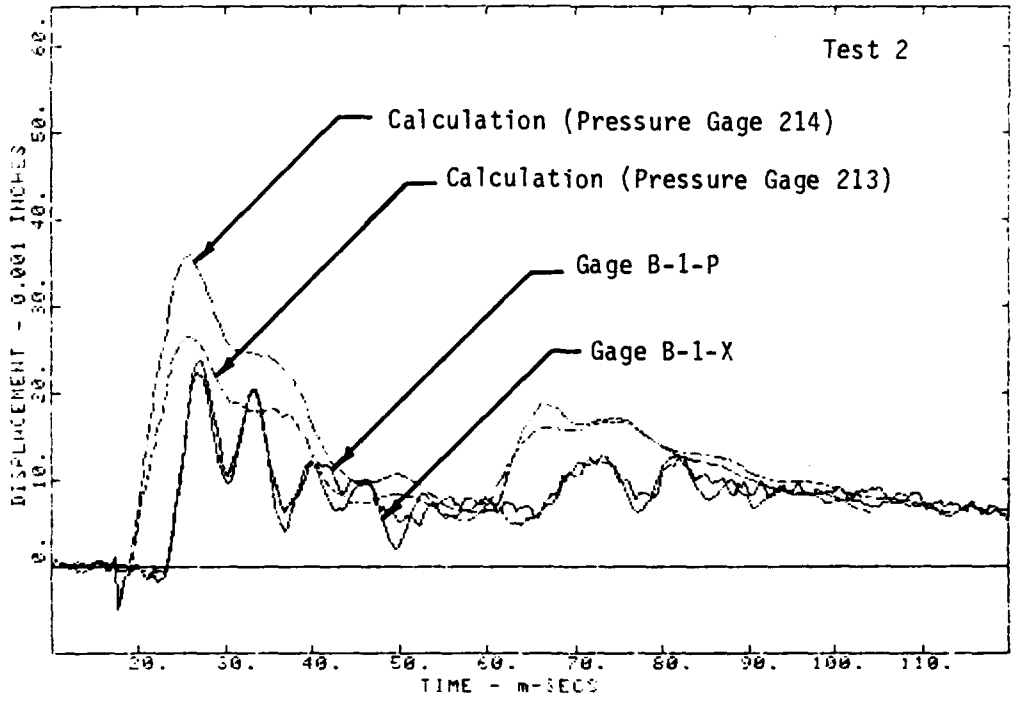

Figure 5-27. Comparison of calculated and measured relative displacements, gages B-1-X and B-1-P.

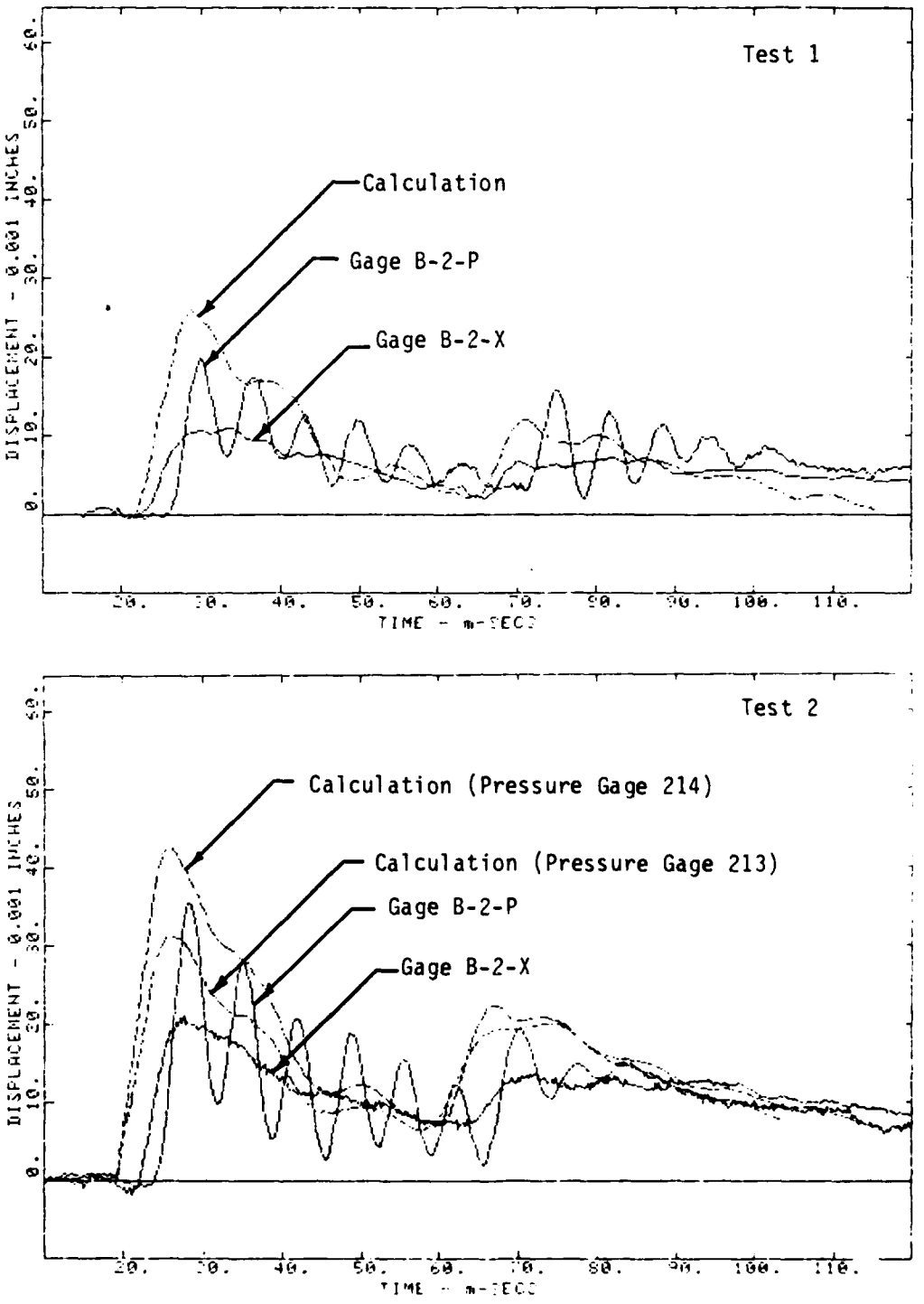

Figure 5-28. Comparison of calculated and measured relative displacements, gages B-2-X and B-2-P.

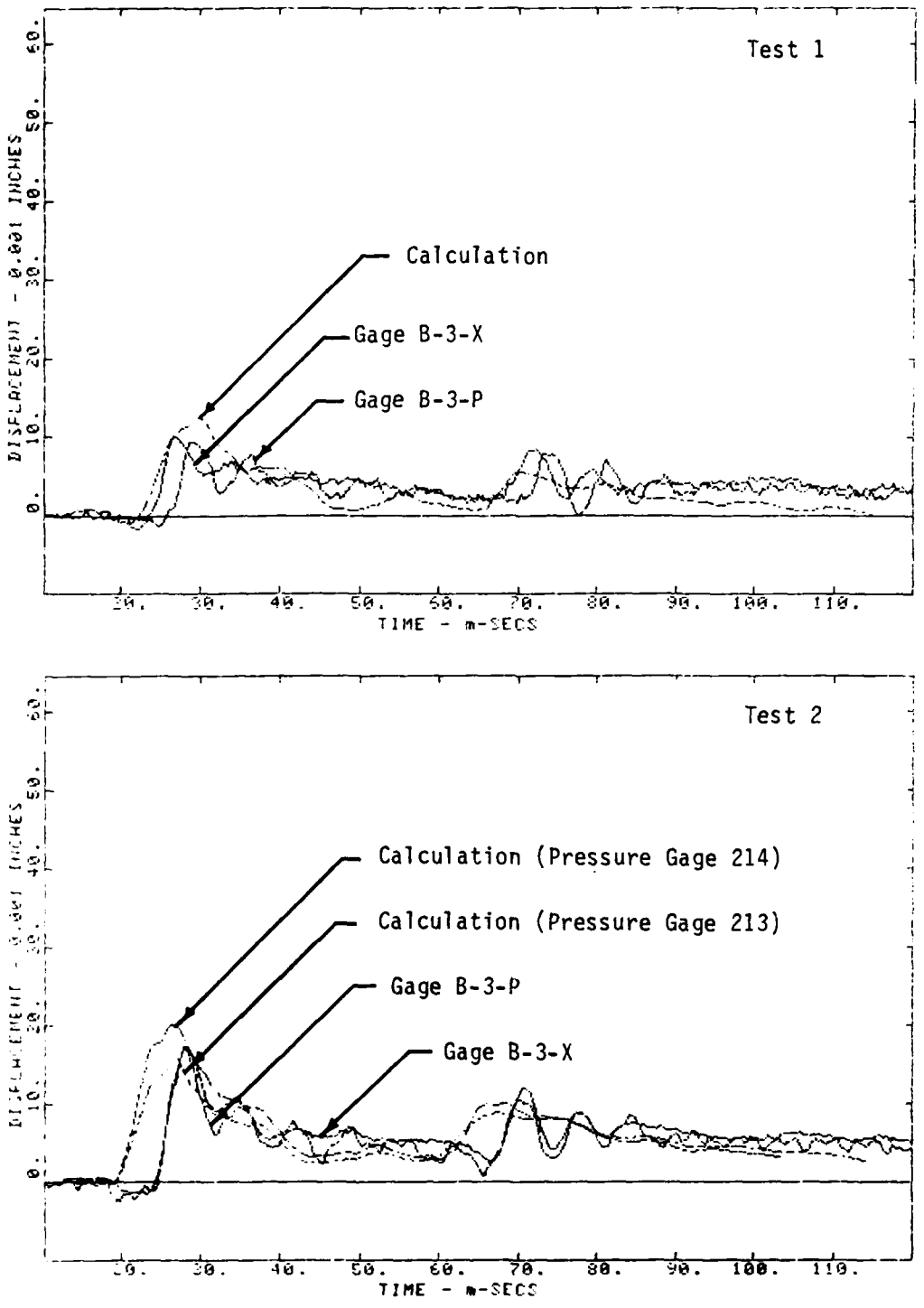

Figure 5-29. Comparison of calculated and measured relative displacements, gages B-3-X and B-3-P.

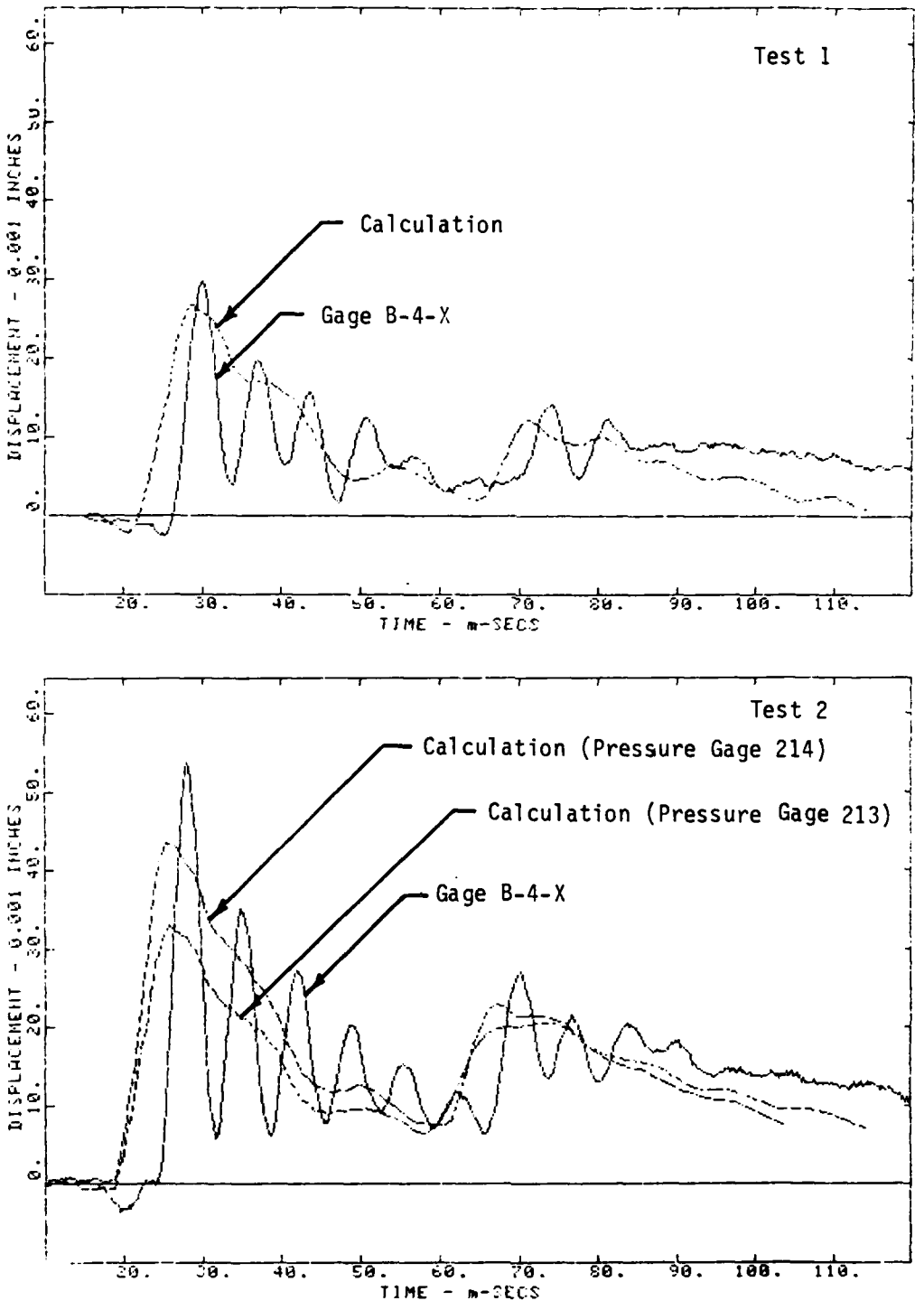

Figure 5-30. Comparison of calculated and measured relative displacements, gage B-4-X.

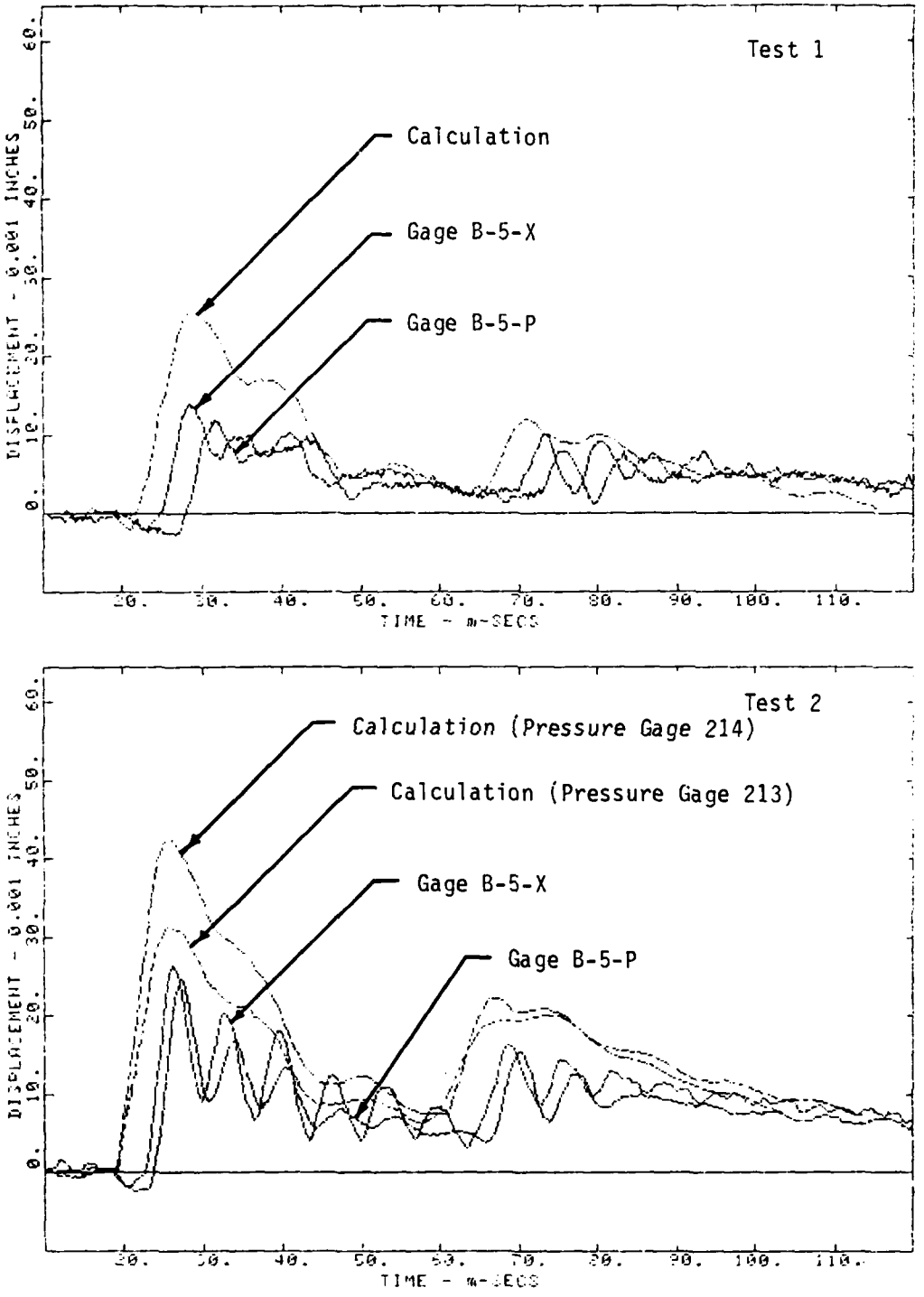

Figure 5-31. Comparison of calculated and measured relative displacements, gages B-5-X and B-5-P.

Comparisons of gage records and calculated relative displacements for the gages located at Section C-C are shown in Figures 5-32 and 5-33. The displacement gages were located at Construction Stations 0+49 and 0+51. The nearest pressure gages were located at Construction Stations 1+50 (100 feet (30.5 m) "upstream") and 0+00 (50 feet (15.2 m) "downstream"). Calculations based on pressure records at both of these locations are shown in the figures. To avoid developing a new finite element grid, the calculation using the station 1+50 pressure record was performed using the same grid (approximately 600 feet (182.9 m) of overburden) as was used for the calculations at Sections A-A and B-B. To aid in the comparisons, the calculated relative displacements have been shifted in time so that first motion occurs between the first positive displacements for the two pressure gages to which they are being compared.

The agreement between calculated and measured relative displacements at the back of the tunnel is quite good for Test 1 (Figure 5-32). There is also reasonable agreement between the measured relative displacements for Test 2 and the values calculated using the pressure record from Construction Station 1+50, although the calculated values are somewhat higher as would be expected since the pressure gage is 100 feet (30.5 m) "upstream" from the displacement gages. On the other hand, there is not good agreement between the measured values and the values calculated using the pressure record from Construction Station 0+00. We believe the large second peak in the calculated relative displacement is caused by the ground shock reflecting off the free surface because the calculational grid used for the portal only provided 20 feet (6.1 m) of overburden above the tunnel. Since the displacement gages were actually located approximately 50 feet (15.2 m) from the portal, the overburden at the gage location is substantially more than 20 feet (6.1 m). To validate this hypothesis, we performed another calculation using the Test 2 station 0+00 pressure record but with the finite element grid providing 600 feet

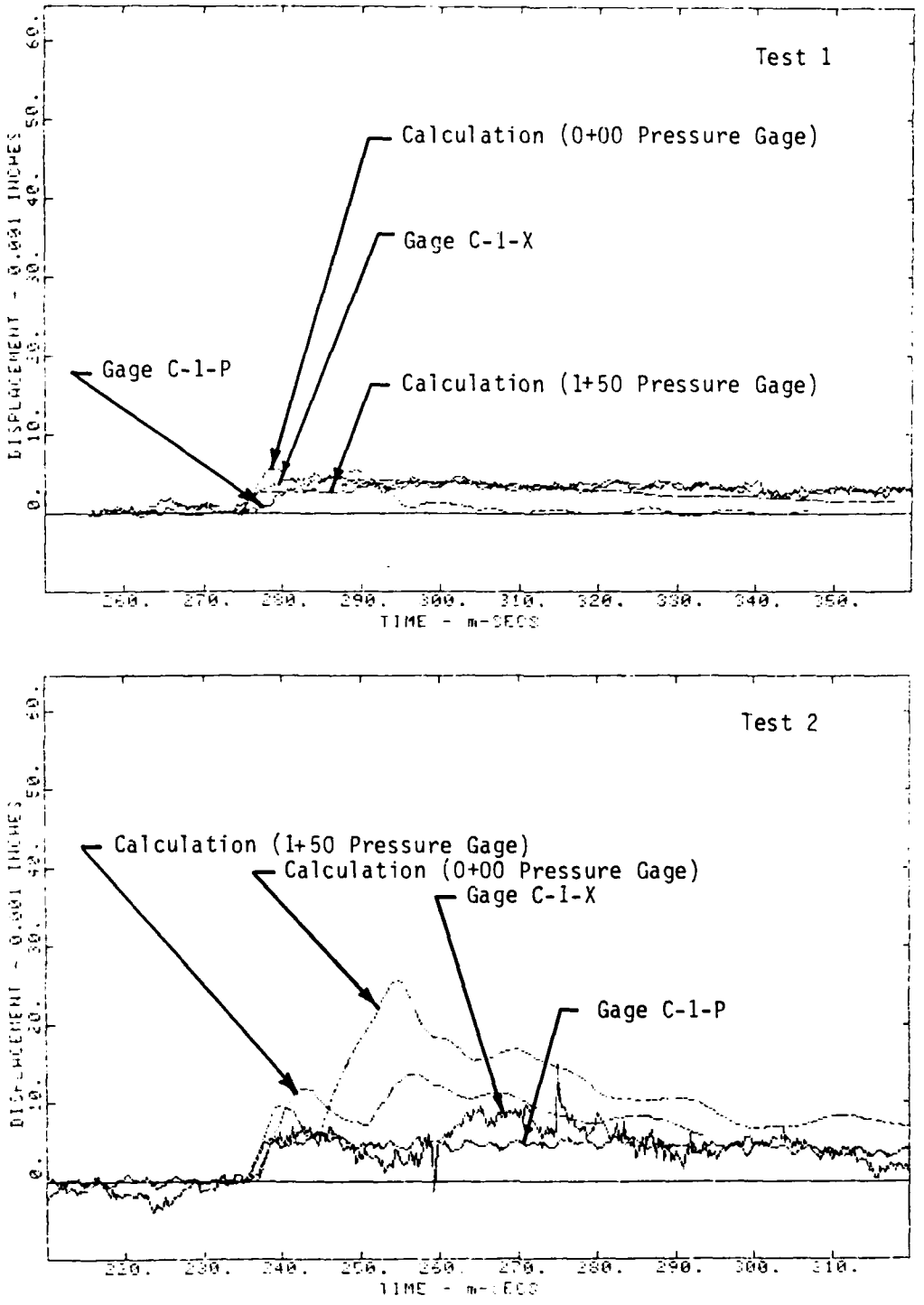

Figure 5-32. Comparison of calculated and measured relative displacements, gages C-1-X and C-1-P (Calculated records shifted so arrival times agree).

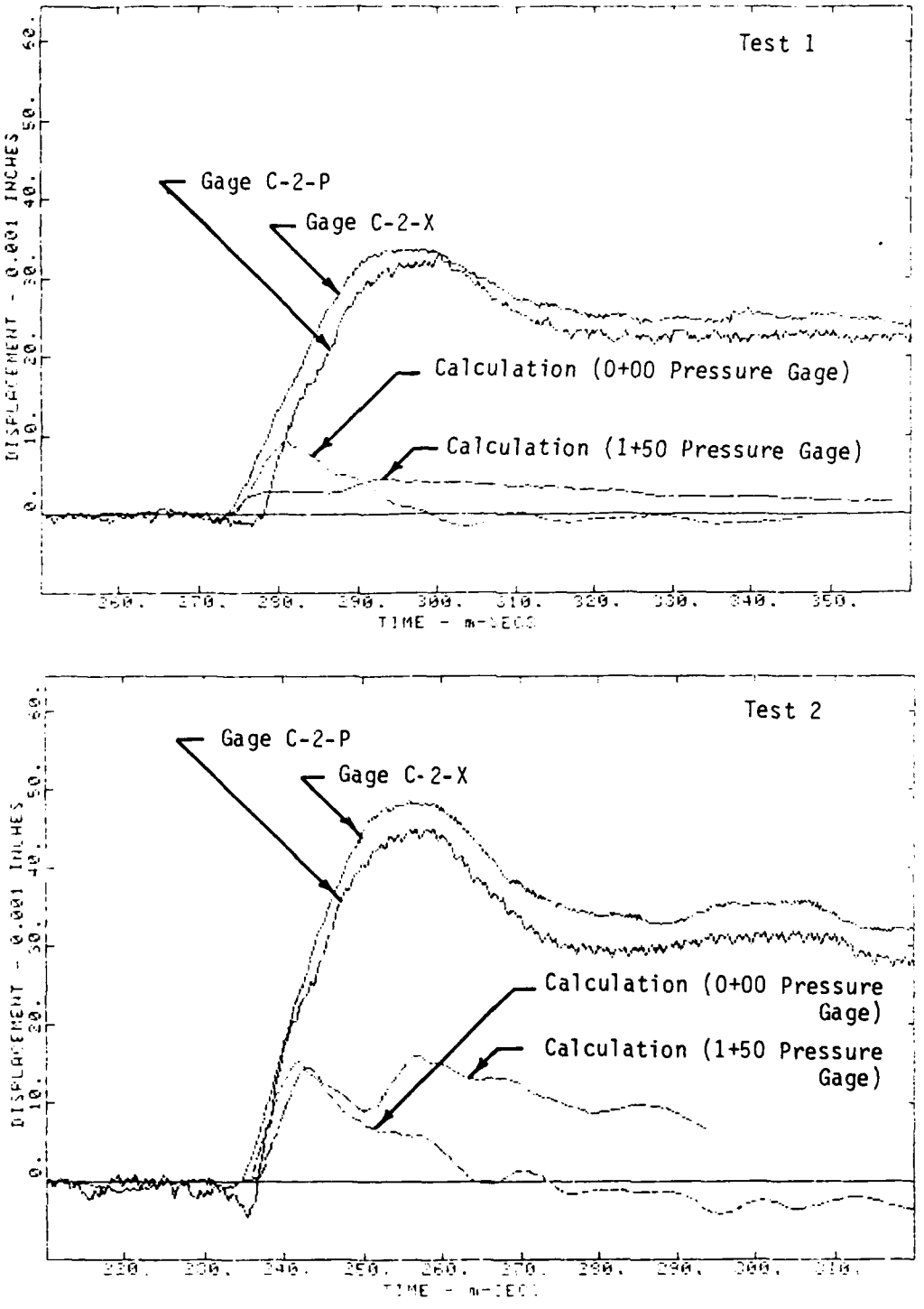

Figure 5-33. Comparison of calculated and measured relative displacements, gages C-2-X and C-2-P (Calculated records shifted so arrival times agree).

(182.9 m) of overburden. The results of this calculation are shown in Figure 5-34 along with the other three plots from Figure 5-32. In this case, the large second peak has disappeared and the measured relative displacements are in reasonably good agreement with both calculations, confirming our hypothesis.

As shown in Figure 5-33, the comparison between calculated and measured relative displacements at the right rib is very poor. As discussed earlier, we have tentatively concluded that gages C-2-X and C-2-P behaved anomalously on both tests.

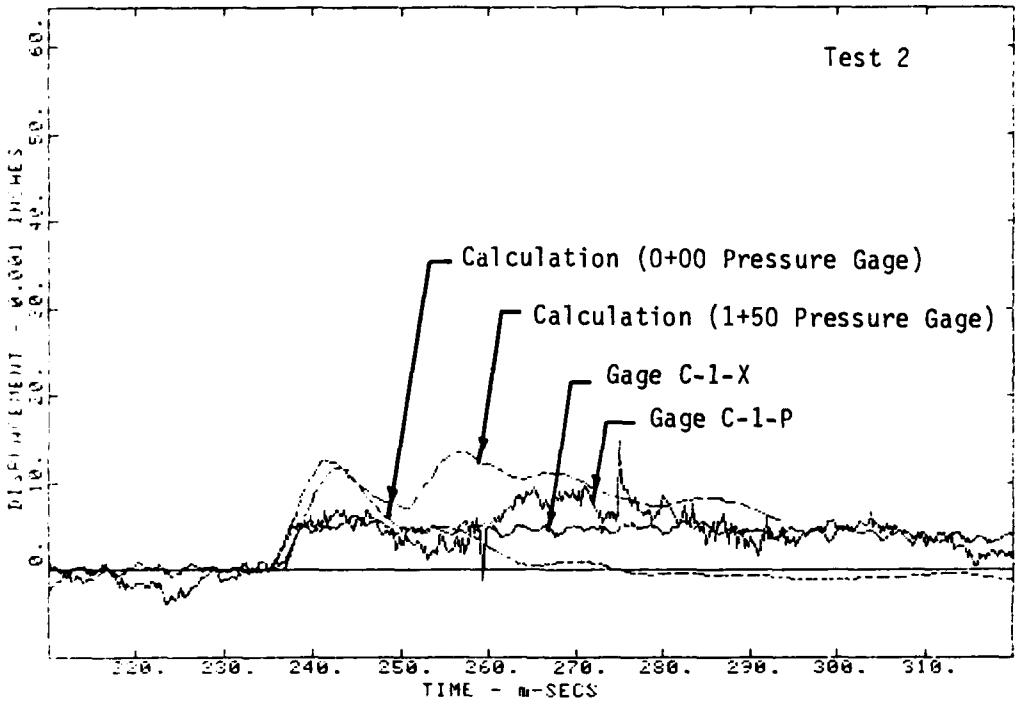

Figure 5-34. Comparison of calculated and measured relative displacements with increased overburden for Construction Station 0+00 calculation, gages C-1-X and C-1-P (Calculated records shifted so arrival times agree).

SECTION 6

PASSIVE MEASUREMENT RESULTS

6.1 RESIDUAL ROCK DEFORMATION DATA

Equipment and procedures used for passively measuring residual rock deformations were described in Section 4. Both tangential and "diametral" measurements were made at Construction Stations 0+50, 5+62, 6+08, and 6+53 as shown in Figure 2-17. For both types of measurement, the distances between gage points were measured both before and after each test, with the differences between measurements being the residual deformations.

As stated in Section 4, our original plan was to repeat all passive measurements both before and after each tunnel response test in order to identify and correct possible reading errors and to provide data with which to assess the accuracy (based on repeatability) of the measurements. Unfortunately, the constraints imposed by the compressed schedule did not permit us to make any repetitive measurements until after the second test. At that time, most tangential measurements were repeated once and selected diametral measurements were repeated twice at Construction Stations 0+50 and 5+62.

Passive tangential measurement data for the four measurement stations are presented in Tables 6-1 through 6-4. The pairs of gage points between which measurements were taken are shown in the first column of each table. The approximate locations of the gage points are as shown earlier in Figures 4-5 through 4-8. Initial gage lengths are shown in the second column and residual displacements are provided in the last three columns of each table. The displacements in the "Test 1" column are the differences between measurements made before and after Test

Table 6-1. Measured residual tangential displacements, Construction Station 0+50.

Gage Points	Initial Gage Length (inches)	Residual Displacement (inches)		
		Test 1	Test 2	Cumulative
101 102	20.0139	-0.0053	0.0173	0.0120
102 103	19.8322	-0.0005	0.0111	0.0106
103 104	19.7433	0.0006	0.0033	0.0039
104 105	20.2256	-0.0034	-0.0159	-0.0193
105 106	19.9940	0.0029	0.0088	0.0118
106 108	19.8800	-0.0105	0.0031	-0.0074
108 109	19.7717	-0.0011	0.0236	0.0225
109 110	19.8555	0.0065	0.0063	0.0128
110 111	19.9262	0.0048	0.0063	0.0111
111 112	19.8939	-0.0060	0.0026	-0.0034
112 113	19.9757	0.0076	-0.0012	0.0064
113 114	20.0886	-0.0015	-0.0006	-0.0021
114 115	19.9380	0.0004	0.0007	0.0011
116 117	19.9652	-0.0015	0.0101	0.0085
117 118	19.7496	0.0034	0.0030	0.0064
118 119	19.8146	-0.0006	0.0110	0.0104
119 120	19.9047	-0.0066	0.0144	0.0077
120 121	20.0015	-0.0044	0.0061	0.0019
121 122	20.1001	-0.0036	0.0115	0.0079
122 123	19.9298	-0.0015	0.0145	0.0130
123 124	20.0865	0.0009	0.0138	0.0148
124 125	19.8979	-0.0005	0.0111	0.0107
125 126	19.8153	0.0093	0.0003	0.0095
126 127	19.8984	-0.0002	0.0126	0.0125
127 128	19.9244	-0.0048	0.0078	0.0030
128 129	19.9875	0.0081	0.0171	0.0252
131 132	20.0448	-0.0018	0.0178	0.0160
132 133	20.0515	0.0139	-0.0003	0.0137
133 134	19.9917	0.0018	-0.0086	-0.0068
134 135	20.0227	0.0039	-0.0101	-0.0062
135 136	20.0122	0.0028	0.0214	0.0241
136 137	20.0623	-0.0070	0.0175	0.0105
137 138	19.9544	0.0001	0.0041	0.0042
138 139	19.8827	0.0177	0.0251	0.0428
139 140	20.1537	0.0057	0.0071	0.0127

Table 6-2. Measured residual tangential displacements, Construction Station 5+62.

Gage Points	Initial Gage Length (inches)	Residual Displacement (inches) Test 1	Test 2	Cumulative
146 147	20.0463	-0.0101	0.0028	-0.0074
147 148	19.9689	-0.0064	0.0046	-0.0018
148 149	19.9877	-0.0044	0.0038	-0.0005
149 150	19.9351	-0.0012	0.0063	0.0051
151 152	19.8198	0.0084	0.0034	0.0118
152 153	20.2123	0.0100	-0.0161	-0.0060
153 154	19.9996	0.0061	0.0040	0.0102
154 155	20.0270	0.0045	-0.0110	-0.0064
155 156	19.8972	0.0053	0.0056	0.0109
156 157	19.9992	0.0020	-0.0069	-0.0049
157 158	19.9421	0.0050	0.0038	0.0089
158 159	20.0232	0.0042	-0.0177	-0.0135
159 160	19.7413	0.0063	0.0152	0.0215
160 161	19.8896	-0.0457	0.0014	-0.0443
161 162	19.9696	0.0130	0.0029	0.0159
162 163	19.9810	-0.0445	0.0119	-0.0327
163 164	20.0892	0.0051	-0.0104	-0.0054
164 165	19.8465	-0.0014	0.0107	0.0093
165 166	19.9180	0.0057	-0.0066	-0.0009
166 167	19.8077	-0.0047	0.0111	0.0064
167 168	19.8252	-0.0006	0.0148	0.0142
168 169	20.0069	-0.0011	-0.0001	-0.0012
169 170	19.9620	0.0079	-0.0049	0.0029
171 172	20.0236	0.0042	-0.0109	-0.0066
172 173	20.0966	-0.0047	0.0152	0.0105
173 174	20.0295	0.0033	0.0223	0.0255
174 175	20.0406	-0.0537	0.0576	0.0039
175 176	19.9427	0.0247	-0.0062	0.0185
176 177	20.2005	0.0073	-0.0368	-0.0294
177 178	19.8769	0.0038	0.0256	0.0294
178 179	20.1932	0.0063	0.0001	0.0064
179 180	20.0234	0.0045	0.0053	0.0098
180 181	20.0059	-0.0007	-0.0011	-0.0019
183 184	19.8069	0.0231	0.0473	0.0704
184 185	20.0005	0.0040	0.0142	0.0181

Table 6-3. Measured residual tangential displacements, Construction Station 6+08.

Gage Points		Initial Gage Length (inches)	Residual Displacement (inches)		
			Test 1	Test 2	Cumulative
186	187	20.0868	0.0080	0.0124	0.0204
188	189	19.8770	-0.0028	0.0156	0.0128
189	190a	20.0612	-0.0034	0.0105	0.0071
190a	190b	19.9591	-0.0155	-0.0188	-0.0343
190b	191	20.0831	-0.0576	0.0077	-0.0499
191	192	19.9835	0.0497	0.0326	0.0824
192	193	19.7353	-0.0259	-0.0012	-0.0270
193	194	20.1425	0.0408	0.0170	0.0578
202	203	19.8175	-0.0222	0.0114	-0.0110
203	204	20.0560	-0.0174	-0.0224	-0.0397
204	206	19.9930**	*	0.0137	*
206	207	19.9226	-0.0187	0.0013	-0.0173
207	208	19.9861	-0.0020	0.0024	0.0003
208	209	19.7720	-0.0368	0.0098	-0.0270
211	212	19.9200	-0.0039	0.0022	-0.0017
212	213	19.8988	-0.0281	0.0075	-0.0206
213	214	19.9717	0.0010	-0.0072	-0.0062
214	215	19.9207	-0.0053	-0.0027	-0.0079
215	216	19.9577	-0.0100	-0.0103	-0.0203
216	217	19.9220	-0.0025	0.0025	-0.0001
217	218	20.0225	-0.0006	-0.0071	-0.0077
218	219	19.9781	-0.0042	-0.0080	-0.0122
219	220	19.9955	-0.0095	-0.0059	-0.0154
220	221	19.9883	-0.0015	0.0006	-0.0010
221	222	20.0817	-0.0111	-0.0043	-0.0154
222	223	20.0027	-0.0077	-0.0027	-0.0105
223	224	20.0725	0.0116	-0.0071	0.0045
224	225	20.0156	0.0012	-0.0097	-0.0084
225	226	19.9763	-0.0083	-0.0030	-0.0114
227	228	20.0672	0.0005	0.0055	0.0060
228	229	20.0168	-0.0128	0.0054	-0.0074
229	230	19.8093	-0.0056	0.0084	0.0029
230	231	19.9940	-0.0112	-0.0018	-0.0129

* Not measured

** Post Test 1 measurement

Table 6-4. Measured residual tangential displacements, Construction Station 6+53.

Gage Points	Initial Gage Length (inches)	Residual Displacement (inches)		
		Test 1	Test 2	Cumulative
235 236	20.0155	0.0123	0.0171	0.0294
236 237	19.8525	0.0014	0.0066	0.0081
237 238	20.2171	0.0050	0.0032	0.0082
238 239	20.1736	0.0627	0.0038	0.0664
239 240	19.8543	-0.0751	0.0178	-0.0573
240 241	19.8994	-0.0660	0.0143	-0.0516
241 242	19.9081	-0.0151	0.0108	-0.0043
242 243	19.9038	-0.0154	0.0215	0.0062
243 244	19.8291	-0.0084	0.0109	0.0025
244 245	20.0168	-0.0020	0.0022	0.0001
245 246	19.8484	-0.0006	0.0129	0.0124
246 247	19.9904	-0.0009	0.0106	0.0098
247 248	19.8710	-0.0034	0.0121	0.0087
248 249	19.9914	-0.0199	0.0274	0.0075
249 250	19.8043	-0.0051	0.0059	0.0009
250 251	19.7240	-0.0058	0.0043	-0.0015
251 252	20.0379	-0.0036	0.0102	0.0066
252 253	20.0777	0.0003	0.0153	0.0156
253 254	19.9437	-0.0039	0.0087	0.0049
254 255	20.0358	-0.0051	0.0090	0.0039
255 256	20.0541	0.0064	-0.0084	-0.0021
256 257	19.8496	-0.0051	0.0162	0.0112
257 258	20.2883	-0.0112	0.0048	-0.0064
258 259	20.0529	0.0214	0.0051	0.0265
259 260	20.1619	0.0092	0.0145	0.0237
260 261	19.9705	0.0003	0.0072	0.0075
261 262	19.9250	0.0146	0.0041	0.0187
262 263	19.8269	-0.0638	-0.1152	-0.1790
263 264	20.0240	0.0213	0.1044	0.1258
264 265	20.0245	-0.0041	-0.0048	-0.0089
265 266	19.8924	0.0038	0.0250	0.0289
266 267	19.8532	0.0106	0.0219	0.0325
267 268	19.8784	0.0015	-0.0061	-0.0047
268 269	19.9167	-0.0013	-0.0009	-0.0022
269 270	19.9809	-0.0037	0.0279	0.0242
270 271	19.9773	0.0235	0.0526	0.0761
271 272	19.9955	0.0022	0.0304	0.0325

1. Similarly, those in the "Test 2" column are the differences between measurements made before and after Test 2. The displacements in the "Cumulative" column are the differences between measurements made before Test 1 and after Test 2. In all cases, the first measurement was subtracted from the second. Therefore, positive values (resulting from the second measurement being larger than the first) indicate increases in displacement corresponding to tensile strain.

As noted earlier, most of the tangential measurements were repeated following Test 2. In all cases where repeat measurements were made, the Test 2 and cumulative residual displacements shown in Tables 6-1 through 6-4 are based on the average of both measurements made after Test 2.

In a few cases (Table 6-3 and some of the tables of diametral measurements discussed below), the same gage points were not measured each time. These are identified by a single asterisk. In the event that the missing measurement was that prior to Test 1, the initial gage length given is the measurement made following Test 1 and is identified by a double asterisk.

Passive diametral measurement data for the four measurement stations are presented in Tables 6-5 through 6-8. The format for these tables is identical to that described above for Tables 6-1 through 6-4. As noted earlier, selected diametral measurements were repeated twice following Test 2 at Construction Stations 0+50 and 5+62. For those cases, the Test 2 and cumulative residual displacements shown in Tables 6-5 and 6-6 are based on the average of the measurements following Test 2.

Table 6-5. Measured residual diametral displacements, Construction Station 0+50.

Gage Points	Initial Gage Length (inches)	Residual Displacement (inches)		
		Test 1	Test 2	Cumulative
103 124	237.7448	-0.0232	0.0823	0.0591
104 124	231.2201	-0.0159	0.0310	0.0151
105 124	227.0626	-0.0185	0.0937	0.0752
106 124	222.9499	-0.0165	0.0588	0.0423
108 122	211.6354	-0.0020	0.0340	0.0320
108 123	217.0452	-0.0085	0.0518	0.0433
108 124	220.9401	-0.0193	0.0621	0.0429
108 125	223.1811	0.0136	0.0269	0.0405
108 126	228.7784	0.0033	0.0915	0.0948
108 127	235.1632	-0.0404	0.0737	0.0333
108 128	240.9410	-0.0109	0.0722	0.0613
109 124	217.3661	-0.0112	0.0513	0.0401
110 124	211.7595	-0.0204	0.0715	0.0511
113 135	211.9035	-0.0249	0.0385	0.0137
114 135	215.8633	-0.0274	0.0455	0.0181
115 135	217.8854	-0.0247	0.0357	0.0110
116 131	230.5425	-0.0286	0.0564	0.0278
116 132	225.0105	-0.0151	0.0424	0.0273
116 133	221.0683	-0.0425	0.0537	0.0112
116 134	218.7961	-0.0270	0.0335	0.0065
116 135	218.2170	-0.0185	0.0409	0.0158
116 136	219.6790	-0.0129	0.0224	0.0095
116 137	223.0870	0.0373	0.0778	0.1151
116 138	227.8132	0.0312	0.0685	0.0997
116 139	232.4518	-0.0275	0.0198	-0.0077
116 140	240.2162	-0.0217	0.0179	-0.0038
117 135	216.6172	-0.0312	0.0443	0.0131
118 135	213.6148	-0.0331	0.0445	0.0114

Table 6-6. Measured residual diametral displacements, Construction Station 5+62.

Gage Points	Initial Gage Length (inches)	Residual Displacement (inches)		
		Test 1	Test 2	Cumulative
147 170	237.2713**	*	0.0623	*
148 170	233.3905**	*	0.0476	*
149 170	230.3665	-0.0256	0.0382	0.0126
150 170	224.5531	0.0379	-0.0156	0.0223
151 167	221.2784**	*	0.0331	*
151 168	222.7654	0.0038	0.0173	0.0211
151 169	222.3453	-0.0062	0.0133	0.0071
151 170	221.1344	-0.0489	0.0112	-0.0152
151 171	224.1619	0.0107	-0.0376	-0.0268
151 172	228.6442	0.0193	0.0098	0.0292
151 173	233.7171	0.0010	0.0284	0.0294
152 170	222.9090	-0.1350	0.0356	-0.0994
153 170	222.9085	-0.0459	0.0447	-0.0011
154 170	220.8570**	*	0.0533	*
157 180	214.0688	-0.0872	0.0182	-0.0689
158 180	219.7073	-0.0831	0.0152	-0.0678
159 180	223.2550**	*	0.0084	*
160 176	236.8465	-0.0877	0.1085	0.0208
160 177	231.2547	-0.0747	0.0207	-0.0540
160 178	227.4475	-0.0673	-0.0577	-0.1250
160 179	225.0546	-0.0999	0.0515	-0.0484
160 180	225.2441	-0.0029	-0.0211	-0.0704
160 181	226.2688	-0.0678	-0.0132	-0.0810
160 183	232.2326	-0.0390	-0.0020	-0.0409
160 184	237.2726**	*	-0.0078	*
161 180	225.1705**	*	-0.0250	*
162 180	223.4867	-0.0883	-0.0141	-0.1024
163 180	219.8322**	*	-0.0111	*
164 180	214.5356**	*	-0.0136	*

* Not measured

** Post Test i measurement

Table 6-7. Measured residual diametral displacements, Construction Station 6+08.

Gage Points		Initial Gage Length (inches)	Residual Displacement (inches)		
			Test 1	Test 2	Cumulative
187	216	240.6034	-0.0212	*	*
188	216	234.2814	-0.0357	*	*
189	216	229.7631	-0.0309	-0.0226	-0.0535
190b	213	212.7785	-0.0159	*	*
190b	214	218.9762	-0.0029	*	*
190b	215	223.8227	-0.0115	*	*
190b	216	226.6918	-0.0084	-0.0280	-0.0364
190b	217	227.6561	0.0307	-0.0401	-0.0094
190b	218	227.0180	0.0409	*	*
190b	219	224.2497	0.0046	*	*
190b	220	220.1088	-0.0043	*	*
190b	221	214.0491	-0.0060	*	*
191	216	227.0455	-0.0269	-0.0850	-0.1118
192	216	229.0420	0.0641	*	*
193	216	232.9358	0.0195	*	*
194	216	238.9270	0.1067	*	*
202	226	239.0707	0.0621	*	*
202	231	224.9648	0.0337	*	*
203	226	230.6538	-0.0154	*	*
204	226	225.3626	0.0015	*	*
206	226	223.6462	-0.0372	0.0150	-0.0222
207	221	212.1642	-0.0024	*	*
207	222	217.4758	-0.0012	*	*
207	223	221.0199	0.0331	*	*
207	224	222.9608	0.0155	*	*
207	225	222.8983	-0.0173	0.0306	0.0133
207	226	220.9977	0.0087	0.0164	0.0250
207	227	225.5195	0.0162	-0.0117	0.0046
207	228	231.4159	-0.0996	*	*
207	229	235.8454	-0.0089	*	*
207	230	239.7522	0.0432	*	*
207	231	240.9213	0.0029	*	*
208	226	222.7542	-0.0257	0.0356	0.0100
209	226	222.2661	-0.0992	*	*
210	226	220.9687	-0.0296	*	*
211	226	217.7064	-0.0773	*	*
212	226	212.2405	-0.0494	*	*

* Not measured

Table 6-8. Measured residual diametral displacements, Construction Station 6+53.

Gage Points	Initial Gage Length (inches)	Residual Displacement (inches)		
		Test 1	Test 2	Cumulative
237 258	220.6531	-0.0280	*	*
238 257	218.3912**	*	0.0118	*
239 254	214.9616	-0.0489	*	*
239 255	217.3097**	*	0.0080	*
239 256	218.5186	0.0442	0.0064	0.0506
239 257	218.7828**	*	0.0270	*
239 258	222.2040	*	*	0.0355
239 260	232.9161	-0.1523	*	*
239 263	232.8060	-0.0378	*	*
240 257	219.0367**	*	0.0155	*
241 257	217.4042**	*	0.0087	*
243 258	219.0497	-0.0255	*	*
245 268	215.9543	-0.0314	*	*
247 268	224.4539	*	*	-0.1194
249 263	239.0769	-0.0305	*	*
249 264	234.9987	-0.0452	*	*
249 266	227.0121	-0.0378	*	*
249 268	224.9318	-0.0553	-0.1044	-0.1597
249 270	228.8472	-0.1245	*	*
249 272	243.0230	-0.1102	*	*
258 272	214.9343	0.0099	*	*

* Not measured

** Post Test 1 measurement

6.2 ASSESSMENT OF MEASUREMENT ACCURACY

As may be seen from Tables 6-1 through 6-8, the measured residual displacements are very small. Consequently, the question of measurement precision naturally arises and must be addressed in order to judge the validity of the data.

As indicated earlier, one of the reasons for making repeat measurements was to provide data for use in assessing measurement accuracy. A total of 142 of the tangential measurements were repeated following the second tunnel response test. These measurements and the differences between them are presented in Tables 6-9 through 6-12.

Selected diametral measurements were repeated twice at Construction Stations 0+50 and 5+62. These measurements are presented in Tables 6-13 and 6-14. Also included in these tables are the differences (totaling 63) between first and second, first and third, and second and third measurements.

If all of the measurements had been made perfectly, the differences recorded in Tables 6-9 through 6-14 would be identically zero. In other words, these differences are an indication of the errors associated with the measurement technique and can be used to assess first the precision and then the relative accuracy of the measurements. Although three, or less, difference values are available for any particular measurement, all measurements of a given type (tangential or diametral) were made using the same instrument and procedures. Therefore, we believe it is reasonable to treat the two sets (one with 142 samples and the other with 63 samples) of data statistically.

In order to determine measurement precision, it was necessary to develop a high confidence estimate of the magnitude of the error which could be compared with individual residual rock deformation measurements to determine their significance.

Table 6-9. Comparison of repeated tangential measurements, Construction Station 0+50.

Gage Points	First Meas. (inches)	Second Meas. (inches)	Difference (inches)
101 102	20.0238	20.0282	0.0044
102 103	19.8449	19.8406	-0.0043
103 104	19.7425	19.7520	0.0095
104 105	20.2121	20.2004	-0.0116
105 106	20.0124	19.9992	-0.0132
106 108	19.8729	19.8723	-0.0005
108 109	19.7941	19.7943	0.0001
109 110	19.8794	19.8573	-0.0221
110 111	19.9365	19.9381	0.0017
111 112	19.8961	19.8848	-0.0113
112 113	19.9778	19.9864	0.0086
113 114	20.0833	20.0897	0.0064
114 115	19.9407	19.9376	-0.0031
116 117	19.9751	19.9725	-0.0026
117 118	19.7551	19.7569	0.0019
118 119	19.8172	19.8329	0.0158
119 120	19.9080	19.9168	0.0088
120 121	19.9974	20.0093	0.0119
121 122	20.1036	20.1124	0.0088
122 123	19.9423	19.9432	0.0008
123 124	20.1038	20.0989	-0.0049
124 125	19.9097	19.9074	-0.0023
125 126	19.8195	19.8302	0.0107
126 127	19.9189	19.9028	-0.0161
127 128	19.9311	19.9238	-0.0073
128 129	20.0179	20.0076	-0.0103
129 130	20.1313	20.1266	-0.0047
130 131	19.9522	19.9399	-0.0123
131 132	20.0749	20.0466	-0.0282
132 133	20.0664	20.0639	-0.0025
133 134	19.9914	19.9786	-0.0127
134 135	20.0143	20.0187	0.0043
135 136	20.0400	20.0328	-0.0073
136 137	20.0880	20.0577	-0.0304
137 138	19.9713	19.9460	-0.0254
138 139	19.9365	19.9147	-0.0217
139 140	20.1793	20.1536	-0.0257

Table 6-10. Comparison of repeated tangential measurements, Construction Station 5+62.

Gage Points	First Meas. (inches)	Second Meas. (inches)	Difference (inches)
146 147	20.0413	20.0366	-0.0047
147 148	19.9760	19.9582	-0.0178
148 149	19.9827	19.9915	0.0089
149 150	19.9352	19.9454	0.0102
151 152	19.8285	19.8348	0.0063
152 153	20.1954	20.2171	0.0217
153 154	20.0037	20.0159	0.0121
154 155	20.0136	20.0275	0.0139
155 156	19.8963	19.9200	0.0237
156 157	19.9930	19.9955	0.0026
157 158	19.9333	19.9687	0.0354
158 159	20.0152	20.0043	-0.0109
159 160	19.7303	19.7953	0.0651
160 161	19.8405	19.8501	0.0096
161 162	19.9679	20.0031	0.0352
162 163	19.9304	19.9663	0.0359
163 164	20.0910	20.0768	-0.0141
164 165	19.8376	19.8741	0.0365
165 166	19.9225	19.9115	-0.0110
166 167	19.8013	19.8269	0.0256
167 168	19.8391	19.8397	0.0005
168 169	20.0050	20.0063	0.0012
169 170	19.9627	19.9671	0.0045
170 171	20.0792	20.1143	0.0351
171 172	20.0014	20.0325	0.0311
172 173	20.1039	20.1102	0.0063
173 174	20.0317	20.0785	0.0468
174 175	20.0289	20.0601	0.0312
175 176	19.9591	19.9634	0.0043
176 177	20.1835	20.1587	-0.0249
179 180	20.0608	20.0055	-0.0553
180 181	20.0026	20.0055	0.0029
183 184	19.9015	19.8533	-0.0482
184 185	20.0386	19.9988	-0.0398

Table 6-11. Comparison of repeated tangential measurements, Construction Station 6+08.

Gage Points		First Meas. (inches)	Second Meas. (inches)	Difference (inches)
186	187	20.1162	20.0982	-0.0180
188	189	19.8897	19.8899	0.0002
189	190a	20.0692	20.0675	-0.0016
190a	190b	19.9350	19.9146	-0.0205
190b	191	20.0330	20.0334	0.0004
191	192	20.0643	20.0675	0.0032
192	193	19.7101	19.7064	-0.0037
193	194	20.2002	20.2004	0.0002
202	203	19.7826	19.8305	0.0479
203	204	20.0043	20.0282	0.0239
204	206	20.0006	20.0128	0.0122
206	207	19.8974	19.9133	0.0159
207	208	19.9842	19.9886	0.0044
208	209	19.7511	19.7387	-0.0124
210	211	20.4063	20.4048	-0.0014
211	212	19.9104	19.9260	0.0156
212	213	19.8736	19.8829	0.0093
213	214	19.9637	19.9672	0.0035
214	215	19.9134	19.9122	-0.0012
215	216	19.9382	19.9369	-0.0013
216	217	19.9237	19.9201	-0.0036
217	218	20.0176	20.0122	-0.0055
218	219	19.9598	19.9720	0.0122
219	220	19.9781	19.9822	0.0040
220	221	19.9858	19.9889	0.0031
221	222	20.0550	20.0775	0.0226
222	223	19.9830	20.0014	0.0184
223	224	20.0650	20.0890	0.0240
224	225	19.9949	20.0196	0.0248
225	226	19.9523	19.9775	0.0252
227	228	20.0712	20.0753	0.0041
228	229	20.0037	20.0150	0.0113
229	230	19.8164	19.8079	-0.0085
230	231	19.9753	19.9867	0.0114

Table 6-12. Comparison of repeated tangential measurements, Construction Station 6+53.

Gage Points	First Meas. (inches)	Second Meas. (inches)	Difference (inches)
235 236	20.0486	20.0414	-0.0072
236 237	19.8589	19.8621	0.0033
237 238	20.2272	20.2235	-0.0037
238 239	20.2380	20.2421	0.0041
239 240	19.7959	19.7980	0.0022
240 241	19.8412	19.8544	0.0132
241 242	19.8947	19.9129	0.0182
242 243	19.9019	19.9179	0.0160
243 244	19.8269	19.8363	0.0094
244 245	20.0233	20.0106	-0.0127
245 246	19.8612	19.8603	-0.0009
246 247	20.0017	19.9988	-0.0029
247 248	19.8829	19.8766	-0.0063
248 249	20.0069	19.9909	-0.0160
249 250	19.8080	19.8024	-0.0057
250 251	19.7269	19.7180	-0.0090
251 252	20.0425	20.0466	0.0041
252 253	20.0935	20.0931	-0.0004
253 254	19.9488	19.9484	-0.0004
254 255	20.0435	20.0359	-0.0076
255 256	20.0570	20.0469	-0.0101
256 257	19.8672	19.8545	-0.0127
257 258	20.2821	20.2817	-0.0004
258 259	20.0821	20.0768	-0.0053
259 260	20.1857	20.1855	-0.0002
260 261	19.9787	19.9774	-0.0013
261 262	19.9455	19.9419	-0.0036
262 263	19.6437	19.6521	0.0083
263 264	20.1559	20.1437	-0.0122
264 265	20.0124	20.0188	0.0065
265 266	19.9210	19.9215	0.0005
266 267	19.8857	19.8858	0.0001
267 268	19.8777	19.8697	-0.0080
268 269	19.9213	19.9077	-0.0136
269 270	20.0048	20.0054	0.0006
270 271	20.0524	20.0544	0.0020
271 272	20.0344	20.0216	-0.0128

Table 6-13. Comparison of repeated diametral measurements, Construction Station 0+50.

Gage Points	First Meas. (inches)	Second Meas. (inches)	Difference (inches)
106 124	222.9802	222.9923	0.0121
108 123	217.0875	217.0862	-0.0013
108 124	220.9912	220.9833	-0.0079
108 125	223.2189	223.2208	0.0019
109 124	217.4050	217.4045	-0.0005
115 135	217.8976	217.8947	-0.0029
116 134	218.8084	218.7978	-0.0106
116 135	218.2319	218.2310	-0.0009
116 136	219.6867	219.6895	0.0028
117 135	216.6294	216.6317	0.0023

	First Meas. (inches)	Third Meas. (inches)	
106 124	222.9802	223.0041	0.0239
108 123	217.0875	217.0917	0.0042
108 124	220.9912	220.9897	-0.0015
108 125	223.2189	223.2250	0.0061
109 124	217.4050	217.4091	0.0041
114 135	215.8788	215.8838	0.0050
115 135	217.8976	217.8970	-0.0006
116 133	221.0784	221.0807	0.0023
116 134	218.8084	218.8017	-0.0067
116 135	218.2319	218.2353	0.0034
116 136	219.6867	219.6891	0.0024
116 137	223.1970	223.2072	0.0102
117 135	216.6294	216.6298	0.0004

	Second Meas. (inches)	Third Meas. (inches)	
106 124	222.9923	223.0041	0.0117
108 123	217.0862	217.0917	0.0055
108 124	220.9833	220.9897	0.0063
108 125	223.2208	223.2250	0.0042
109 124	217.4045	217.4091	0.0045
115 135	217.8947	217.8970	0.0023
116 134	218.7978	218.8017	0.0039
116 135	218.2310	218.2353	0.0043
116 136	219.6895	219.6891	-0.0004
117 135	216.6317	216.6298	-0.0019

Table 6-14. Comparison of repeated diametral measurements, Construction Station 5+62.

Gage Points	First Meas. (inches)	Second Meas. (inches)	Difference (inches)
150 170	224.5841	224.5738	-0.0103
151 169	222.3601	222.3502	-0.0099
151 170	221.1259	221.1183	-0.0076
151 171	224.1164	224.1689	0.0525
152 170	222.8118	222.8117	-0.0001
159 180	223.2670	223.2628	-0.0042
160 179	224.9851	224.9849	-0.0002
160 180	225.1800	225.1716	-0.0084
160 181	226.1925	226.1841	-0.0084
161 180	225.1515	225.1402	-0.0114

	First Meas. (inches)	Third Meas. (inches)	
150 170	224.5841	224.5684	-0.0157
151 169	222.3601	222.3470	-0.0131
151 170	221.1259	221.1134	-0.0125
151 171	224.1164	224.1199	0.0035
152 170	222.8118	222.8054	-0.0064
159 180	223.2670	223.2604	-0.0067
160 179	224.9851	225.0486	0.0636
160 180	225.1800	225.1696	-0.0104
160 181	226.1925	226.1869	-0.0056
161 180	225.1515	225.1449	-0.0066

	Second Meas. (inches)	Third Meas. (inches)	
150 170	224.5738	224.5684	-0.0053
151 169	222.3502	222.3470	-0.0031
151 170	221.1183	221.1134	-0.0049
151 171	224.1689	224.1199	-0.0490
152 170	222.8117	222.8054	-0.0063
159 180	223.2628	223.2604	-0.0024
160 179	224.9849	225.0486	0.0638
160 180	225.1716	225.1696	-0.0020
160 181	226.1841	226.1869	0.0028
161 180	225.1402	225.1449	0.0047

A review of Tables 6-9 through 6-14 does not indicate any obvious bias in the differences (errors). Therefore, we assumed the measurement errors to be normally distributed around the theoretical mean of zero. Following this assumption, we computed the standard deviation for each of the two measurement types. Tolerance limit factors (K), for the appropriate sample size, were then selected from tables of "Factors for two-sided tolerance limits for normal distributions" in Reference 9. These factors were selected so that the probability is 95 percent that at least 95 percent of the error distribution will be included between $\bar{X} \pm KS$, where $\bar{X}$ and S are the mean (assumed to be the theoretical zero value, in our case) and the standard deviation. In other words, if the magnitude of a displacement measurement (either positive or negative) exceeds the product KS, there is high confidence that it truely indicates rock displacement. This approach, of course, has the potential for eliminating some "real" rock displacement data from consideration. However, we believe this is the best way to confidently identify those measurements which actually represent displacements.

Considering the 142 tangential measurement differences contained in Tables 6-9 through 6-12, the standard deviation is 0.01722. From Reference 9, the K factor for a sample population of 142 is 2.182. The product of these two values is 0.0376. In other words, the estimated precision of the tangential measurements is $\pm$0.0376 inches ($\pm$0.0955 cm). Therefore, if the magnitude of a tangential rock displacement measurement (either positive or negative) is greater than 0.0376 inches (0.0955 cm), we can say we are 95 percent confident that it is beyond the 0.95 area of the normal distribution for measurement uncertainty and very likely indicates a "real" residual displacement. Dividing the estimated precision by the nominal gage length of 20 inches (50.8 cm) (actual values ranged from 19.74 to 20.29 inches (50.14 to 51.54 cm)) yields a relative error of $\pm$0.00188 inches per inch ($\pm$0.188 percent). This implies a residual tangential strain measurement accuracy of better than 0.2 percent.

A similar treatment of the 63 diametral measurement differences contained in Tables 6-13 and 6-14 yields a standard deviation of 0.01608, a K factor of 2.322, and an estimated measurement precision of ±0.0373 inches (±0.0947 cm). This precision estimate is not significantly different from that for the tangential measurements. However, when the estimated precision is divided by the median gage length of 227.3 inches (5.77 m) (values ranged from 211.6 to 243.0 inches (5.37 to 6.17 m)), the relative error is found to be ±0.000164 inches per inch (±0.0164 percent), more than an order of magnitude less than that for the tangential measurements. This implies a residual diametral strain measurement accuracy of better than 0.02 percent.

6.3 EVALUATION OF PASSIVE MEASUREMENT DATA

As described in Section 2, our pretest predictions for the first tunnel response test indicated that the maximum dynamic diametral strain would be approximately 0.0008 inches per inch (0.08 percent) with comparable maximum tangential strains.[1] Because this indicates essentially elastic behavior of the rock, the residual strains were expected to be very much smaller. A separate pretest prediction calculation was not performed for the second test, but maximum strains were expected to be about twice as large since the driver pressure was approximately doubled.

---

[1]The predicted maximum dynamic strain should not be compared to any of the residual displacements or strains presented in this section. It is repeated here only to emphasize the elastic nature of the expected tunnel response.

As may be seen from Tables 6-1 through 6-4, a large majority of the tangential measurements yielded values less than the estimated measurement precision (±0.0376 inches (±0.0955 cm)). In fact, only 28 of the 418 values (6.7 percent) exceed this value and may legitimately be considered to be data. Of these 28 values, 20 occurred at the high pressure locations (Construction Stations 6+08 and 6+53) as might be expected. Also, 21 of the 28 values occurred in the invert or "flat" portions of the ribs, again as might be expected. The largest measured displacement (between gage points 262 and 263 at Construction Station 6+53) was -0.1790 ±0.0376 inches (-0.4547 ±0.0955 cm), representing a cumulative (after two tests) compressive tangential strain of 0.00903 ±0.00188 inches per inch (0.903 ±0.188 percent).

Ninety-three of the 233 diametral displacements (39.9 percent) shown in Tables 6-5 through 6-8 equal or exceed the estimated measurement precision (±0.0373 inches (±0.0947 cm)) and, therefore, are judged to be significant. Tables 6-5 through 6-8 are repeated as Tables 6-15 through 6-18, but only the significant data are shown. These tables have been annotated to identify measurements which were generally horizontal and vertical, even though none of the measurements was exactly horizontal or vertical. Note that the "vertical" measurement data are at the top of Table 6-17 because of the order in which the gage points were numbered.

The largest measured displacement (between gage points 249 and 268 at Construction Station 6+53) was -0.1597 ±0.0373 inches (-0.4056 ±0.0947 cm), representing a cumulative compressive diametral strain of 0.000710 ±0.000164 inches per inch (0.0710 ±0.0164 percent). Most other residual strains were substantially less than this value.

The residual rock displacement data exhibit a generally random pattern. There is no apparent basis for drawing conclusions regarding differing aspects (e.g., horizontal versus vertical, low pressure versus high pressure, etc.) of tunnel

Table 6-15. Significant residual diametral displacements, Construction Station 0+50.

Gage Points	Initial Gage Length (inches)	Residual Displacement (inches) Test 1	Test 2	Cumulative	
103 124	237.7448		0.0823	0.0591	
105 124	227.0626		0.0937	0.0752	
106 124	222.9499		0.0588	0.0423	
108 123	217.0452		0.0518	0.0433	
108 124	220.9401		0.0621	0.0429	Generally
108 125	223.1811			0.0405	Horizontal
108 126	228.7784		0.0915	0.0948	
108 127	235.1632	-0.0404	0.0737		
108 128	240.9410		0.0722	0.0613	
109 124	217.3661		0.0513	0.0401	
110 124	211.7595		0.0715	0.0511	
113 135	211.9035		0.0385		
114 135	215.8633		0.0455		
116 131	230.5425		0.0564		
116 132	225.0105		0.0424		
116 133	221.0683	-0.0425	0.0537		Generally
116 135	218.2170		0.0409		Vertical
116 137	223.0870	0.0373	0.0778	0.1151	
116 138	227.8132		0.0685	0.0997	
117 135	216.6172		0.0443		
118 135	213.6148		0.0445		

Table 6-16. Significant residual diametral displacements, Construction Station 5+62.

Gage Points	Initial Gage Length (inches)	Residual Displacement (inches) Test 1	Test 2	Cumulative	
147 170	237.2713		0.0623		
148 170	233.3905		0.0476		
149 170	230.3665		0.0382		
150 170	224.5531	0.0379			Generally
151 170	221.1344	-0.0489			Horizontal
151 171	224.1619		-0.0376		
152 170	222.9090	-0.1350		-0.0994	
153 170	222.9085	-0.0459	0.0447		
154 170	220.8570		0.0533		
157 180	214.0688	-0.0872		-0.0689	
158 180	219.7073	-0.0831		-0.0678	
160 176	236.8465	-0.0877	0.1085		
160 177	231.2547	-0.0747		-0.0540	
160 178	227.4475	-0.0673	-0.0577	-0.1250	Generally
160 179	225.0546	-0.0999	0.0515	-0.0484	Vertical
160 180	225.2441			-0.0704	
160 181	226.2688	-0.0678		-0.0810	
160 183	232.2326	-0.0390		-0.0409	
162 180	223.4867	-0.0883		-0.1024	

Table 6-17. Significant residual diametral displacements, Construction Station 6+08.

Gage Points		Initial Gage Length (inches)	Residual Displacement (inches)			
			Test 1	Test 2	Cumulative	
189	216	229.7631			-0.0535	
190b	217	227.6561		-0.0401		Generally Vertical
190b	218	227.0180	0.0409			
191	216	227.0455		-0.0850	-0.1118	
192	216	229.0420	0.0641			
194	216	238.9270	0.1067			
202	226	239.0707	0.0621			
207	228	231.4159	-0.0996			
207	230	239.7522	0.0432			Generally Horizontal
209	226	222.2661	-0.0992			
211	226	217.7064	-0.0773			
212	226	212.2405	-0.0494			

Table 6-18. Significant residual diametral displacements, Construction Station 6+53.

Gage Points	Initial Gage Length (inches)	Residual Displacement (inches) Test 1	Test 2	Cumulative	
239 254	214.9616	-0.0489			
239 256	218.5186	0.0442		0.0506	Generally
239 260	232.9161	-0.1523			Horizontal
239 263	232.8060	-0.0378			
247 268	224.4539			-0.1194	
249 264	234.9987	-0.0452			
249 266	227.0121	-0.0378			Generally
249 268	224.9318	-0.0553	-0.1044	-0.1597	Vertical
249 270	228.8472	-0.1245			
249 272	243.0230	-0.1102			

behavior. This is not surprising, since the measured residual displacements are very small. It is also completely consistent with our pretest prediction that the tunnel would respond essentially elastically, with the small relative displacements measured actively, and, most importantly, with the nearly complete absence of damage observed following both tunnel response tests.

SECTION 7

CONCLUDING REMARKS

The dynamic relative displacement gages developed for and fielded at Little Skull Mountain performed very well during both tunnel response tests, providing detailed dynamic response data. Following the first test, the finite element calculational model was calibrated against two of the gage records, using a pressure record provided by NMERI. The calibrated model was then used to calculate relative displacement-time histories at the other gage locations for Test 1 and at all gage locations for Test 2. Except for five gages which appeared to provide anomalous records, the calculated peak relative displacements were within a few percent of measured values for the majority of the gages. The calculations also provided reasonably good matches to the "structure" of the gage records beyond the peaks. We concluded that the objective of obtaining dynamic displacement data and calibrating the calculational model was satisfied. We are confident that the calculational technique is suitable for use during the design of a large scale underground simulator.

The precision and relative accuracy of the passive measurements of residual rock deformation were not as good as we previously experienced on the HURON LANDING structures experiment. However, the measurement technique is sufficiently accurate (better than 0.2 percent for tangential strain and 0.02 percent for diametral strain) to measure any strains which are large enough to cause significant damage to the tunnel. Because of the extremely compressed schedule for the tunnel response tests, we did not (a) use Sulfaset® during installation of the gage points, (b) countersink the small holes drilled in the heads of the lag screws which served as receptacles for the index points of the gage, and (c) repeat any measurements until

after the second test. The reduced measurement precision is attributed to these factors, all of which may easily be remedied in any future test, given sufficient time in the fielding schedule.

In the 25 feet (7.62 m) of the driver section nearest the portal, the rock was covered with two coats of latex paint. In the remaining 50 feet (15.2 m) of the driver section, the rock was covered with two inches (5.08 cm) of fibercrete followed by a single coat of latex paint. The remainder of the tunnel was treated with a single coat of latex paint. Prior to the second test, the entire length (704 feet (214.6 m)) of the tunnel was treated with an additional coat of latex paint. Additional details of tunnel preparation may be found in Reference 10.

The tunnel surface treatments described in the previous paragraph prevented scouring of the rock surface and minimized the amount of dust introduced into the atmosphere. The tunnel was able to withstand two high explosive detonations with negligible damage.

The measured (both active and passive) rock displacements were very small. These measurements, when coupled with pretest predictions and observations of negligible damage following both tests, led us to conclude that the tunnel response was essentially elastic. Consequently, there is a high degree of confidence that a one-half scale (on the order of 50 feet (15.2 m) in diameter) simulator could be constructed and repeatedly operated successfully at Little Skull Mountain or in a similar geology.

SECTION 8

LIST OF REFERENCES

1. Scowcroft, B., "Report of the President's Commission on Strategic Forces," April 1983.

2. Kuhl, A. and Wright, M., "Preliminary Design Calculations, HML Airblast Simulator Development Program," Briefing, R & D Associates, 12 October 1983.

3. Stockham, L.W., "Hard Mobile Launcher Test Series, Tunnel Survivability, Tests 1 and 2, Airblast Data Report," NMERI/CERF TA9-90, Subtask Statement 9.29, New Mexico Engineering Research Institute, 24 July 1984.

4. Sweet, J., "SATURN - A Multi-Dimensional Two-Phase Computer Program which Treats the Nonlinear Behavior of Continua Using the Finite Element Approach," Report No. JSA-79-016, Joel Sweet and Associates, September 1979.

5. _____, "ICBM Deep Basing Egress System, Feasibility Test Data Analysis Report, Technical Operating Report," Draft prepared under Contract F04704-82-C-0031, Bechtel National, July 1983.

6. Sweet, J., "Nonlinear Response of Buried Structures in a Stress Wave Environment," DNA 4360F, Systems, Science and Software, June 1977.

7. Shunk, R.A., "Soil Strain Measurements on MISERS BLUFF - Phase II," DNA 4833T, Electromechanical Systems of New Mexico, 30 April 1979.

8. Den Hartog, J.P., Mechanical Vibrations, 4th edition, McGraw-Hill Book Company, 1956.

9. Natrella, M.G., Experimental Statistics, NBS Handbook 91, U.S. Government Printing Office, 1963.

10. LaComb, J.W., et al, "TUNNEL SURVIVABILITY TESTS. Test Execution and Data Report," DNA POR 7151, Test Directorate, Field Command DNA, 19 March 1985.

DISTRIBUTION LIST

DEPARTMENT OF DEFENSE

Defense Intelligence Agency
ATTN: RTS-2A, Tech Lib
ATTN: RTS-2B

Defense Nuclear Agency
ATTN: SPAS ROHR
2 cys ATTN: SPSS
4 cys ATTN: STTI-CA

Defense Technical Information Center
12 cys ATTN: DD

Department of Defense Explo Safety Board
ATTN: Chairman

Field Command, Defense Nuclear Agency
ATTN: LTC J. Lee

DEPARTMENT OF THE ARMY

BMD Advanced Technology Center
ATTN: ATC-T
ATTN: 1CRDABH-X

US Army Ballistic Research Lab
ATTN: DRDAR-BLT, J. Keefer
2 cys ATTN: DRDAR-BLA-S, Tech Lib

US Army Concepts Analysis Agency
ATTN: CSSA-ADL, Tech Lib

US Army Engineer Div Ohio River
ATTN: ORDAS-L, Tech Lib

US Army Engr Waterways Exper Station
ATTN: Library
ATTN: WESSD, J. Jackson

US Army Nuclear & Chemical Agency
ATTN: Library

DEPARTMENT OF THE AIR FORCE

Air Force Systems Command
ATTN: DEB

Air Force Geophysics Laboratory
ATTN: LWH, H. Ossing

Air Force Institute of Technology
ATTN: Library

Air Force Weapons Laboratory
ATTN: J. Renick
ATTN: SUL

Air University Library
ATTN: AUL-LSE

Assistant Chief of Staff, Intelligence
ATTN: IN

Ballistic Missile Office
ATTN: ENS, W. Weisinger
ATTN: ENSN, D. Emary

DEPARTMENT OF THE AIR FORCE (Continued)

Strategic Air Command
ATTN: DOWE
ATTN: INAO
ATTN: NRI/STINFO
ATTN: XPQ

DEPARTMENT OF ENERGY

Department of Energy
Albuquerque Operations Office
ATTN: CTID
ATTN: R. Jones

Department of Energy
Office of Military Application, GTN
ATTN: OMA/RD&T

Department of Energy
Nevada Operations Office
ATTN: Doc Con for Technical Library

Sandia National Laboratories
ATTN: Library & Security Classification Div

Sandia National Laboratories
ATTN: F. Mathews

OTHER GOVERNMENT AGENCIES

Central Intelligence Agency
ATTN: OSWR/NED

Bureau of Mines
ATTN: Tech Lib

Federal Emergency Management Agency
ATTN: Asst Assoc. Dir for Rsch, J. Kerr
ATTN: W. Chipman, NP-CP

DEPARTMENT OF DEFENSE CONTRACTORS

ACTA, Inc
ATTN: Dr J. Collins

Aerospace Corp
ATTN: Library Acquisition, M1/199

California Research & Technology, Inc
ATTN: M. Rosenblatt

California Research & Technology, Inc
ATTN: F. Sauer

California Research & Technology, Inc
ATTN: Technical Library

University of Denver, Colorado Seminary
ATTN: Sec Officer for J. Wisotski

Electro-Mech Systems, Inc
ATTN: R. Shunk

General Research Corp
ATTN: Technical Information Office

DEPARTMENT OF DEFENSE CONTRACTORS (Continued)

H-TECH Labs, Inc
ATTN: B. Hartenbaum

IIT Research Institute
ATTN: Documents Library

Information Science, Inc
ATTN: W. Dudziak

Institute for Defense Analyses
ATTN: Classified Library

Kaman Sciences Corp
ATTN: Library

Kaman Tempo
ATTN: DASIAC

Kaman Tempo
ATTN: DASIAC

Merritt CASES, Inc
ATTN: J. Merritt
ATTN: Library
2 cys ATTN: D. Burgess
2 cys ATTN: G. Wintergerst
2 cys ATTN: H. Davis
2 cys ATTN: K. Morrill

University of New Mexico
New Mexico Engineering Research Institute
ATTN: Leo Stockham

DEPARTMENT OF DEFENSE CONTRACTORS (Continued)

Pacific-Sierra Research Corp
ATTN: H. Brode, Chairman SAGE

Physics International Co
ATTN: W. Wampler

R & D Associates
ATTN: A. Kuhl
ATTN: Technical Information Center

R & D Associates
ATTN: G. Ganong

Science & Engrg Assoc, Inc
ATTN: B. Chambers

Science Applications International Corp
ATTN: G. Binninger

SRI International
ATTN: M. Sarai

Tech Reps, Inc
ATTN: B. Homes

TRW Electronics & Defense Sector
ATTN: Technical Information Center

Weidlinger Assoc, Consulting Engrg
ATTN: T. Deevy

Weidlinger Assoc, Consulting Engrg
ATTN: J. Isenberg

END

FILMED

DTIC